NASA

Technical Memorandum 81984

Variations in the Nimbus-7 Scanning Multichannel Microwave Radiometer Cold Reference Antenna Signals and Temperatures During Two Orbital Periods

Per Gloersen, D.J. Cavalieri and H.V.Soule

AUGUST 1980

National Aeronautics and
Space Administration

Goddard Space Flight Center
Greenbelt, Maryland 20771

(NASA-TM-81984) VARIATIONS IN THE NIMBUS-7 SCANNING MULTICHANNEL MICROWAVE RADIOMETER COLD REFERENCE ANTENNA SIGNALS AND TEMPERATURES DURING TWO ORBITAL PERIODS (NASA) 73 p HC A04/MF A01 CSCL 22B G3/15

N80-30355

Unclas
31329

VARIATIONS IN THE NIMBUS-7 SCANNING MULTICHANNEL MICROWAVE RADIOMETER COLD REFERENCE ANTENNA SIGNALS AND TEMPERATURES DURING TWO ORBITAL PERIODS

Per Gloersen
D. J. Cavalieri
Goddard Space Flight Center
Greenbelt, Maryland

Harold V. Soule
OAO Corporation
Beltsville, Maryland

ABSTRACT

This paper discusses a study of the observed effects of solar radiance on the Nimbus 7 Scanning Multichannel Microwave Radiometer (SMMR) cold reference signal. Unexpected diurnal responses in this signal sometimes larger than the typical cold reference signal resulted from acquisition of the solar disc. Solar heating of the SMMR components as a function of orbital locations was correlated with the cold reference radiances for two sets of sequential orbit six months apart.

TABLE OF CONTENTS

TABLES

ILLUSTRATIONS

ILLUSTRATIONS (continued)

1. INTRODUCTION

The Nimbus-7 Scanning Multichannel Microwave Radiometer (N-7/SMMR) utilizes a two-point radiance reference scheme to provide radiance measurement adjustment information when the radiometer gain changes. One point is the radiation from a waveguide load for which the temperature is carefully monitored; the other is free space radiation (2.7K) monitored by a set of three horn antennas (ref. 1). In order to avoid interception in the main beam of the earth-viewing antenna, observation of the limb of the earth and of the Nimbus-7 solar panels, the horns shown in Figure 1 were aimed 15^{o} above the local horizontal and 10^{o} to the right of the spacecraft velocity vector. As a result, an unavoidable observation of solar radiation occurs once every orbital period, because Nimbus-7 is in a sun-synchronous orbit i.e., crosses the equator at approximately local noon when in the south-to-north portion of the orbit, and has an orbit tilt of 99.3^{o} with respect to the equatorial plane. Since the N-7/SMMR gain varies approximately with orbital period, response to the solar disc can be filtered out and the cold reference signal synthesized by interpolation over the solar acquisition interval.

This report describes a study of the solar radiance as observed with the cold reference horns, and an unexpected diurnal response, sometimes larger than the normal signal resulting from the solar disc acquisition, which cannot be attributed to re-radiation from the N-7/SMMR radio frequency (r.f.) components.

2. PERTINENT SMMR CHARACTERISTICS

Figure 2 shows the SMMR location onboard the Nimbus 7 spacecraft. Note that there is a rather large shield behind the earth-viewing antenna dish. When that shield and the main antenna dish face the sun, concentrated heating can occur. At other times they operate as heat radiators to the earth and space, cooling the SMMR components.

In the schematics in Figure 3, it will be noted that the microwave radiation travels from the multifrequency feed horn via the coaxial or standard waveguides through the bulkhead to the ferrite switch. Note that there are different flow paths and temperature measurements for the horizontal and vertical polarizations for most of the frequencies. However, in some cases, the same temperature measurement is used for more than one frequency. In a similar manner the microwaves received by the calibration horns pass from the receiver via the coaxial or standard waveguide through the bulkhead to the ferrite switch block.

An offset voltage is used to make the output counts increase with increasing detected radiances. However, there is always a possibility that the reference voltage will change during the course of an orbit. It is therefore desirable to remove this offset signal by taking the difference between the warm counts (C_W) and the cold counts (C_C). The parameter (C_W-C_C) represents the true response of the N-7/SMMR Dicke type radiometer to the radiance received by the cold horn, (ref. 1).

The component temperatures were measured by accurate platinum resistance units which were compared with a constant temperature reference. Their locations on the N-7/SMMR are indicated in Figure 3, along with the engineering block word numbers, corresponding to the SMMR Data Format shown in Table I.

3. COUNT CONVERSION FACTORS

For the (C_W-C_C) counts, corresponding approximate radiance differences were computed using the value of 0.12 Kelvin/count. This value corresponds to the ratio (300-100)/(C_W-C_C) thermal - vacuum chamber where 300 and 100 were the physical temperatures of the warm and cold reference used during the thermal-vacuum chamber calibrations.

Table I

SMMR DATA FORMAT
DATA BLOCK 16
SUB-MULTIPLEXER

6.6 GHz + XTL Current 1	10.69 GHz + XTL Current 2	18 GHz + XTL Current 3	21 GHz + XTL Current 4	6.6 GHz Dicke SW. Temp. Plat. 5	10.69 GHz Dicke SW. Temp. Plat. 6	18 GHz Dicke SW. Temp. Plat. 7	21 GHz Dicke SW. Temp. Plat. 8
6.6 GHz - XTL Current 9	10.69 GHz - XTL Current 10	18 GHz - XTL Current 11	21 GHz - XTL Current 12	Antenna Feed Horn Temp #1 Aperture Plat. 13	Antenna Feed Horn Temp #2 6.6 GHz-H Port Plat. 14	37 GHz Horiz. Dicke SW. Temp. Plat. 15	37 GHz Vert. Dicke SW. Temp. Plat. 16
37 GHz Horiz. + XTL Current 17	6.6 GHz Dicke SW. Temp. Eng. 18	37 GHz Vert. +XTL Current 19	10.69 GHz Dicke SW. Temp. Eng. 20	6 & 10 GHz Calibration Horn Temp. #1 Plat. 21	18 GHz V Feed Horn Wave Guide Temp. #1 Plat. 22	18 & 21 GHz Calibration Horn Temp. #2 Plat. 23	21 GHz V Feed Horn Wave Guide Temp. #6 Plat. 24
37 GHz Horiz. - XTL Current 25	6.6 GHz Local Osc. Temp. Eng. 26	37 GHz Vert. - XTL Current 27	10.69 GHz Local Osc. Temp. Eng. 28	6.6 GHz Chassis Bulkhead Temp. #1 Plat. 29	18 GHz-H Feed Horn Wave Guide Temp. #2 Plat. 30	37 GHz Calibration Horn Temp. #3 Plat. 31	21 & 37V GHz Chassis Bulkhead Temp. #4 Plat. 32
18 GHz Dicke SW. Temp. Eng. 33	Motor Commutator Temp. Eng. 34	21 GHz Dicke SW. Temp. Eng. 35	6.6 GHz Chassis Bulkhead Temp. Eng. 36	10.69 GHz Chassis Bulkhead Temp. #2 Plat. 37	37 GHz V Feed Horn Wave Guide Temp. #3 Plat. 38	18 & 37H GHz Chassis Bulkhead Temp. #3 Plat. 39	Antenna Feed Horn Temp. #4 6.6 GHz-V Port Plat. 40
18 GHz Local Osc. Temp. Eng. 41	Antenna Feed Horn Temp. Eng. Aperture 42	21 GHz Local Osc. Temp. Eng. 43	10.69 GHz Chassis Bulkhead Temp. Eng. 44	6.6 GHz Cal. Horn Wave Guide Temp. #1 Plat. 45	37 GHz-H Feed Horn Wave Guide Temp. #4 Plat. 46	21 GHz Cal. Horn Wave Guide Temp. #4 Plat. 47	Antenna Feed Horn Temp. #3 37 GHz Ortho Plat. 48
37 GHz Horiz. Dicke SW. Temp. Eng. 49	6 & 10.69GHz Calibration Horn Temp. Eng. 50	37 GHz Vert. Dicke SW. Temp. Eng. 51	18 & 37H GHz Chassis Bulkhead Temp. Eng. 52	10.69 GHz Cal. Horn Wave Guide Temp. #2 Plat. 53	21 GHz-H Feed Horn Wave Guide Temp. #5 Plat. 54	37 GHz-V Cal. Horn Wave Guide Temp. #5 Plat. 55	37 GHz-H Cal. Horn Wave Guide Temp. #6 Plat. 56
37 GHz Local Osc. Temp. Eng. 57	Power Supply Temp. Eng. 58	Eng. Mux. Calibrate High 59	Eng. Mux. Calibrate Low 60	18 GHz Cal. Horn Wave Guide Temp. #3 Plat. 61	Data Chassis Temp. Plat. 62	Temp. Mux. Calibrate High 63	Temp. Mux. Calibrate Low 64

The relationship between the component temperature counts and the actual temperatures is given by the following equation:

$$T = A_o + A_1 \left[(R_1 - R_o) + \frac{(R_2 - R_1) \times (C - C_1)}{C_2 - C_1} \right] \ldots \text{(Kevins)} \ldots (1.0)$$

Where: C = counts
C_1 = Calibration Temperature (low) = 1001
C_2 = Calibration Temperature (high) = 3048
R_1 = 500.00
R_2 = 598.85
T = Measured Temperature (K)

The other values in equation (1.0) vary as a function of the unit temperature being measured. Values for the other constraints are shown in Table II.

Table II
COUNT/TEMPERATURE CONVERSION FACTORS

Calibration Horn Values

	(1)	(2)	(3)
A_o	293.16	293.16	293.16
A_1	0.513	0.514	0.511
R_o	536.46	535.81	538.93

SWITCH (SW)

Freq (GHz)	6.6	10.7	18.0	21.0	37(H)	37(V)
A_o	293.16	293.16	293.16	293.16	293.16	293.16
A_1	0.510	0.510	0.512	0.509	0.509	0.510
R_o	539.76	539.34	537.27	540.05	540.2	538.87

BULKHEAD

Freq (GHz)	6.6	10.7	18/37(H)	21/37(V)
A_o	293.16	293.16	293.16	293.16
A_1	0.512	0.514	0.510	0.510
R_o	536.9	535.44	540.14	539.51

4. OBSERVATIONS

Figures 4 through 15 show the manner in which (C_W-C_C) varied through a sequence of successive orbits. On 24 Jan. 1979, the start of the first pass (#1269) across the equator on the descending node was about 10 minutes after SMMR turn-on. The abrupt rise in (C_W-C_C) values near the South Pole in figures 4 and 5 were due to direct viewing of solar produced microwave energy by the reference cold horns. It will be noted that in figures 6 through 9 the radiance difference due to this solar produced effect decreases with increasing orbits after SMMR power-on. After about the fourth orbit, these appears in the data to be little or no direct solar radiation viewing by the 18, 21 and 37 GHz calibration horns.

The same effects occurred during sequential orbits on 23 July, 1979, shown in figures 10 through 15. This sequence of orbits six months later were in a plane almost exactly over the same earth surface locations. In this case, orbit #3760 also started about ten minutes after SMMR turn-on. However, because of the changed sun position with respect to the Nimbus-7 orbit, there was a shift in the time at which solar radiation struck the cold horns. In these figures use of different scale factors for some of the frequencies produced a distortion of the apparent magnitude of this effect.

However, as is indicated in figures 16 through 21 when the same (C_W-C_C) scale factor was used for all frequencies, there is a consistant trend between data taken six months apart. The true radiance corresponding to the (C_W-C_C) counts has not as yet been determined. For this reason in all of these figures the computed radiance was arbitrarly determined using 300-0.13 (C_W-C_C) counts (K) producing a decreasing radiance for increasing counts. Thus the addition of solar microwave energy produces an increasing (C_W-C_C) radiance.

In Figures 22 through 30 the temperature variations along each frequency microwave flow path for the horizontal and vertical polarizations is shown for the first orbit (#1269). Figures 31 through 39 show the same parameters for the 4th orbit (#1272 after SMMR power-on on 24 Jan. 1979.

Simular SMMR component temperature measurements made 6 months later for orbits #3760 and #3763 are shown in figures 40 through 46 and 47 through 53 respectively. For convenience the time have all been normalized and equivalent latitude positions indicated in all of these figures.

To indicate the nature of the changes in the feed horn and reference horn temperatures for several sequential orbits, figures 54 through 57 give a comparison for the two orbital sets of measurements. Figures 54 compares the temperature of the feed-horn surfaces used for all frequencies but 6.6 GHz. Figure 55 shows the 6.6 GHz horizontal polarization feed-horn temperature variation. Figures 58 through 61 indicate the manner in which the ferrite switch temperatures, change as a function of time. It will be noted that except for the expected shift in the temporal position of the peak temperatures, there was little change in the manner in which the temperatures varied for the two series of orbits.

4.1 Comments

The shape of the component temperature curves more or less follow expectations during the course of an orbital period The Nimbus-7 spacecraft is in sunlight for about 70% of its 104 minute orbit; the cyclic variation of the components follow this trend. The somewhat sharper peak on the multifrequency receiving horn temperatures may be attributed to shadowing effects that differ from those on the cold reference horns. Proceeding from the exposed components in towards the radiometer bulkheads and interior switch temperature, the amplitude of the diurnal variation in component temperatures is seen to decrease. Since it is anticipated that the instrument calibration algorithm based on the assumption of in-phase instrument temperature variations will be impacted, the phase shift in the diurnal component temperature variations along the radiometric paths is noteworthy. Indeed, slight day/night differences have been noted in the radiometer signals received (Reference 3) from a given ocean area (averaged over 300 orbits).

Solar acquisition by the cold horns was expected at all frequencies. The amplitudes measured were also expected (Ref. 4). Superimposed upon

this however, is a diurnal response that was not expected. This additional signal cannot be attributed to re-radiation from the instrument components, since the signal is in the opposite sense to the potential re-radiation source temperatures, i.e., the radiometer readings decrease when the component temperatures increase. This usually occurred between the South Pole and the Equator on the ascending portion of the orbit. In Figures 58 through 61 it will be noted that even the Dicke temperatures increased during this portion of the orbits.

REFERENCES

1). Per Gloersen and Frank T. Barath, (1977) "A Scanning Multichannel Microwave Radiometer for Nimbus-G and Seasat A,". IEEE J of Oceanic Engr. Vol. OE-2, No. 2, pg. 172 (April 1977)

2). Per Gloersen and J. M. Stacey (1979) Prelaunch Calibration Report Nimbus-7 SMMR Instrument Jet Propulsion Lab., Cal Inst. of Tech. Pasadena, Calif.

3). Per Gloersen, D. Cavalieri and H. Sou'e, (1980) "An Alternate Algorithm for correction of the Scanning Multichannel Microwave Radiometer Polarization Radiances using Nimbus-7 Observed Data NASA TM 80672.

4). Stacey, J. M., "Sun and Moon in the Sky Calibration Horns" Tech Memo JPL, Oct. 14, 1977 (Unpublished).

5). Stacey, J. M., "Private Communication".

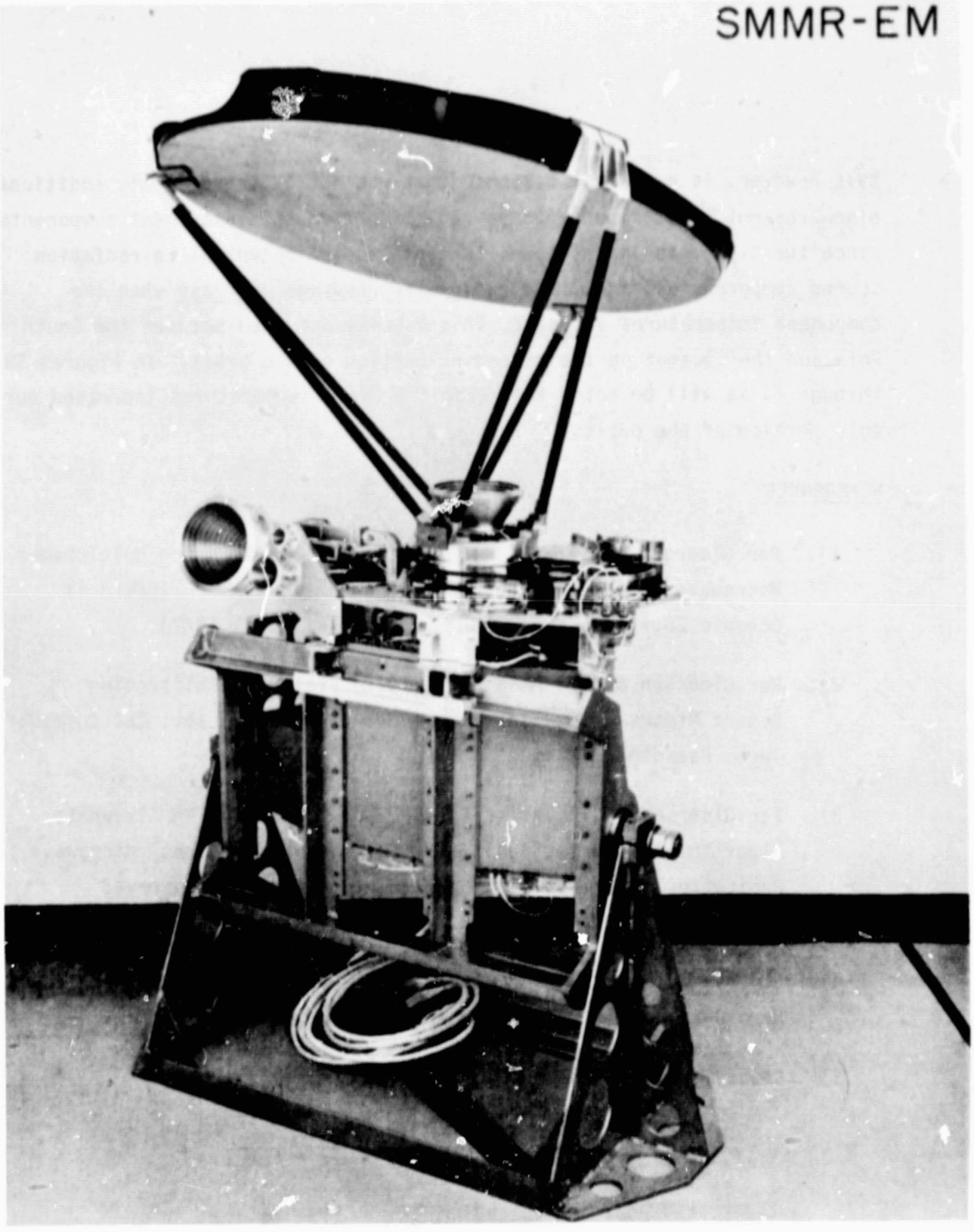

Figure 1. SMMR Sensor System

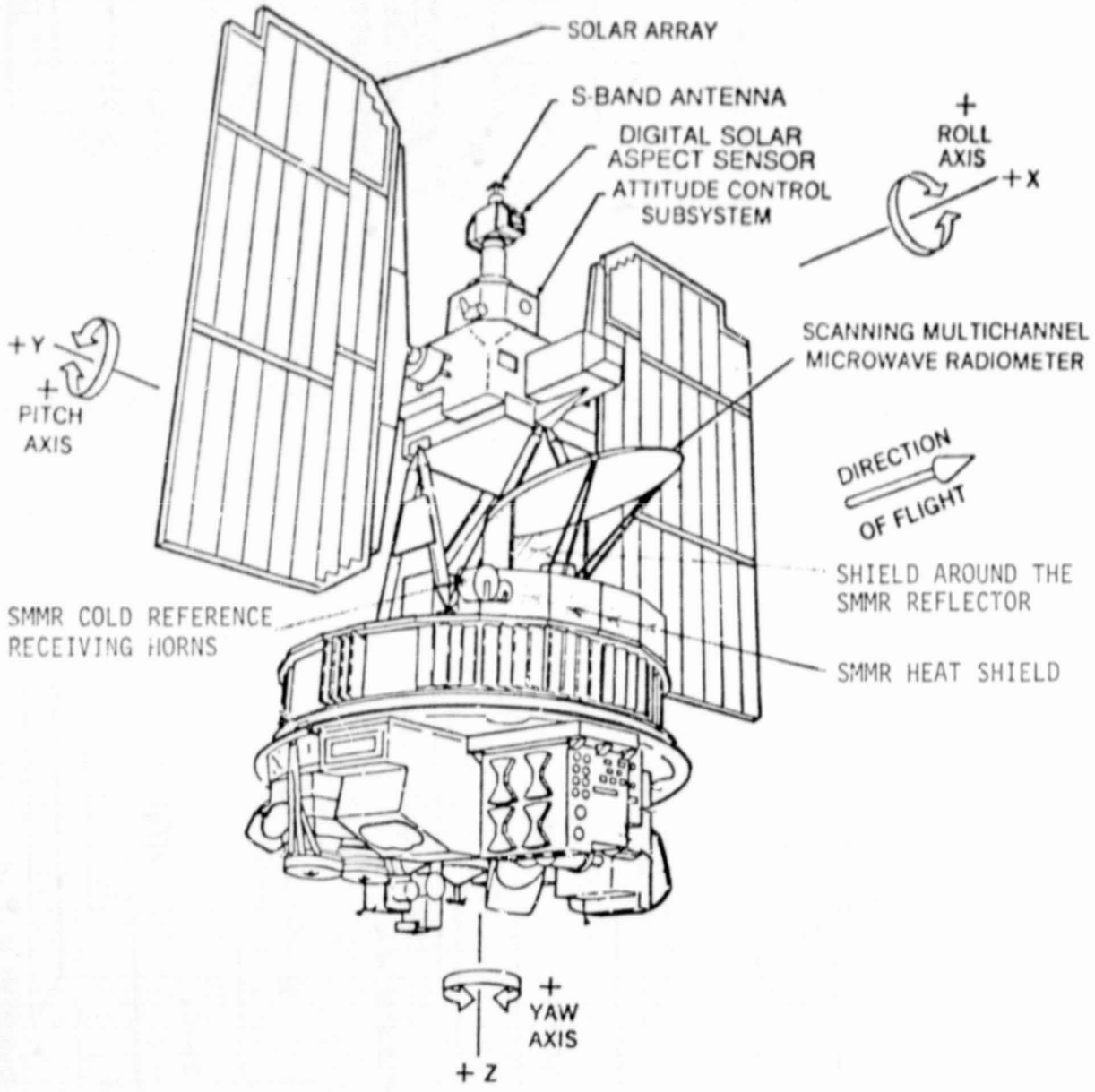

Figure 2. Assembly Details of the Scanning Multichannel Microwave Radiometer on the Nimbus 7.

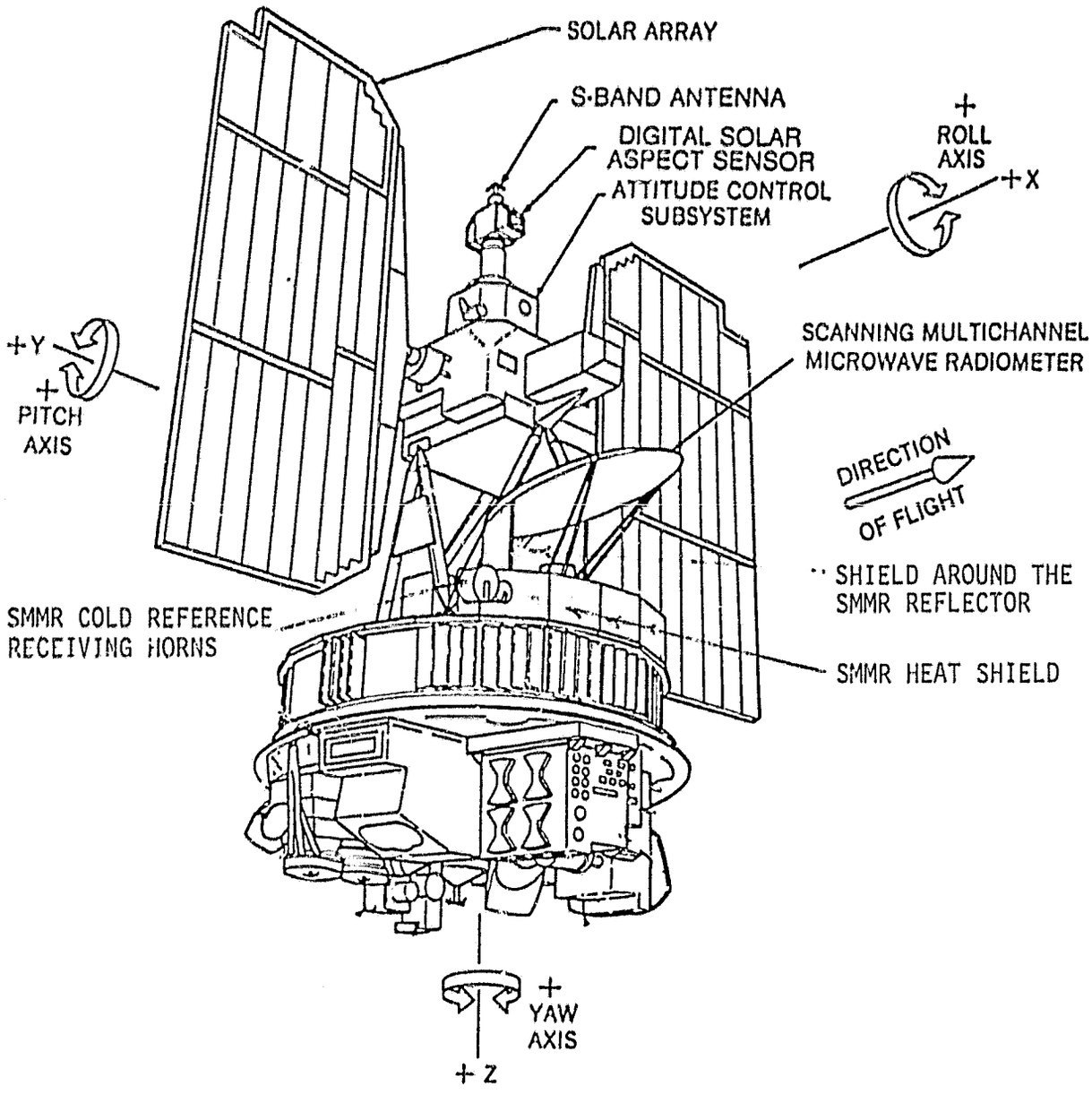

Figure 2. Assembly Details of the Scanning Multichannel Microwave Radiometer on the Nimbus 7.

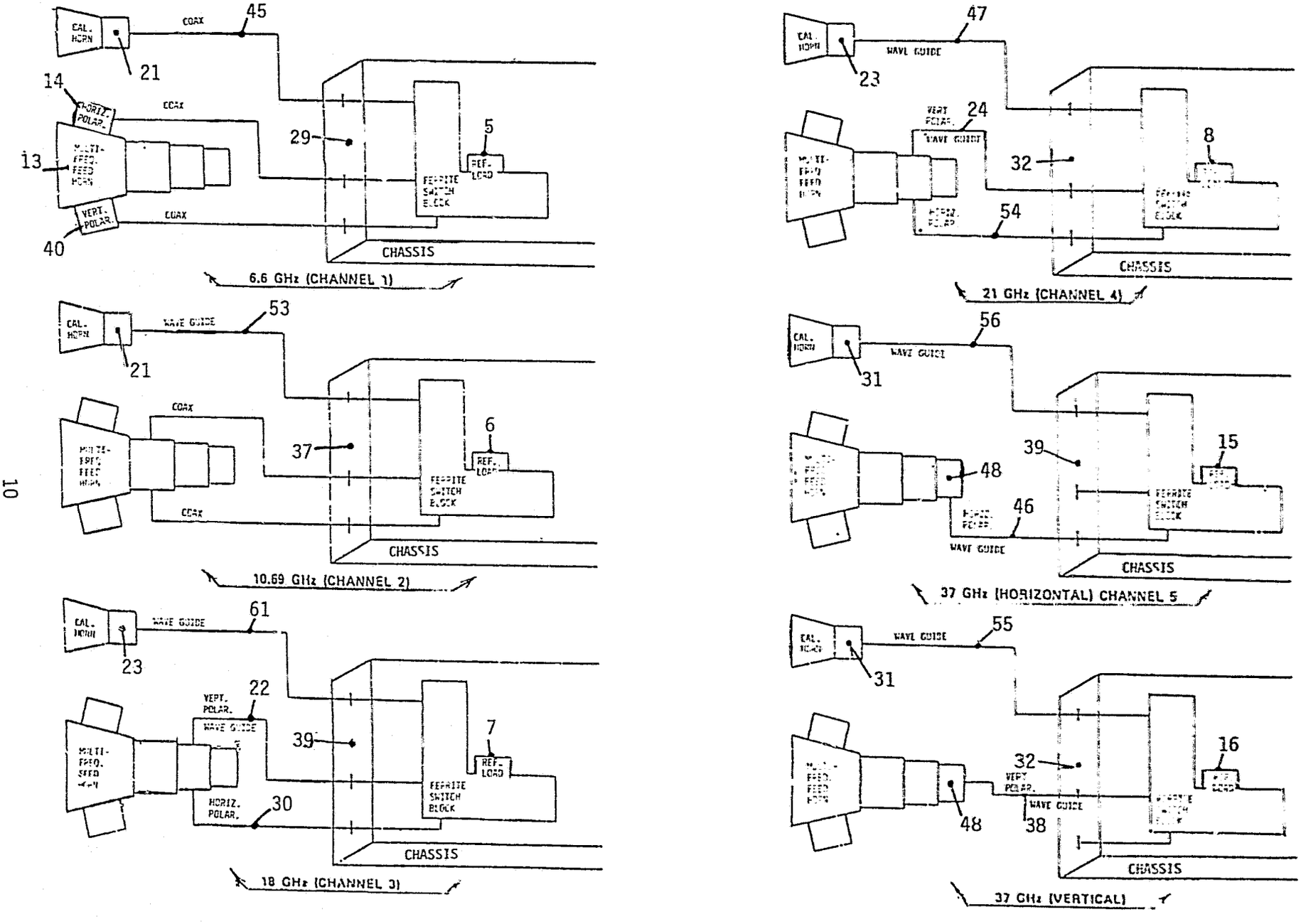

Figure 3. SMMR channel schematics showing the approximate location of the platinum temperature sensors identified in Table II by block numbers.

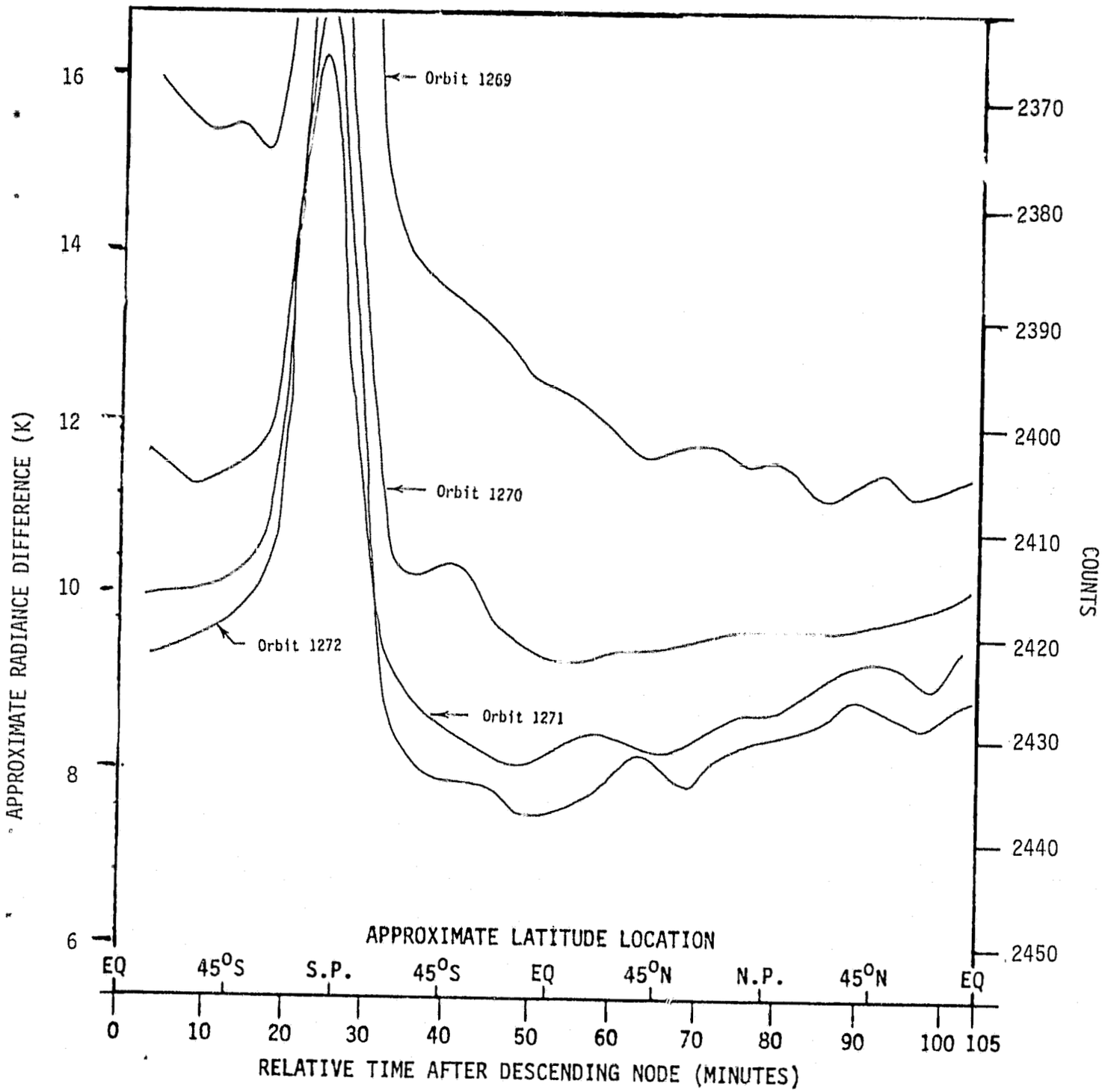

Figure 4. SMMR radiance difference (C_W-C_C) as a function of sequential orbits for 6.6 GHz. Orbits 1269 through 1272 (24 Jan. 1979).

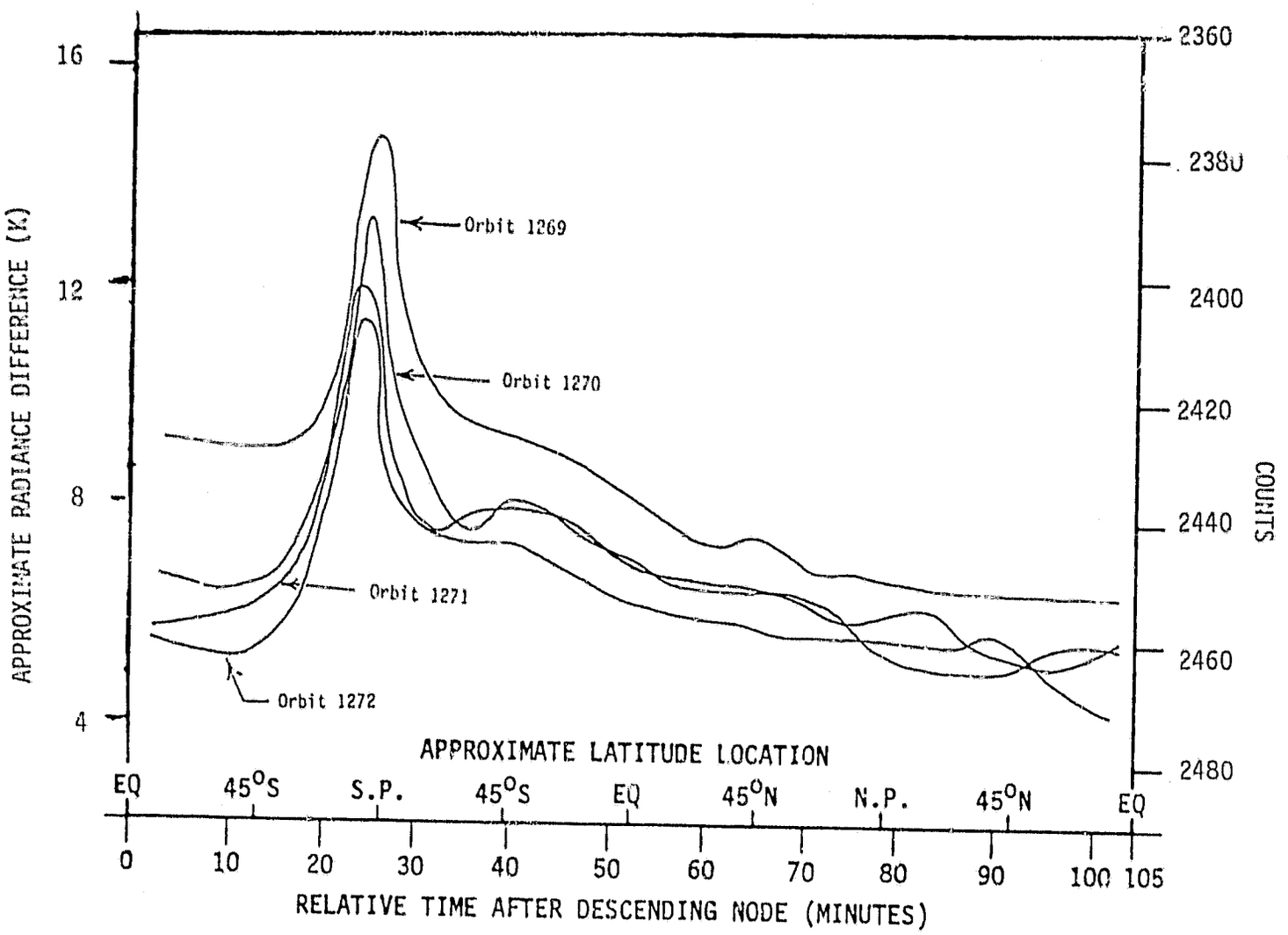

Figure 5. SMMR radiance difference (C_W-C_C) as a function of sequential orbits for 10.7 GHz. Orbits 1269 through 1272 (24 Jan. 1979).

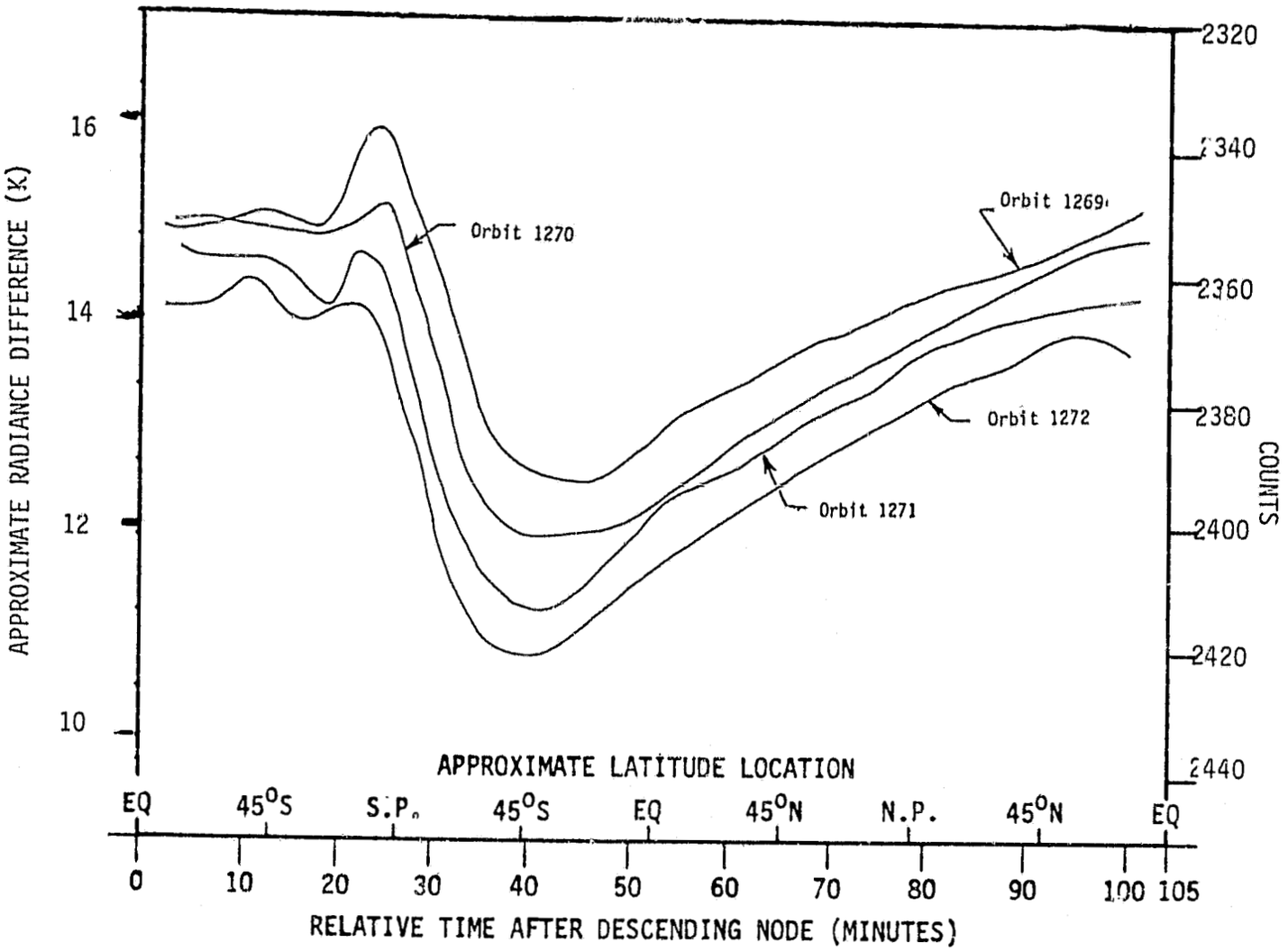

Figure 6. SMMR radiance difference (C_W-C_C) as a function of sequential orbits for 18.0 GHz. Orbits 1269 through 1272 (24 Jan. 1979).

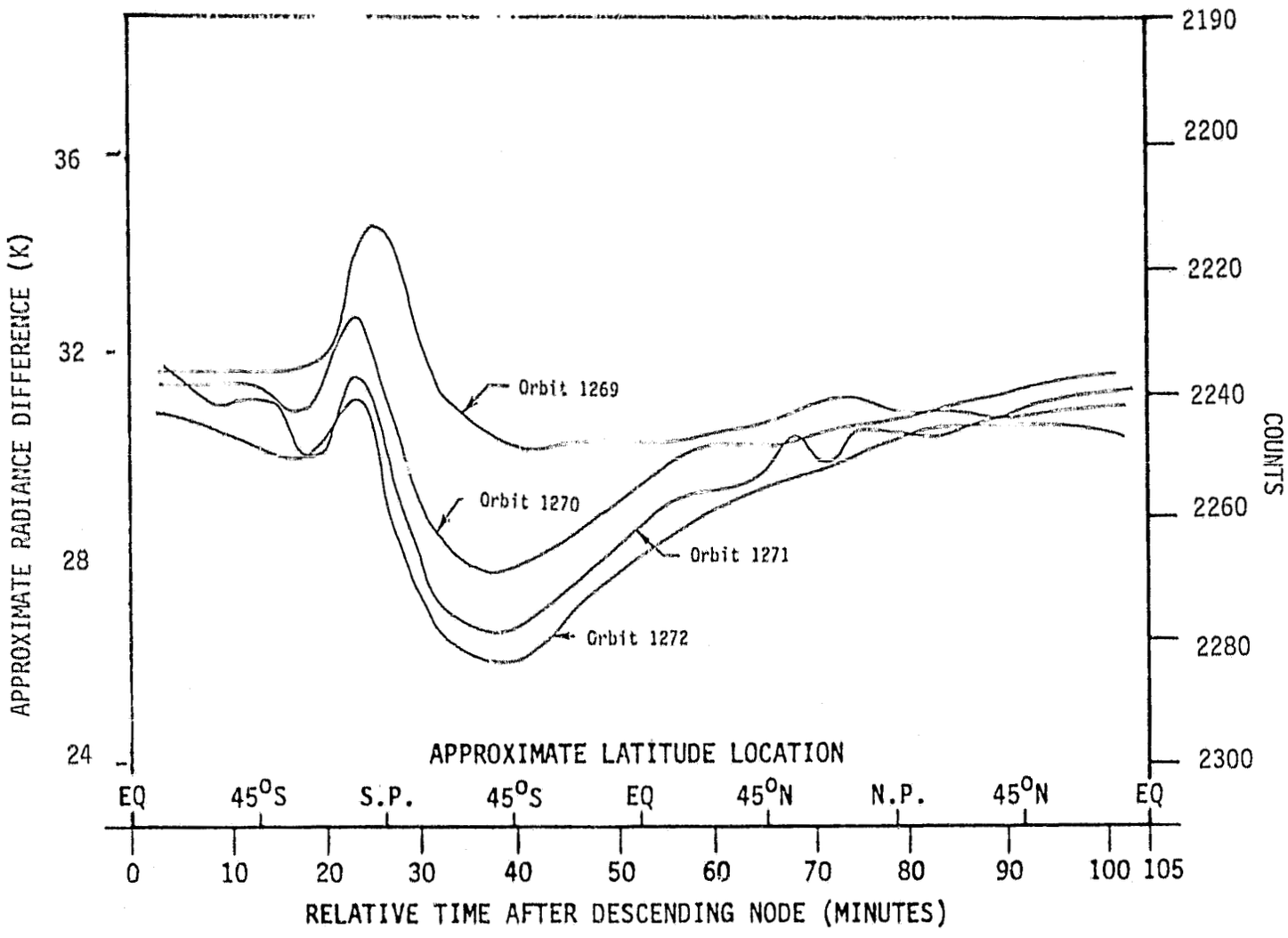

Figure 7. SMMR radiance difference (C_W-C_C) as a function of sequential orbits for 21.0 GHz. Orbits 1269 through 1272 (24 Jan. 1979).

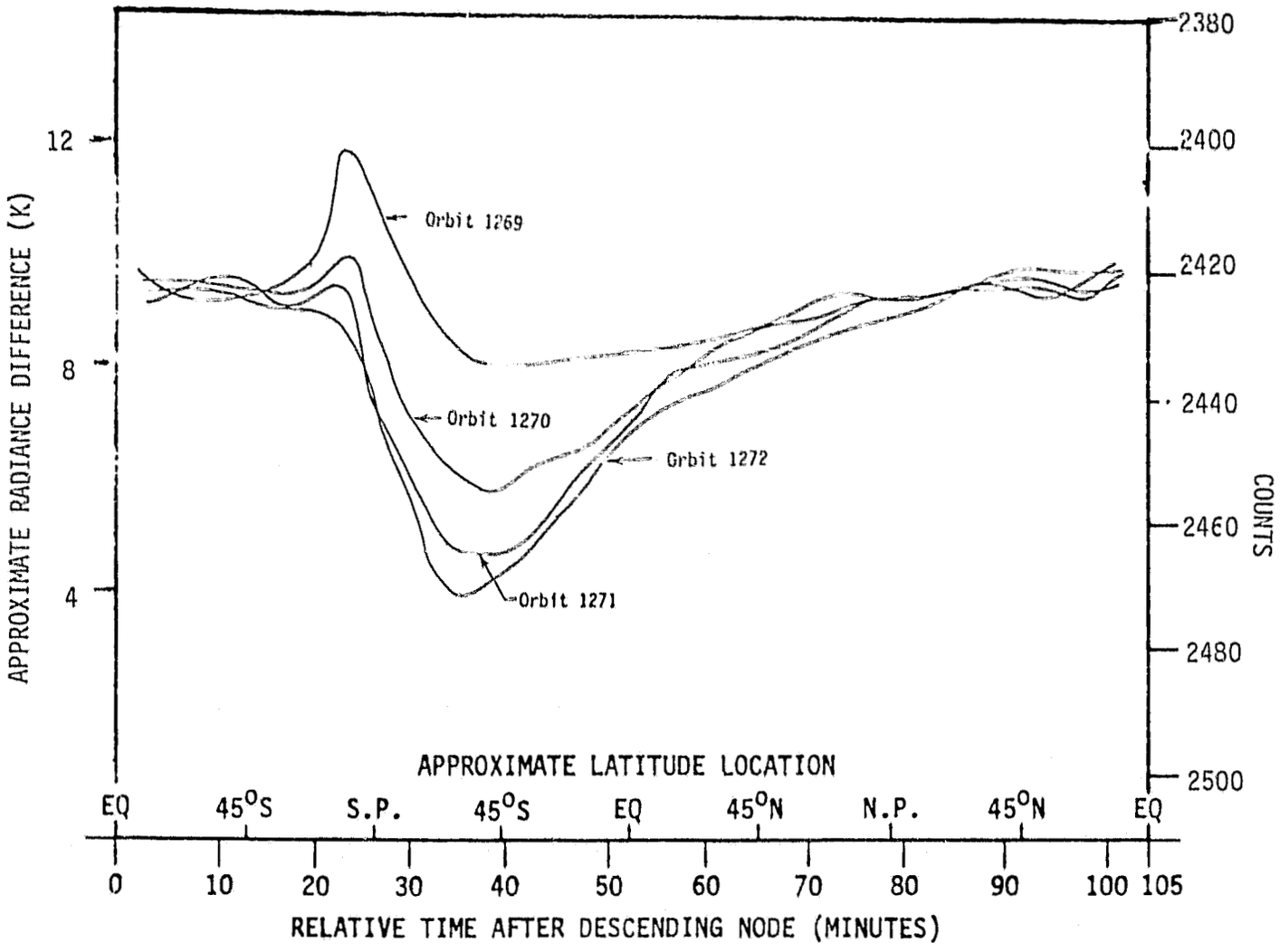

Figure 8. SMMR radiance difference (C_W-C_C) as a function of sequential orbits for 37.0 GHz vertical polarization. Orbits 1269 through 1272 (24 Jan. 1979).

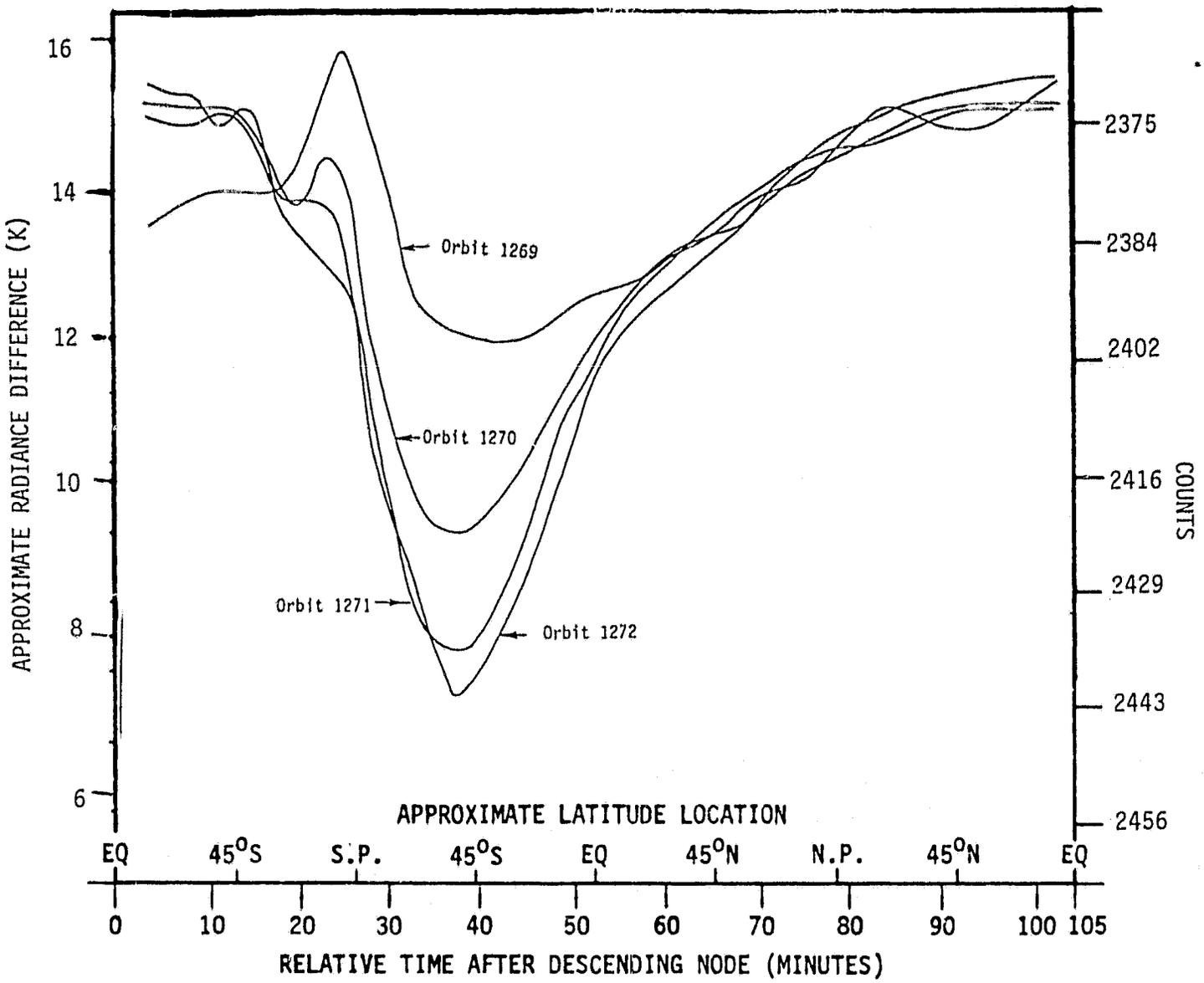

Figure 9. SMMR radiance difference (C_W-C_C) as a function of sequential orbits for 37.0 GHz horizontal polarization. Orbits 1269 through 1272 (24 Jan. 1979).

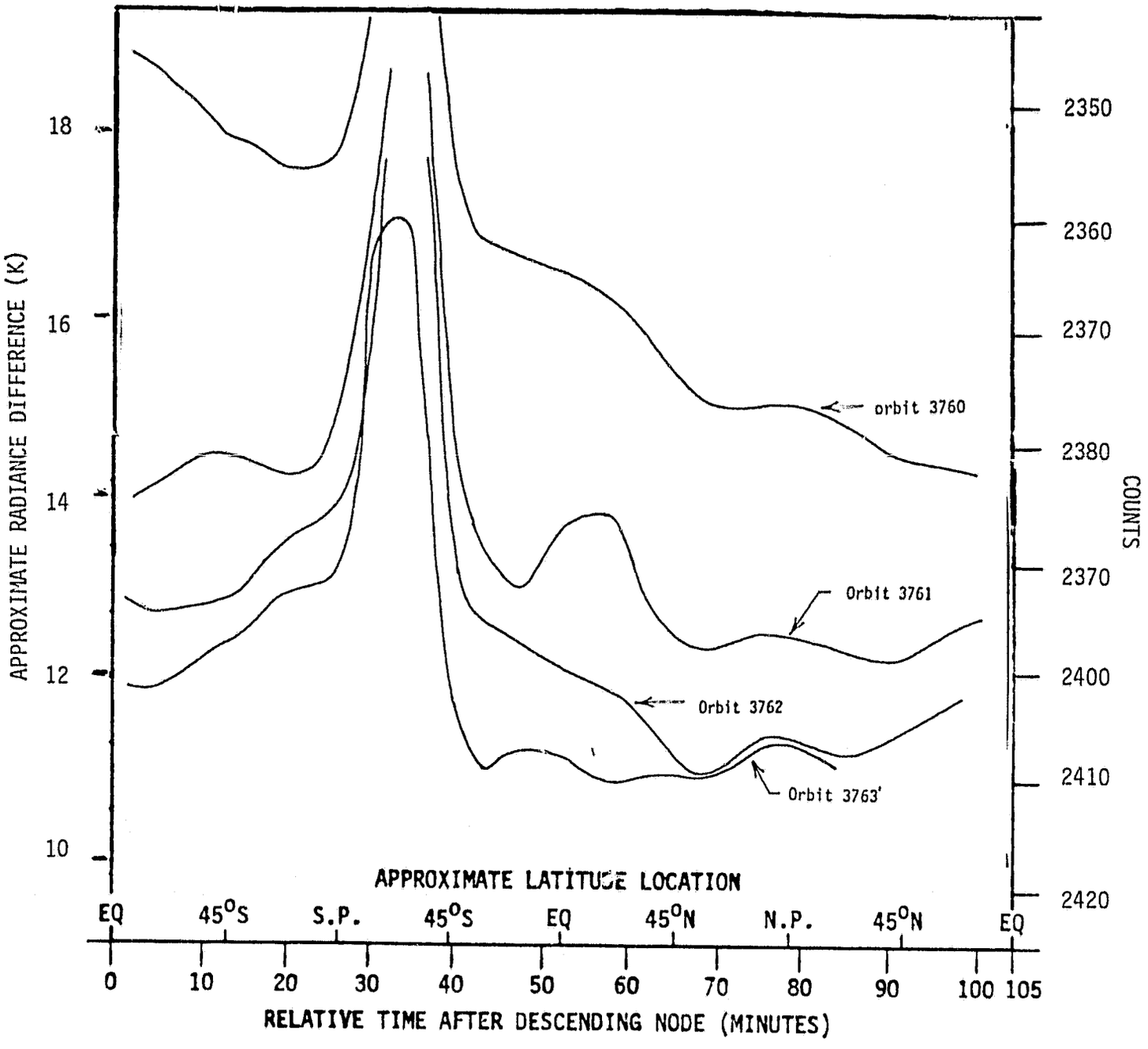

Figure 10. SMMR radiance difference (C_W-C_C) a function of sequential orbits for 6.6 GHz. Orbits 3760 through 3763 (23 July 1979).

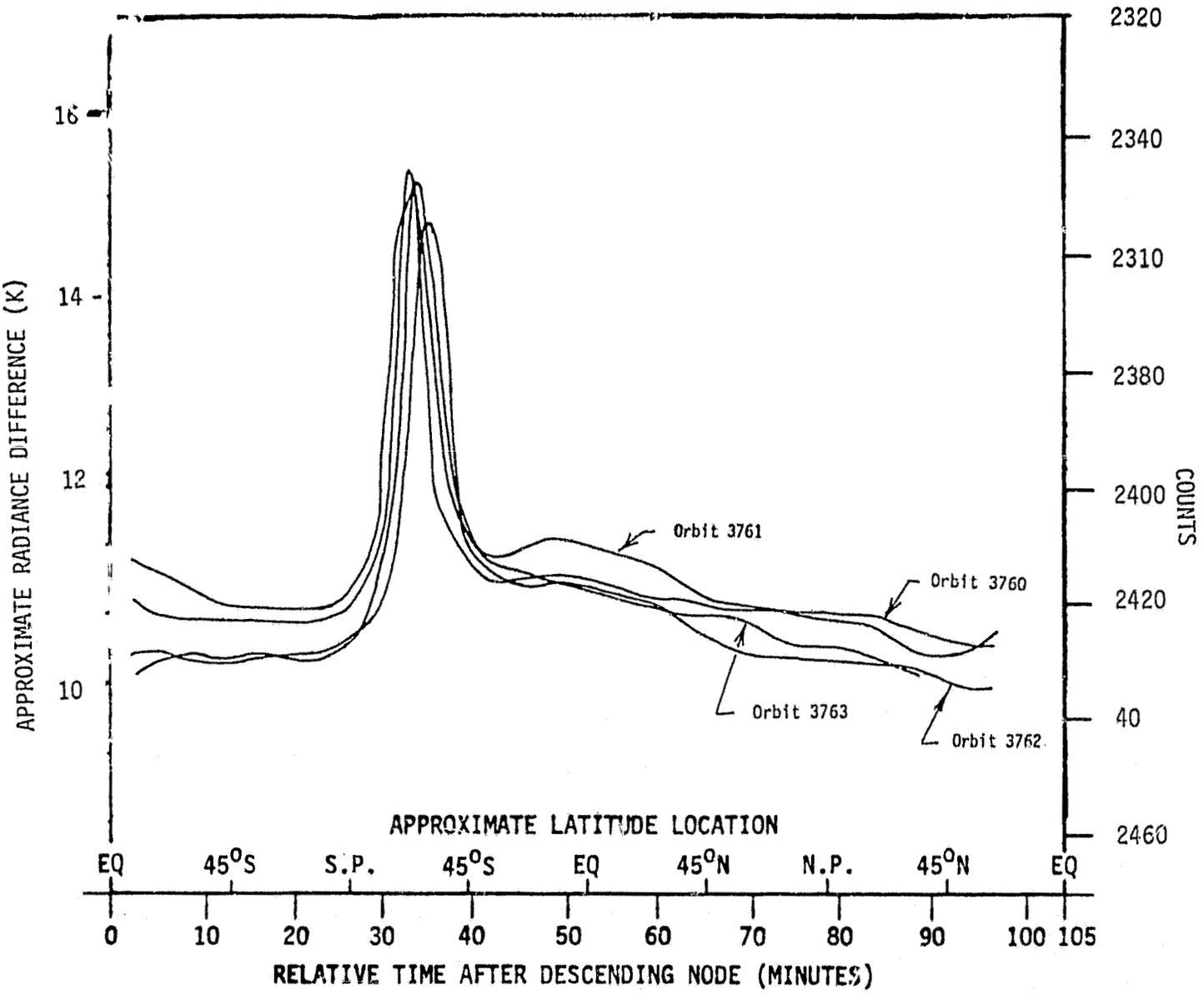

Figure 11. SMMR radiance difference (C_W-C_C) as a function of sequential orbits for 10.7 GHz. Orbits 3760 through 3763 (23 July 1979)

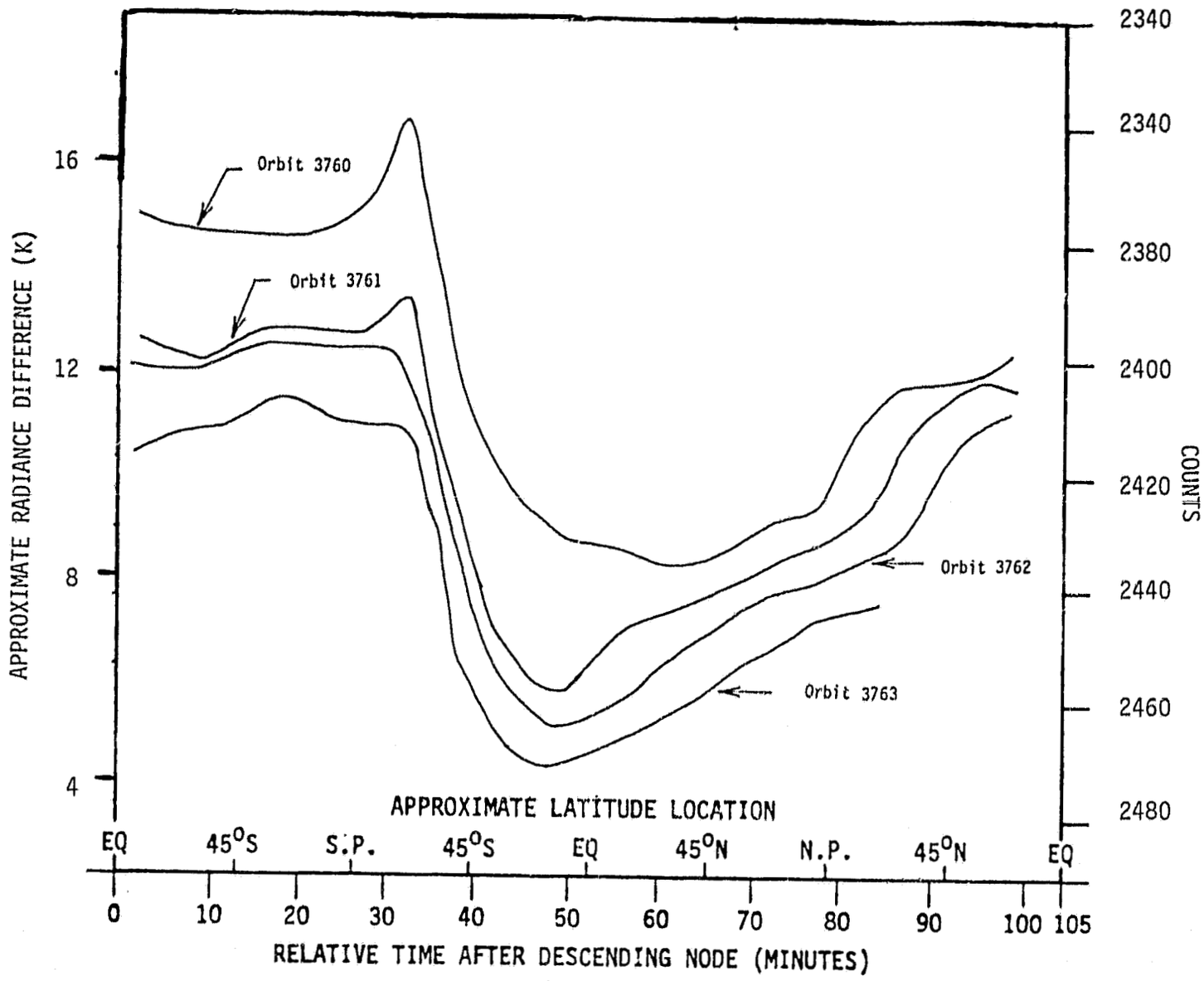

Figure 12. SMMR radiance difference (C_W-C_C) as a function of sequential orbits for 18 GHz. Orbits 3760 through 3763 (23 July 1979).

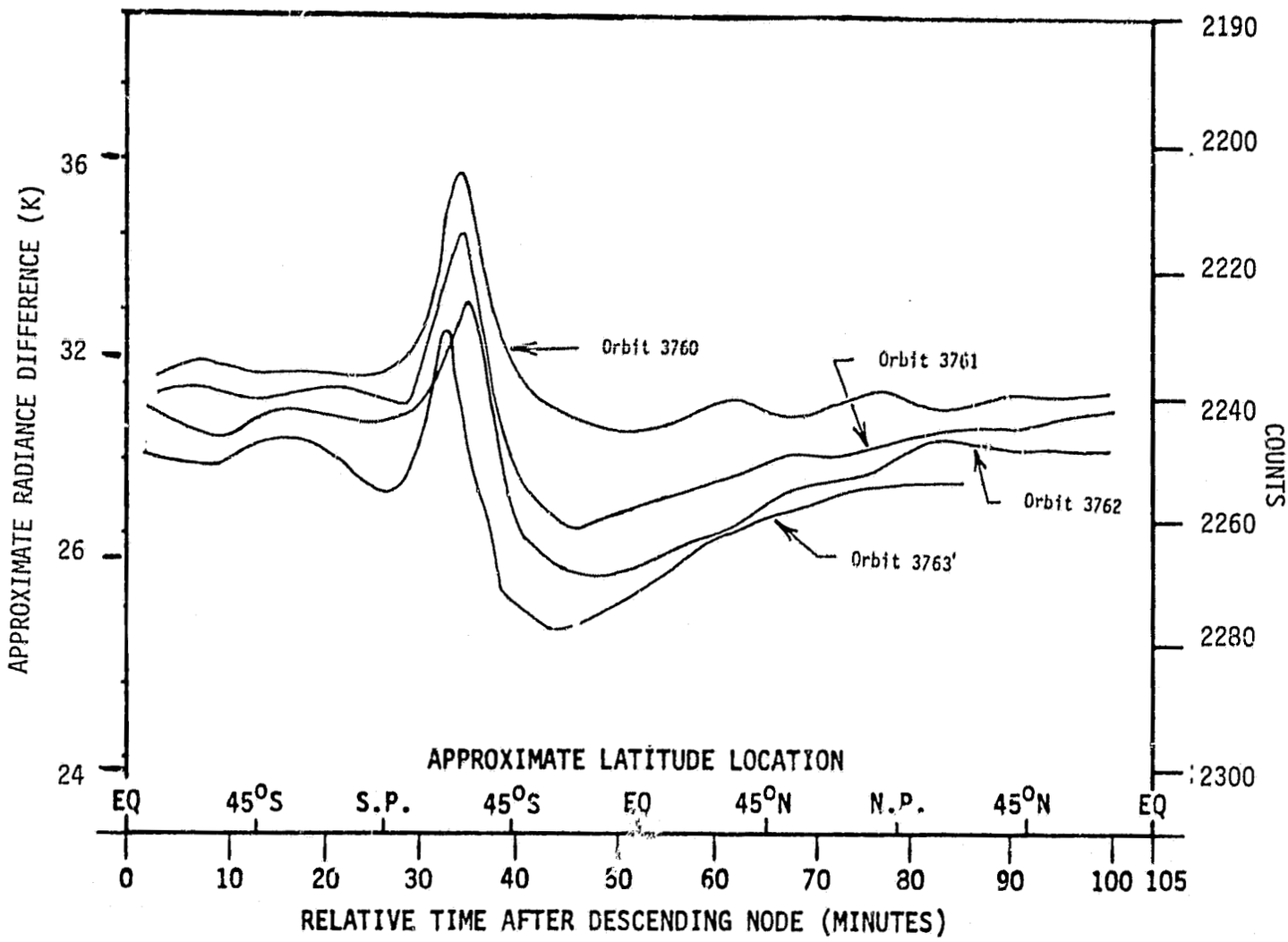

Figure 13. SMMR radiance difference (C_W-C_C) as a function of sequential orbits for 21 GHz. Orbits 3760 through 3763 (23 July 1979).

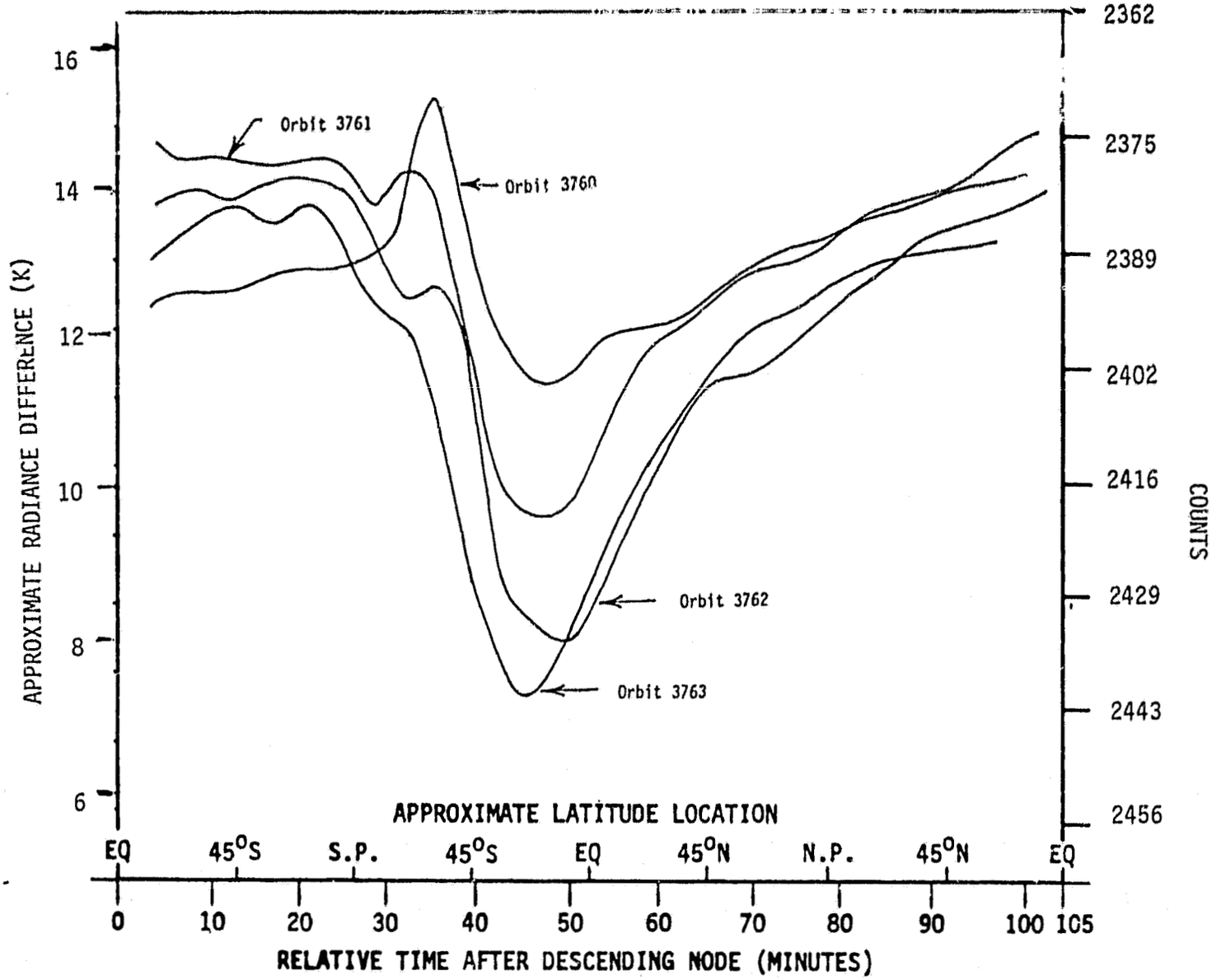

Figure 14. SMMR radiance difference (C_W-C_C) as a function of sequential orbits for 37 (H) GHz. Orbits 3760 through 3763 (23 July 1979).

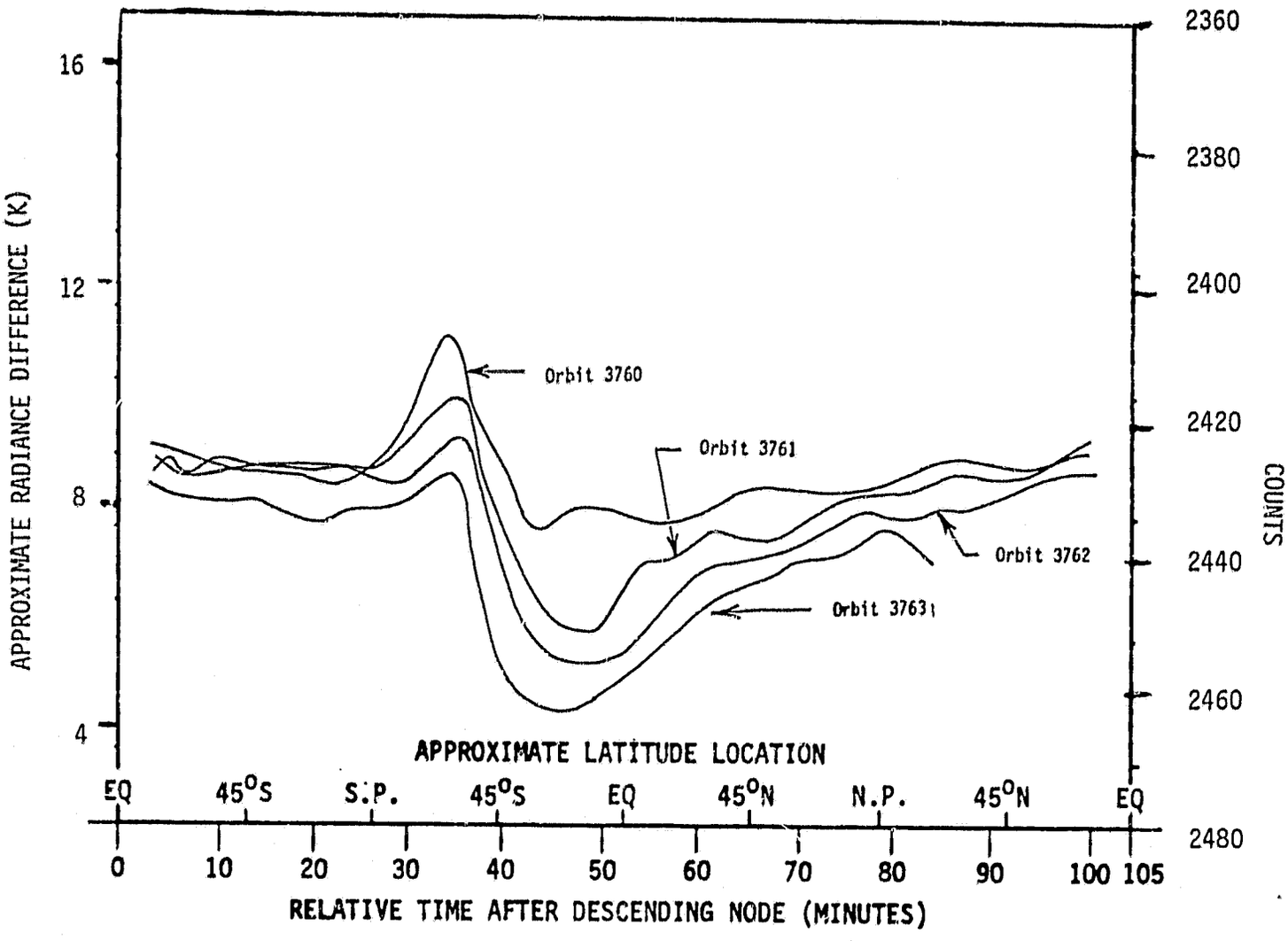

Figure 15. SMMR radiance difference between C_W and C_C as a function of sequential orbits for 37 (V) GHz. Orbits 3760 through 3763 (23 July 1979).

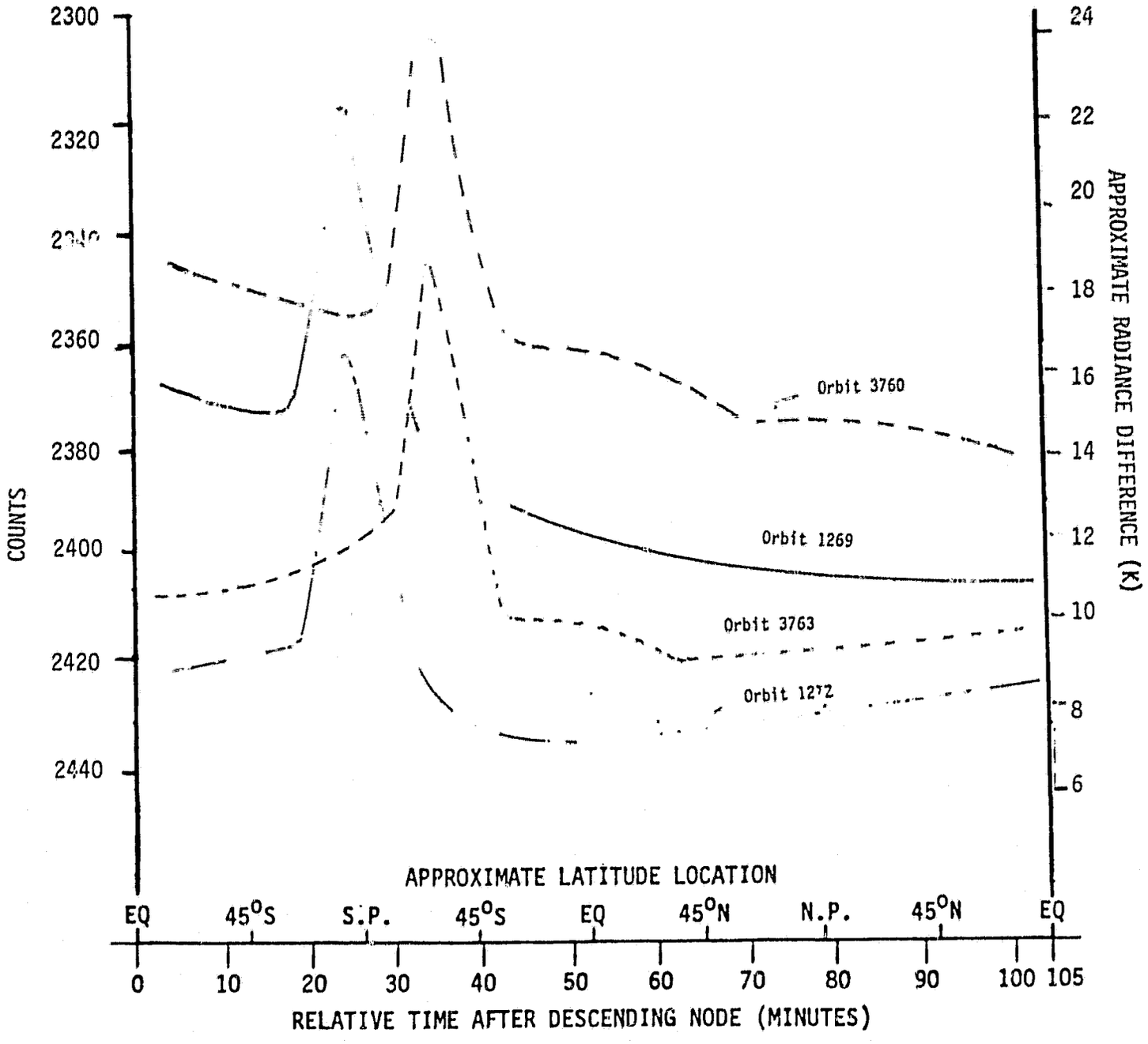

Figure 16. Comparison of 6.6 GHz (C_W-C_C) for 1st and 4th orbits after power-on for 24 January 1979 and 23 July 1979.

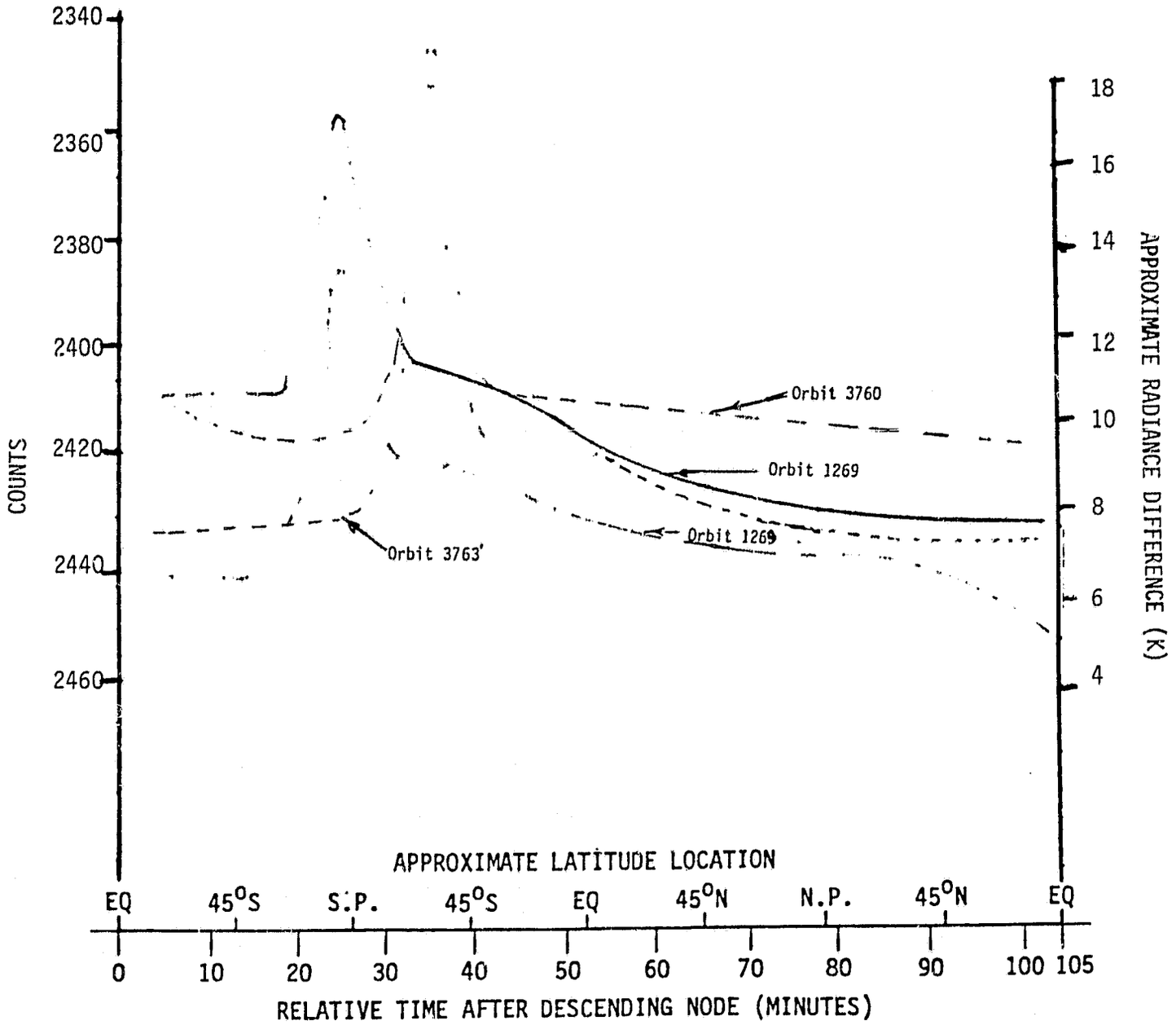

Figure 17. Comparison of 10.7 GHz (C_W-C_C) for 1st and 4th orbits after power-on for 24 January 1979 and 23 July 1979.

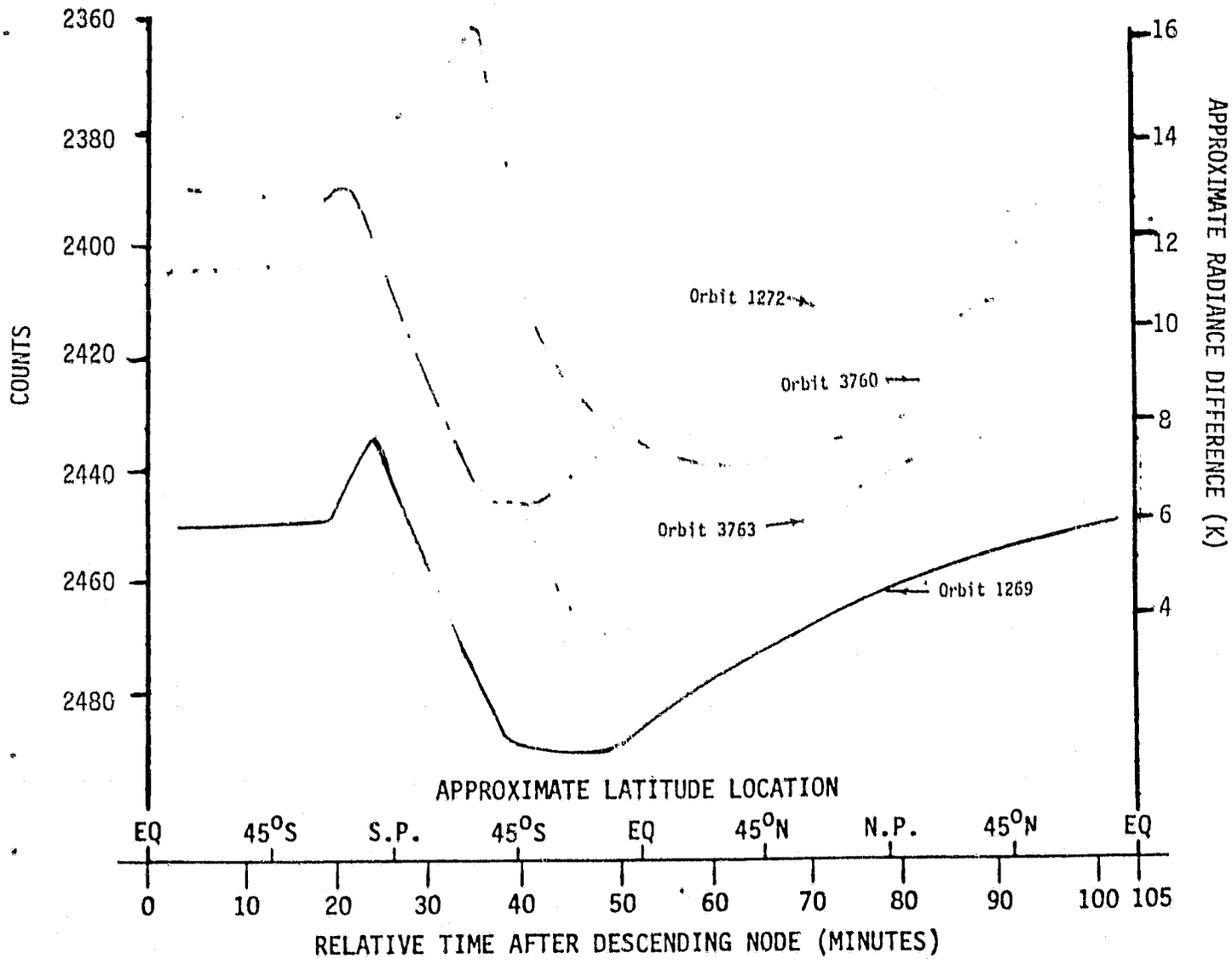

Figure 18. Comparison of 18 GHz (C_W-C_C) for 1st and 4th orbits after power-on for 24 January 1979 and 23 July 1979.

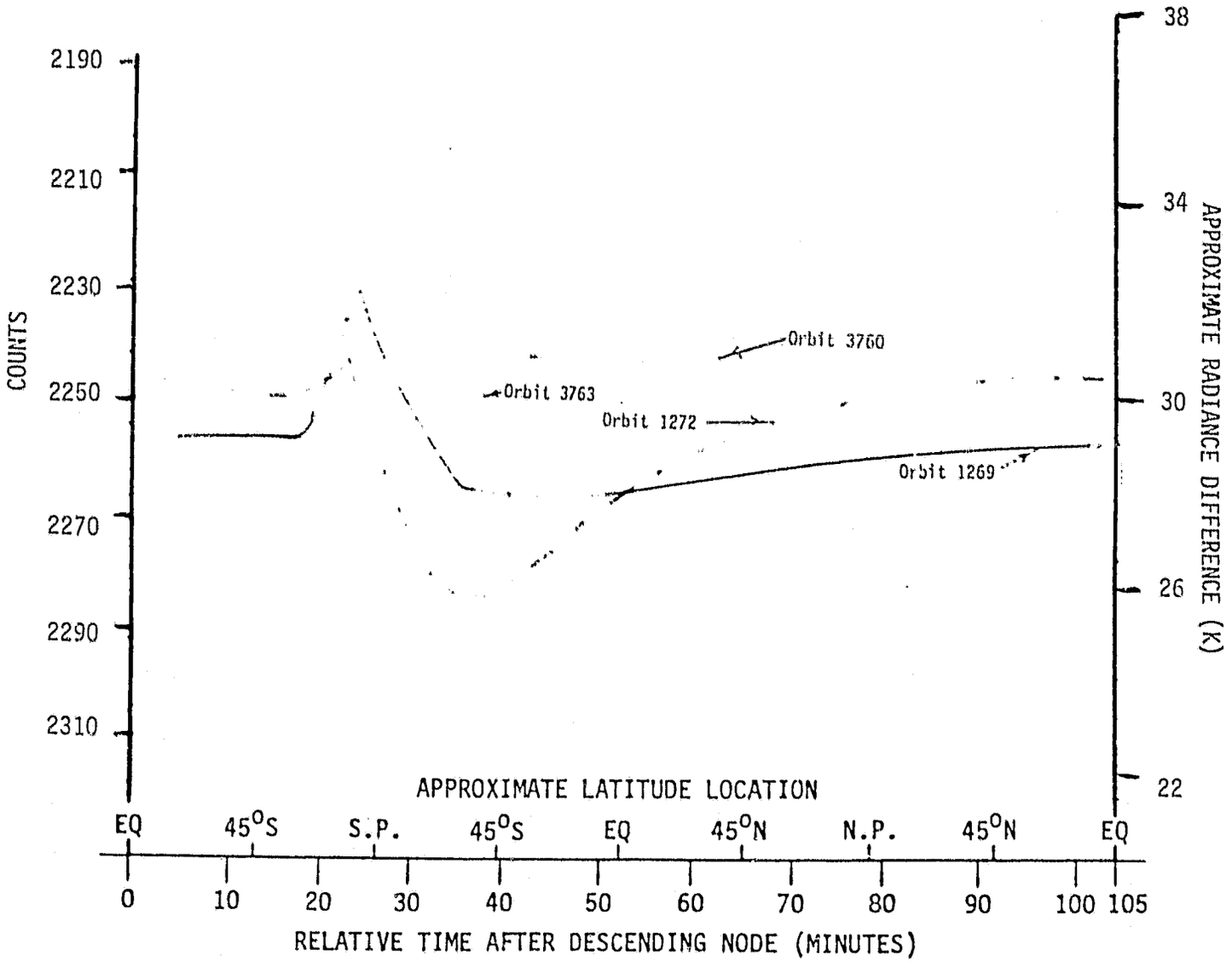

Figure 19. Comparison of 21 GHz (C_W-C_C) for 1st and 4th orbits after power-on for 24 January 1979 and 23 July 1979.

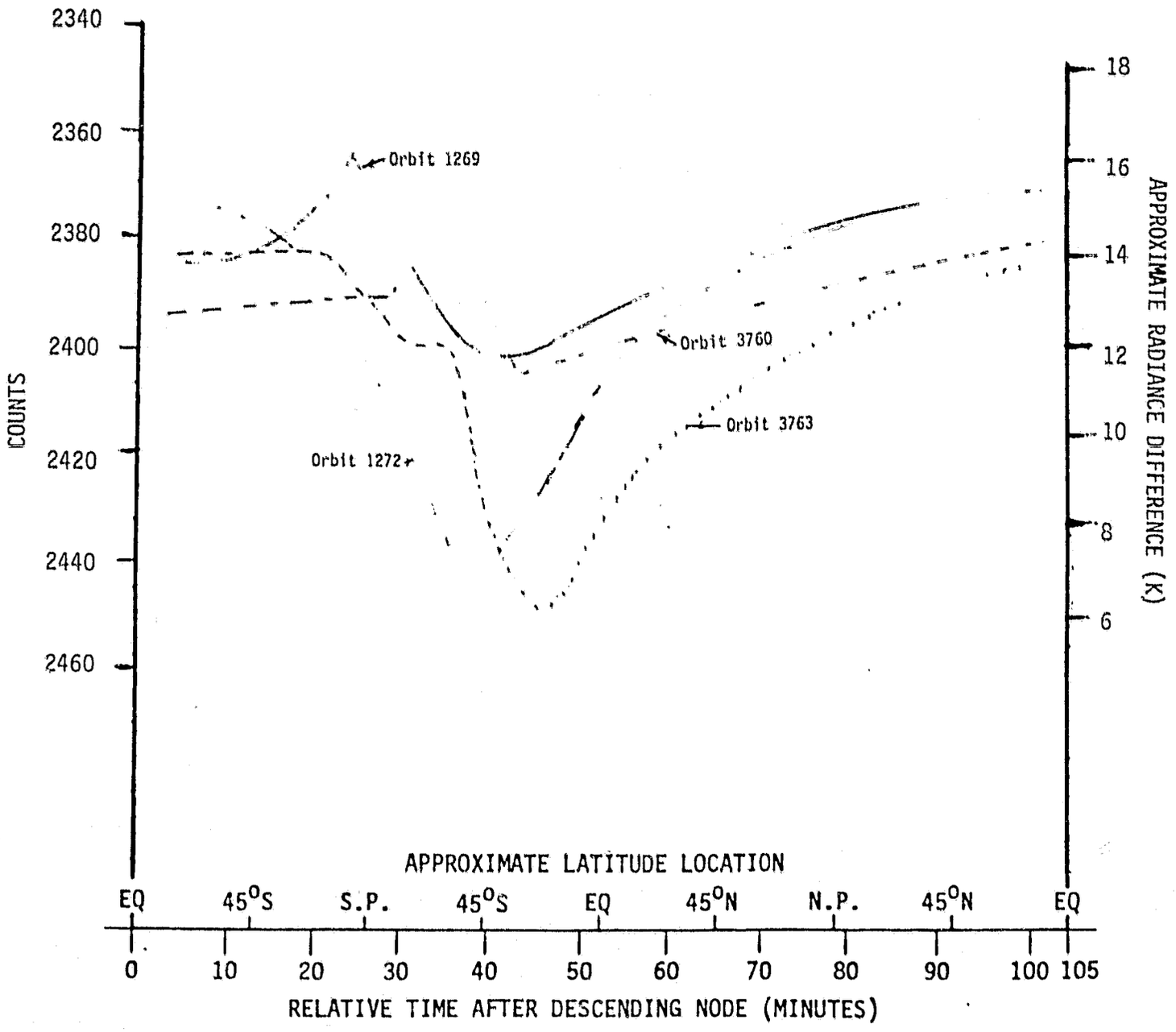

Figure 20. Comparison of 37 GHz horizontal (C_W-C_C) for 1st and 4th orbits after power-on for 24 January 1979 and 23 July 1979.

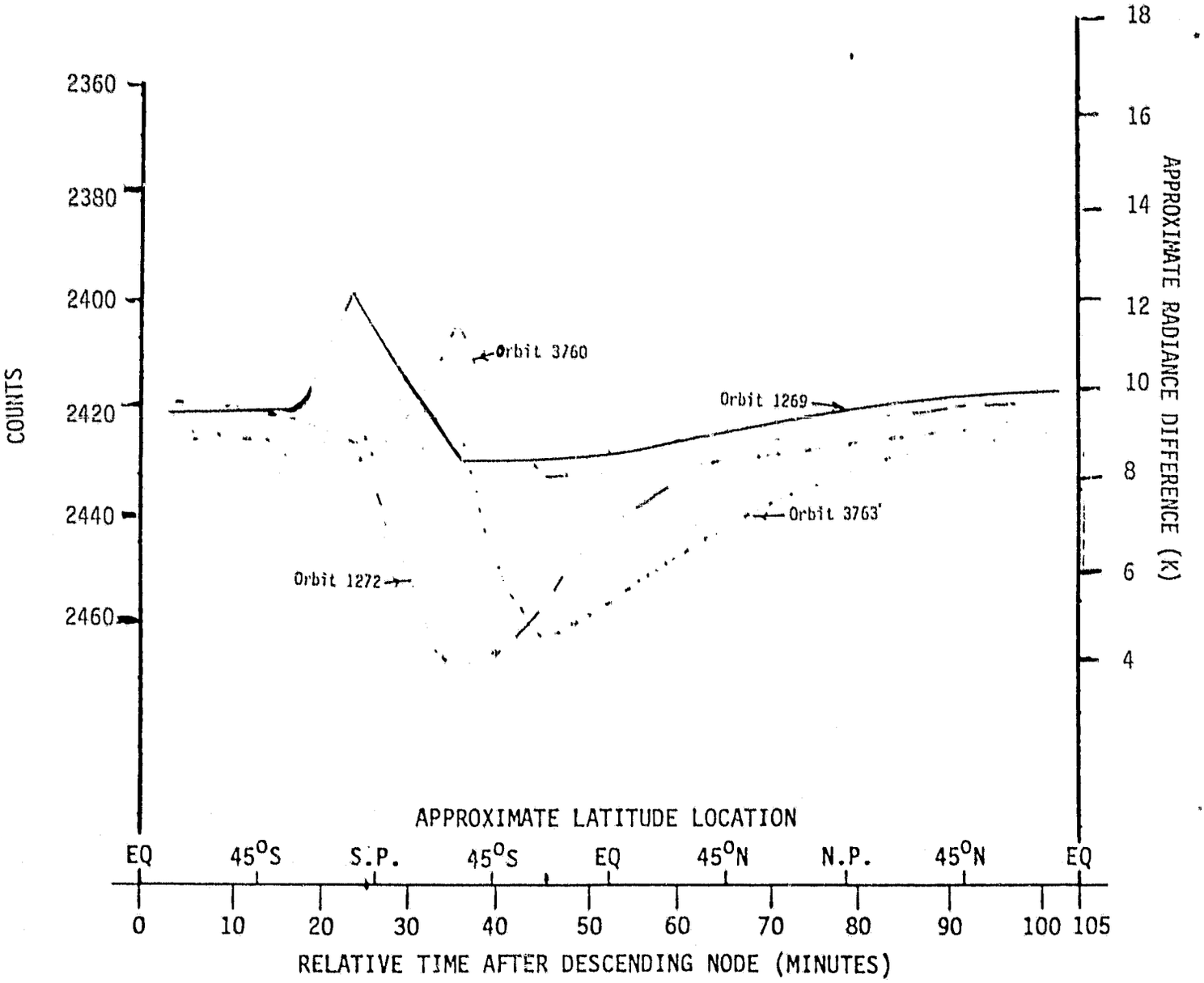

Figure 21. Comparison of 37 GHz vertical (C_W-C_C) for 1st and 4th orbits after power-on for 24 January 1979 and 23 July 1979.

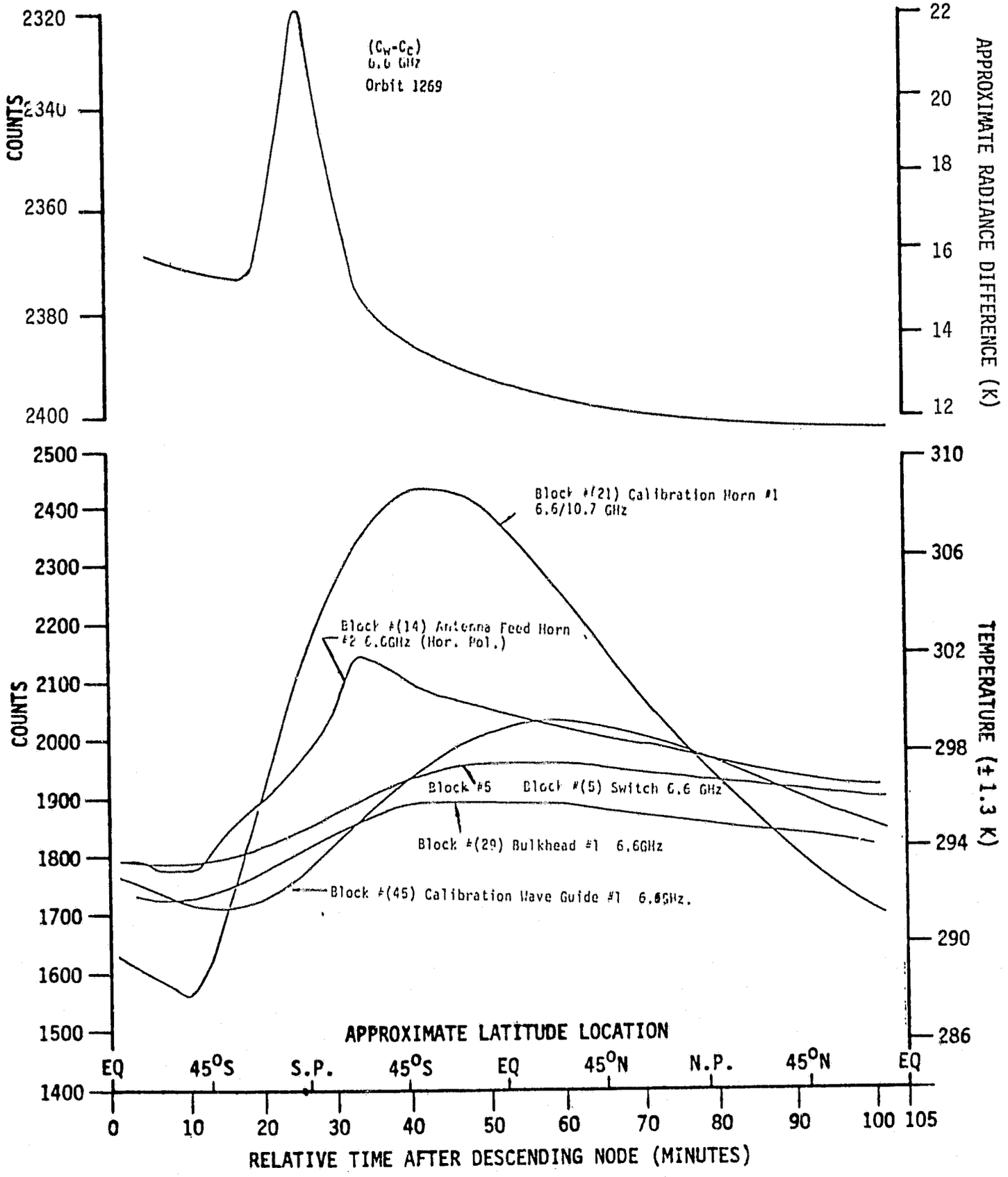

Fig. 22 SMMR 6.6 GHz horizontal polarization transmission path counts/ temperatures vs. orbit times/latitudes compared with (C_W-C_C) radiances. Orbit #1269, 24 January 1979.

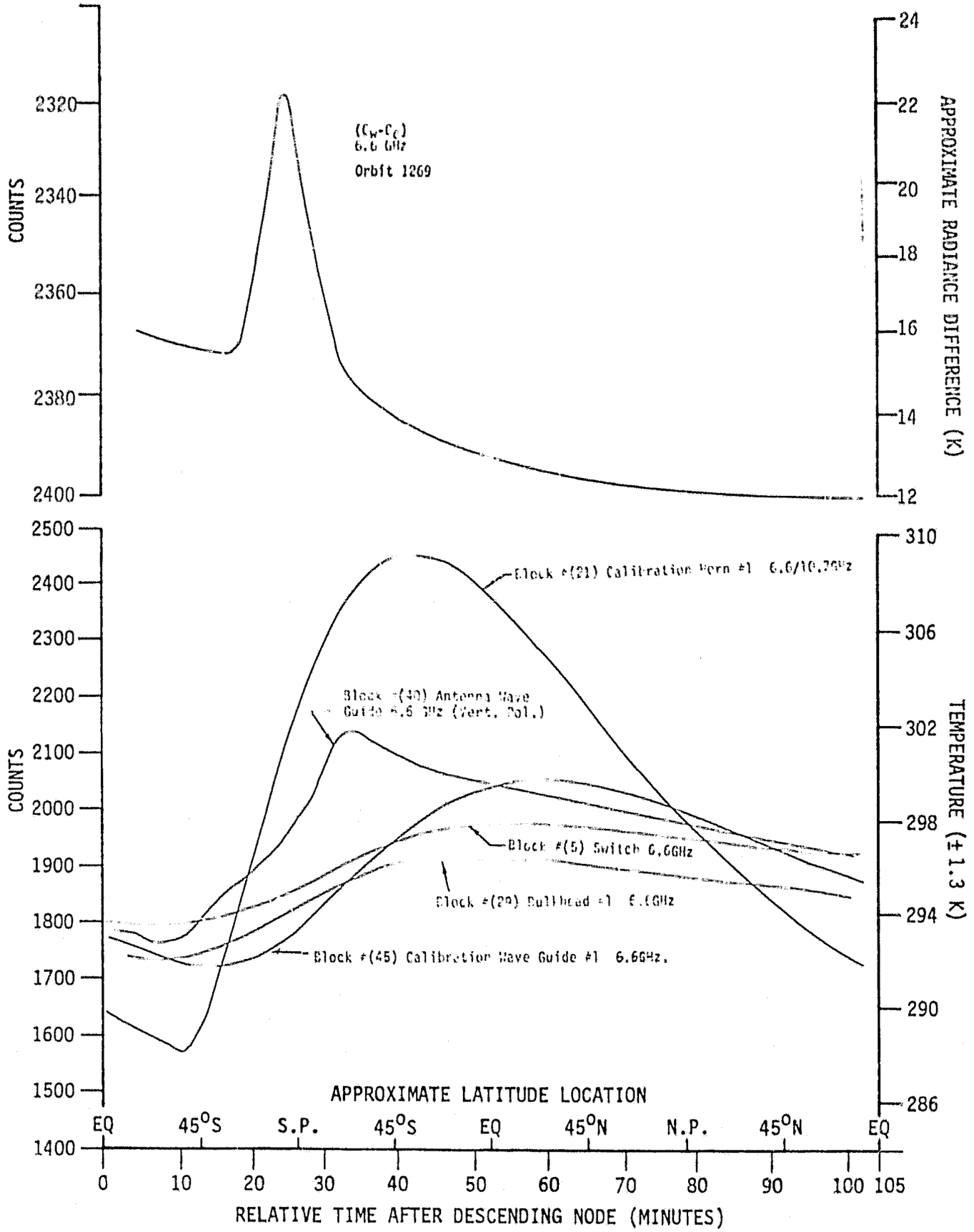

Fig. 23 SMMR 6.6 GHz vertical polarization transmission path counts/ temperatures vs. orbit times/latitudes compared with (C_W-C_C) radiances. Orbit #1269, 24 January 1979.

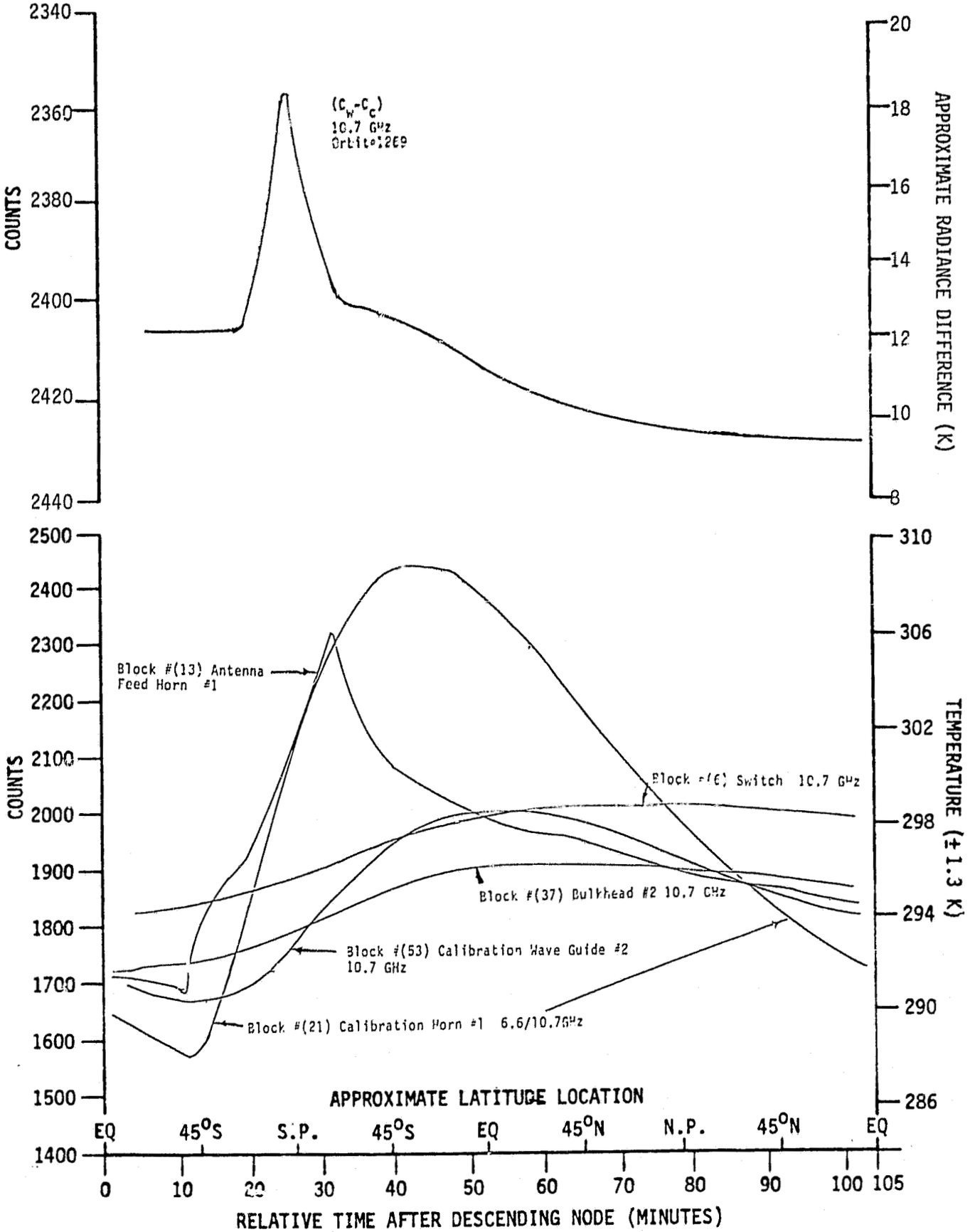

Fig. 24 SMMR 10.7 GHz polarization transmission path counts/temperatures vs. orbit times/latitudes compared with (C_W-C_C) radiances. Orbit #1269, 24 January 1979.

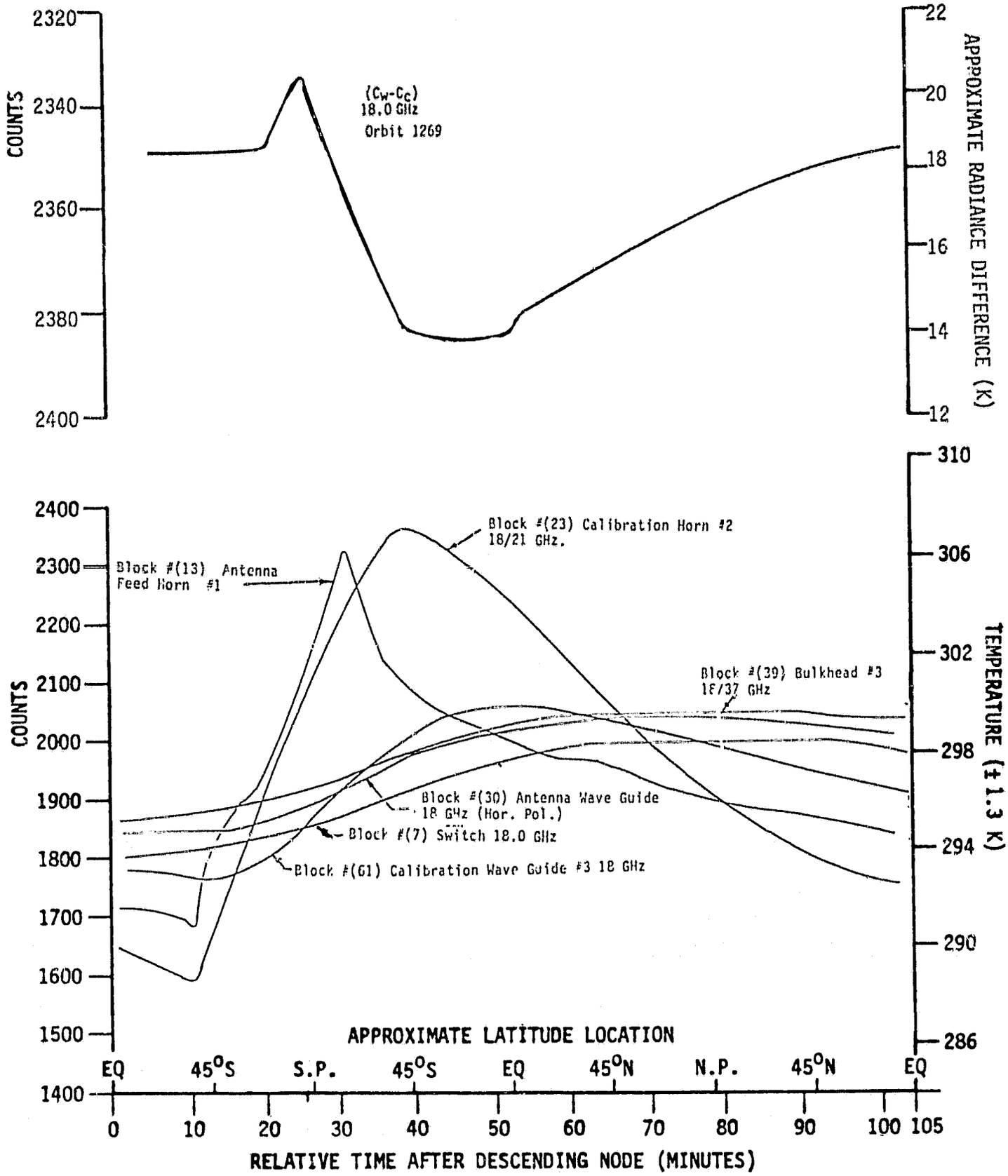

Fig. 25 SMMR 18 GHz horizontal polarization transmission path counts/ temperatures vs. orbit times/latitudes compared with (C_W-C_C) radiances. Orbit #1269, 24 January 1979.

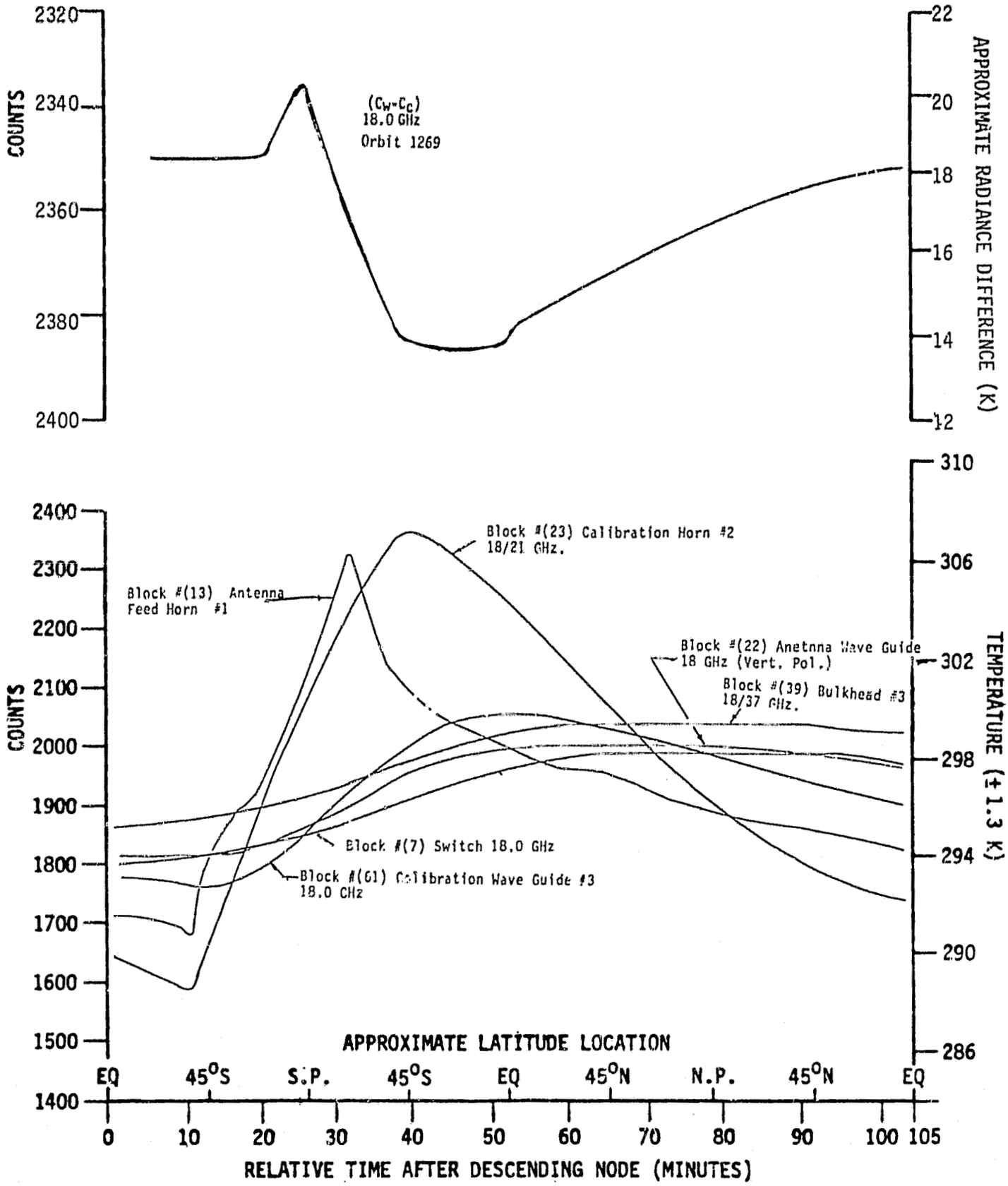

Fig. 26 SMMR 18 GHz vertical polarization transmission path counts/ temperatures vs. orbit times/latitudes compared with (C_W-C_C) radiances. Orbit #1269, 24 January 1979.

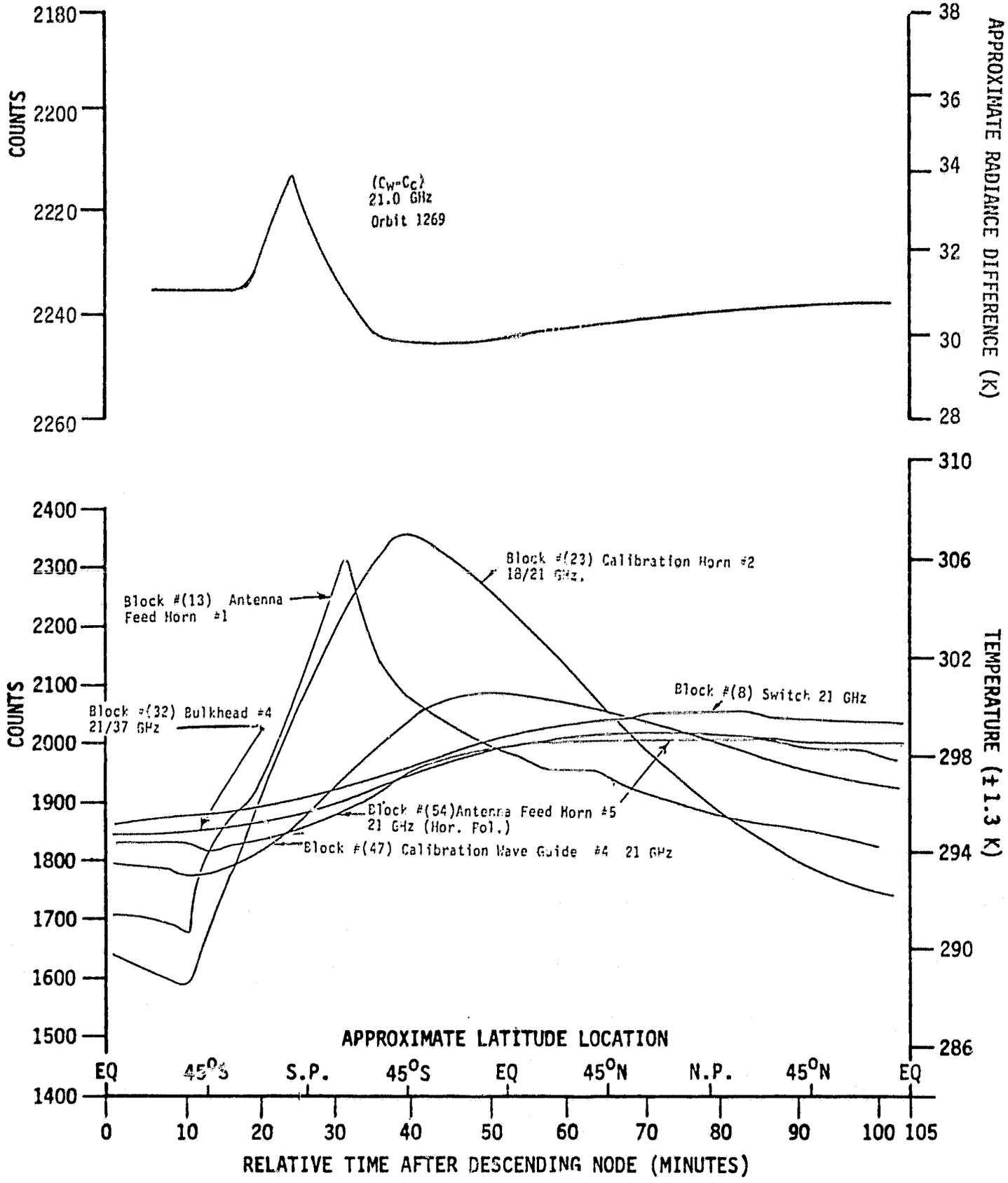

Fig. 27 SMMR 21 GHz horizontal polarization transmission path counts/ temperatures vs. orbit times/latitudes compared with (C_W-C_C) radiances. Orbit #1269, 24 January 1979.

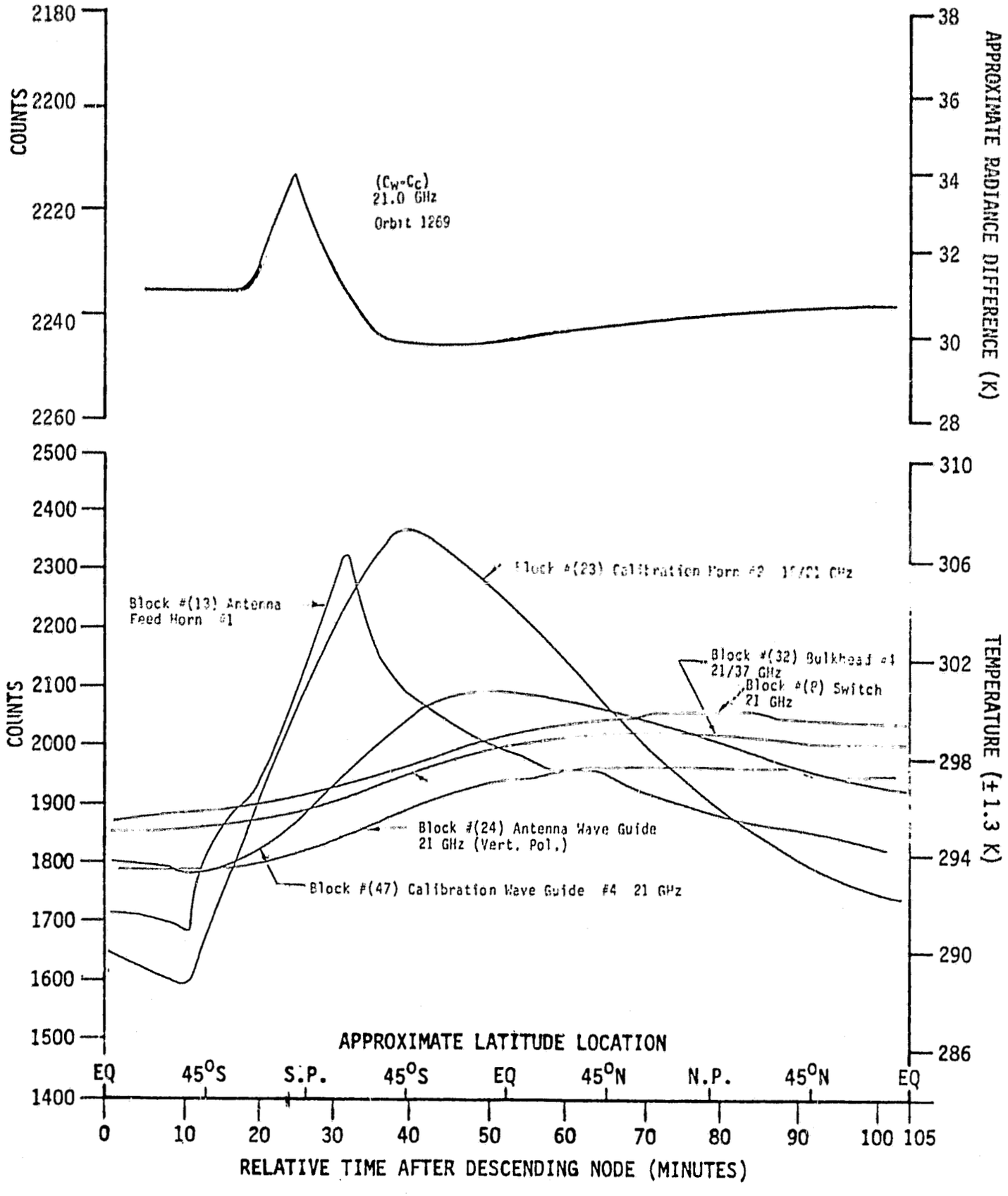

Fig. 28 SMMR 21 GHz vertical polarization transmission path counts/ temperatures vs. orbit times/latitudes compared with (Cw-Cc) radiances. Orbit #1269, 24 January 1979.

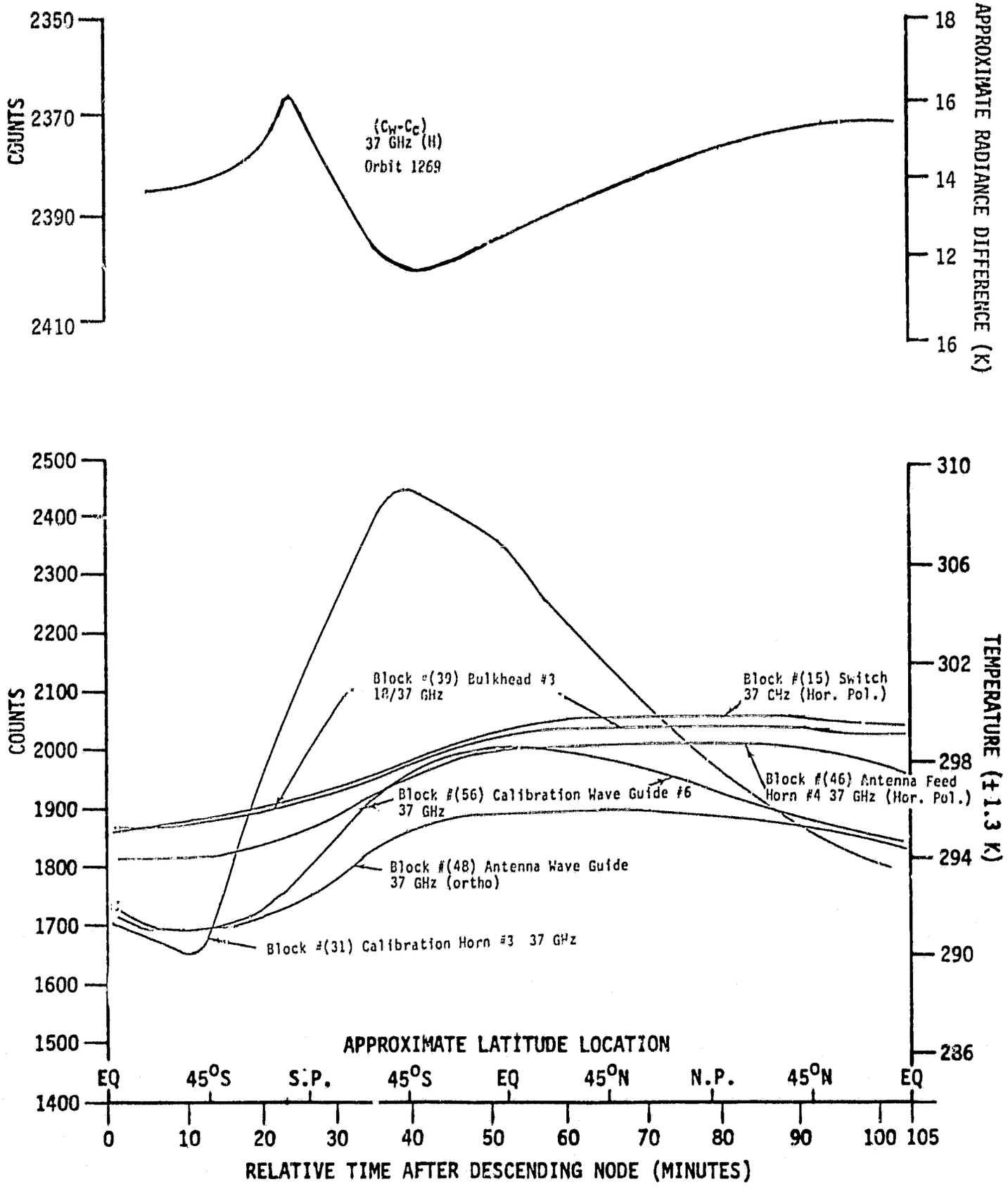

Fig. 29 SMMR 37 GHz horizontal polarization transmission path counts/ temperatures vs. orbit times/latitudes compared with (C_W-C_C) radiances. Orbit #1269, 24 January 1979.

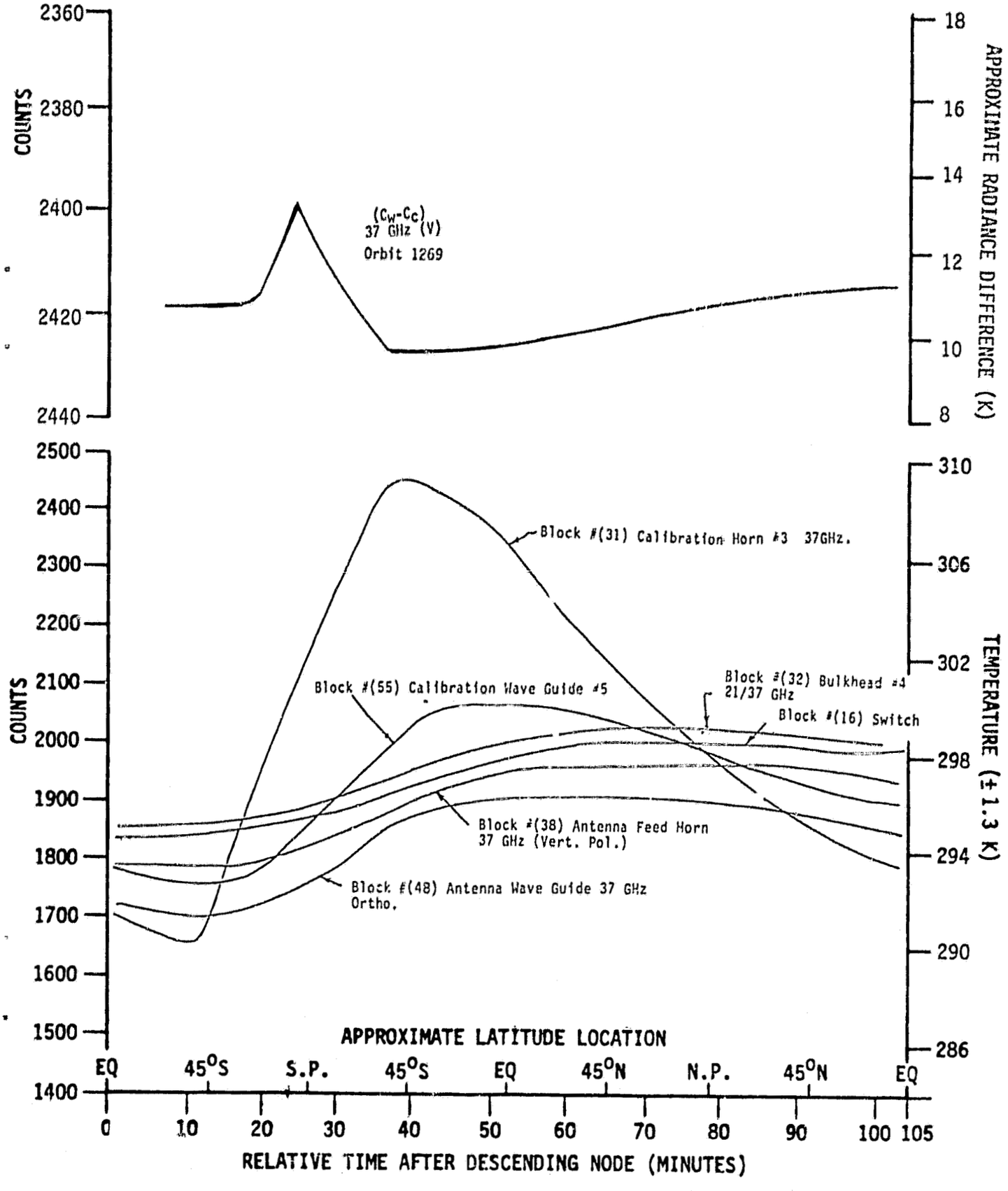

Fig. 30 SMMR 37 GHz vertical polarization transmission path counts/ temperatures vs. orbit times/latitudes compared with (C_W-C_C) radiances. Orbit #1269, 24 January 1979.

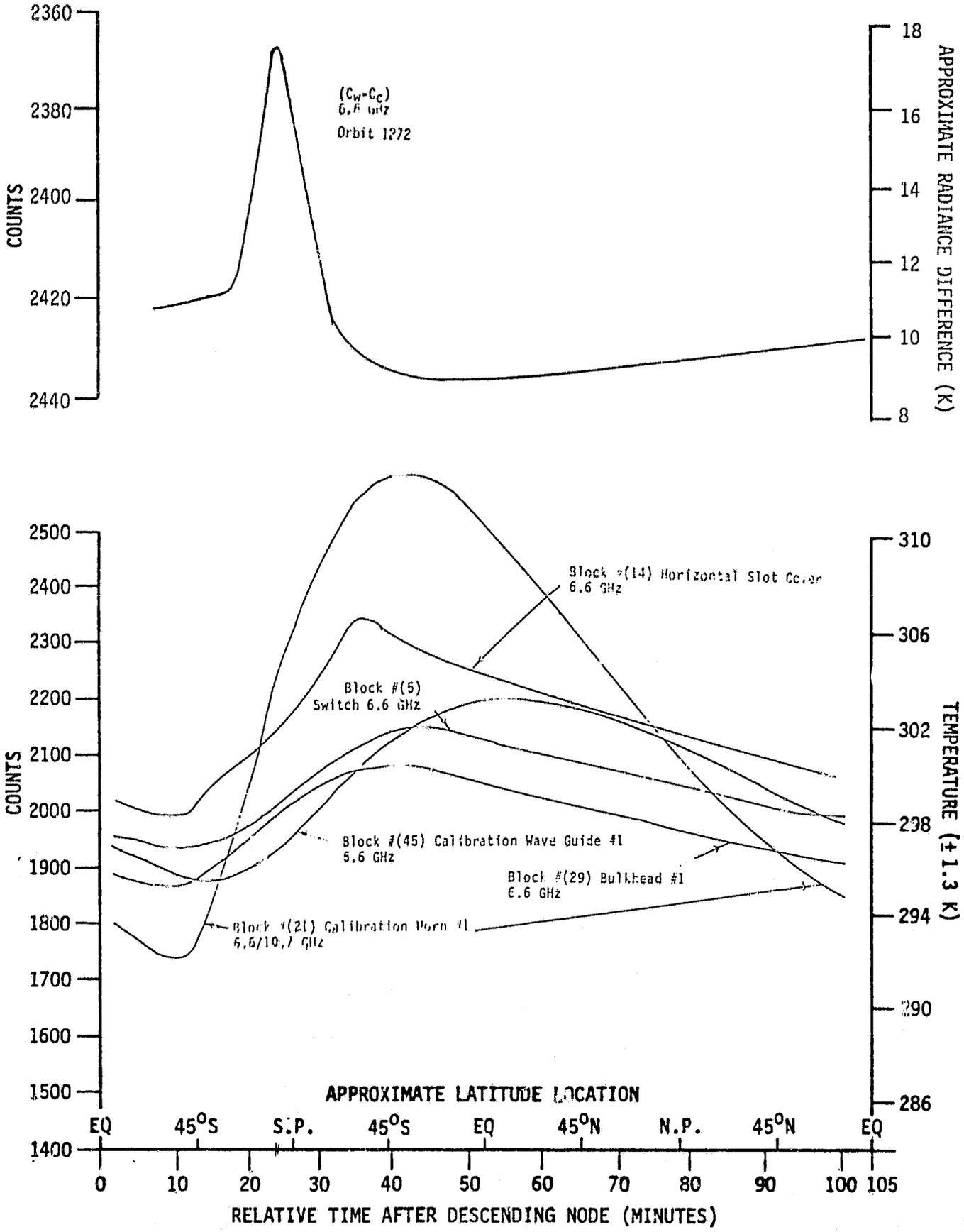

Fig. 31 SMMR 6.6 GHz horizontal polarization transmission path counts/ temperatures vs. orbit times/latitudes compared with (C_W-C_C) radiances. Orbit #1272, 24 January 1979.

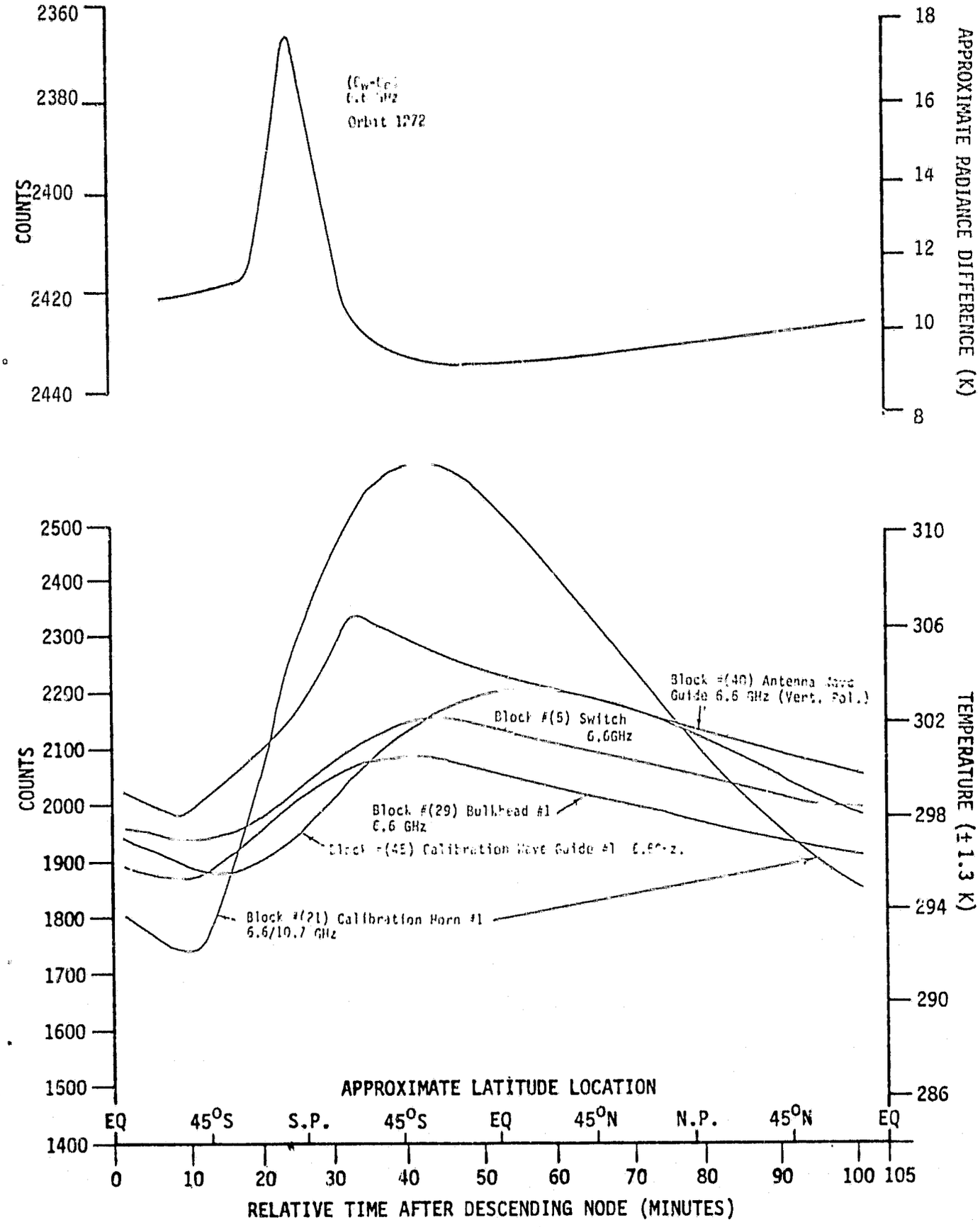

Fig. 32 SMMR 6.6 GHz vertical polarization transmission path counts/ temperatures vs. orbit times/latitudes compared with (C_W-C_C) radiances. Orbit #1272, 24 January 1979.

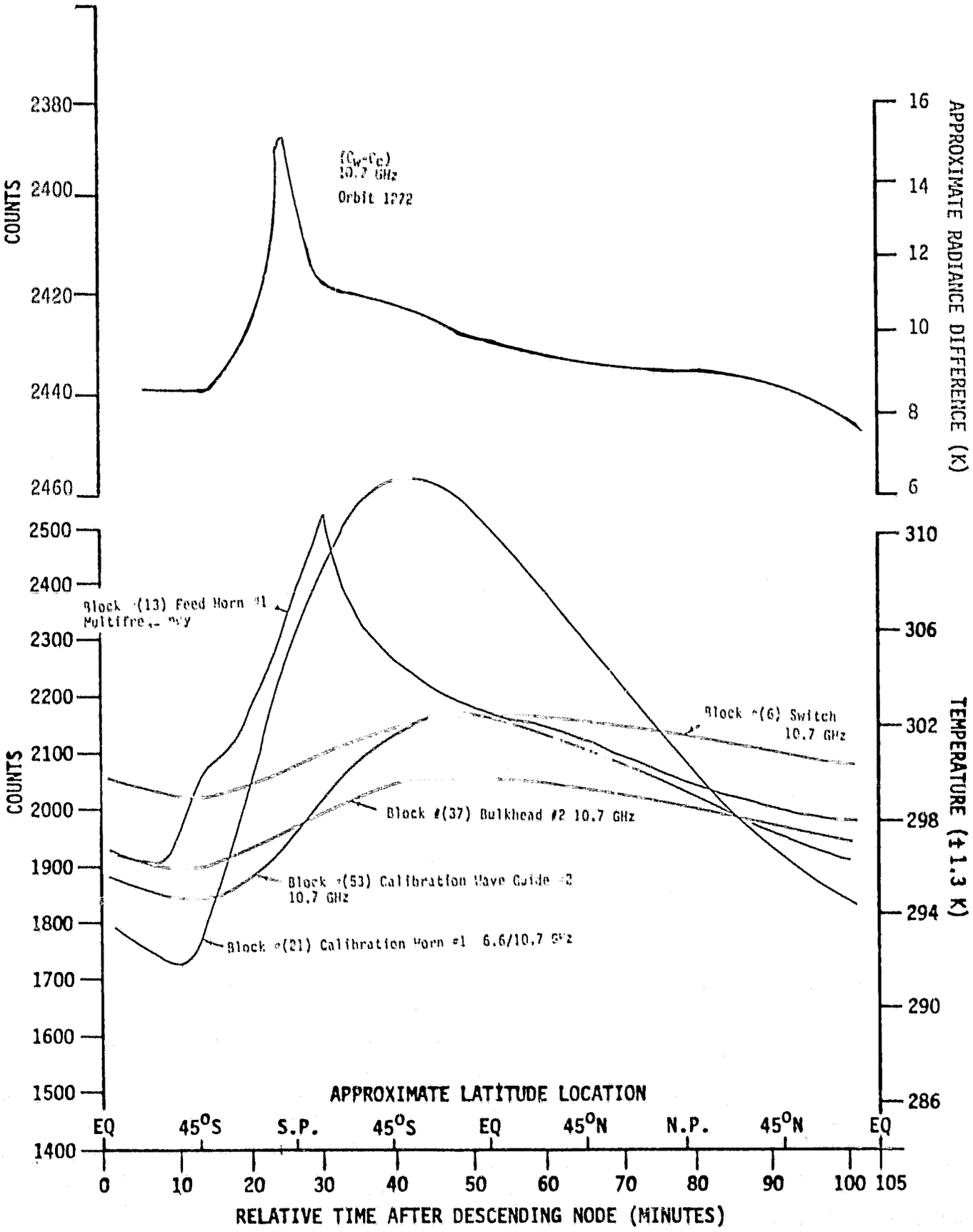

Fig. 3? SMMR 10.7 GHz polarization transmission path counts/temperatures vs. orbit times/latitudes compared with (C_W-C_C) radiances. Orbit #1272, 24 January 1979.

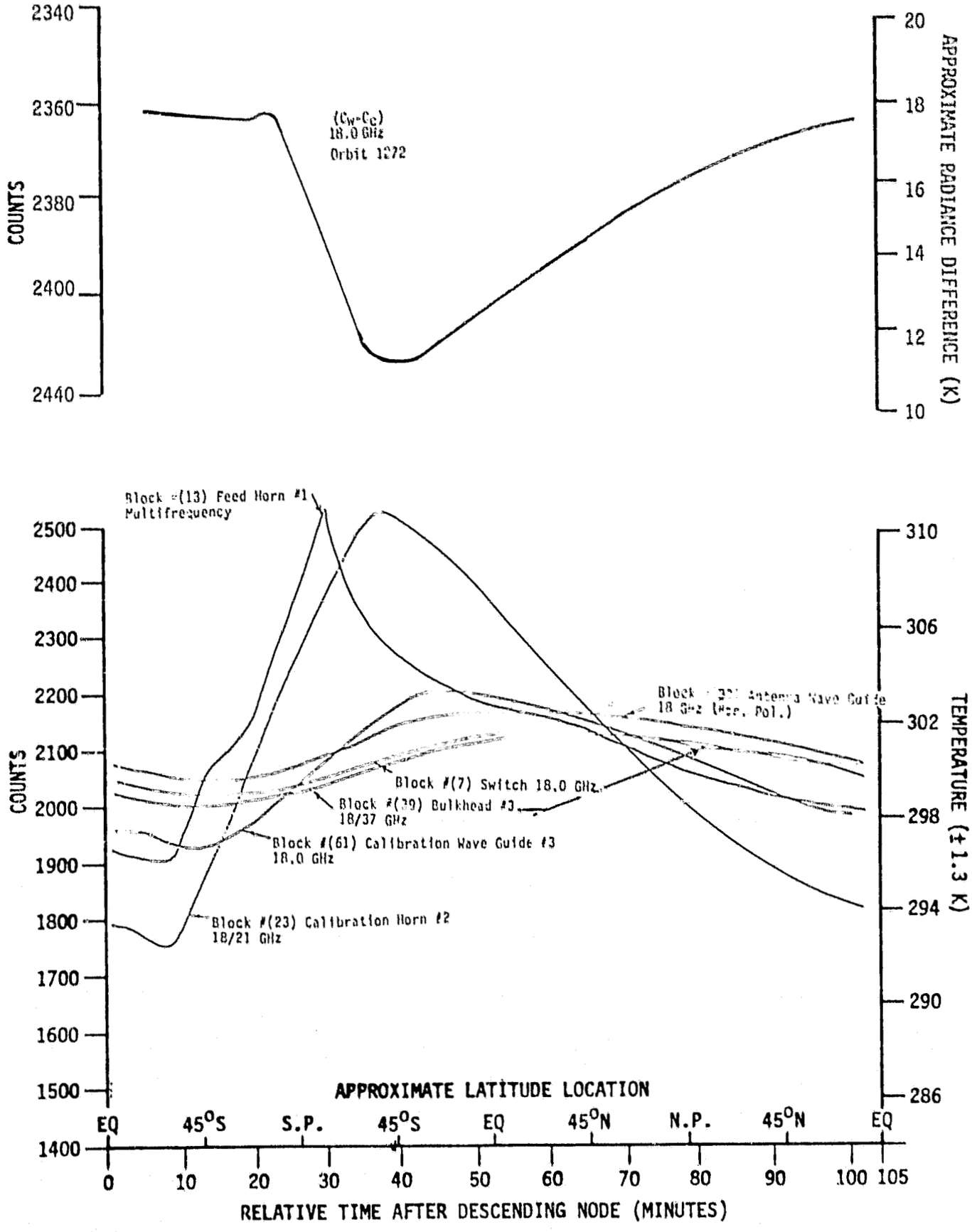

Fig. 34 SMMR 18 GHz horizontal polarization transmission path counts/ temperatures vs. orbit times/latitudes compared with (C_W-C_C) radiances. Orbit #1272, 24 January 1979.

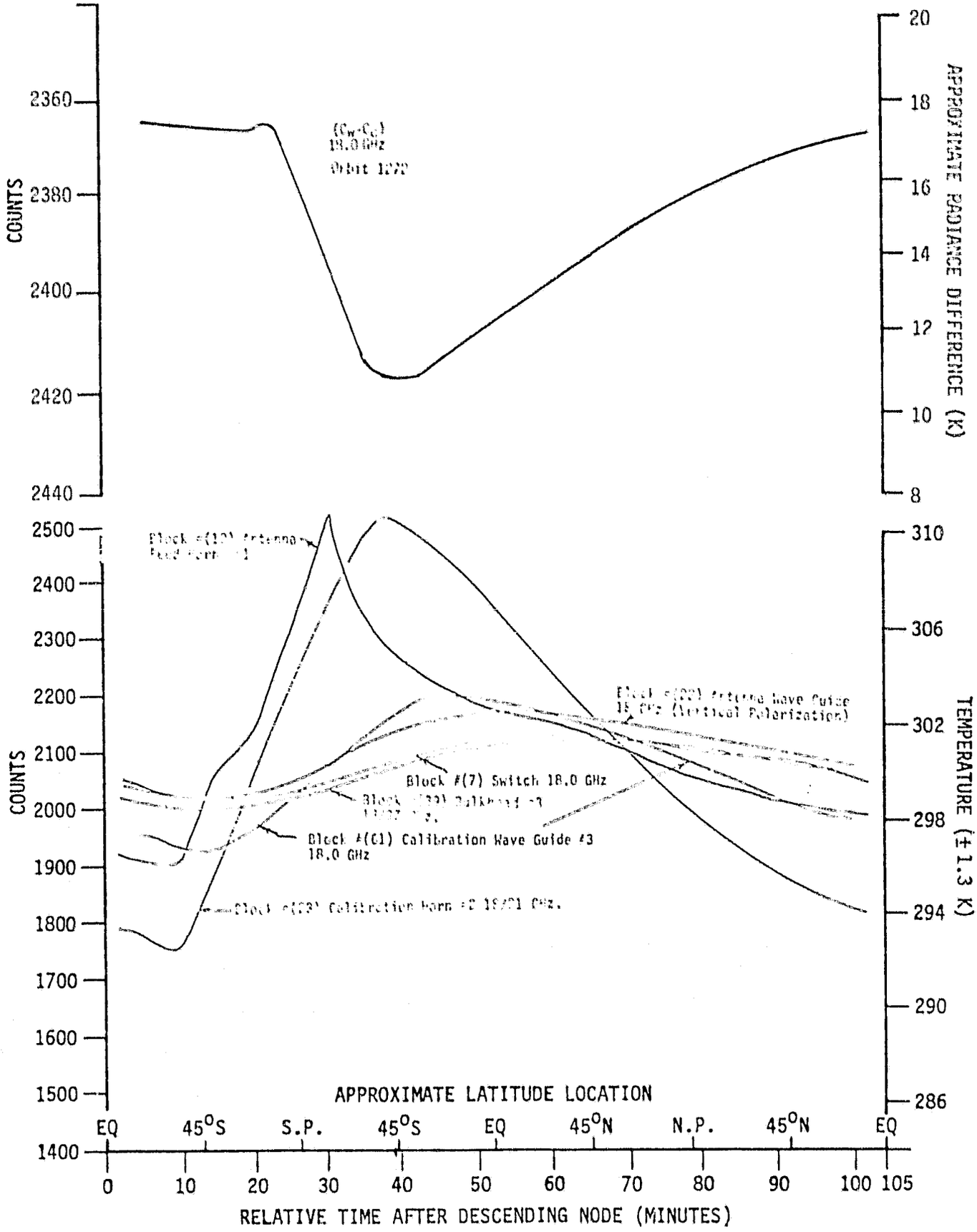

Fig. 35 SMMR 18 GHz vertical polarization transmission path counts/ temperatures vs. orbit times/latitudes compared with (C_W-C_C) radiances. Orbit #1272, 24 January 1979.

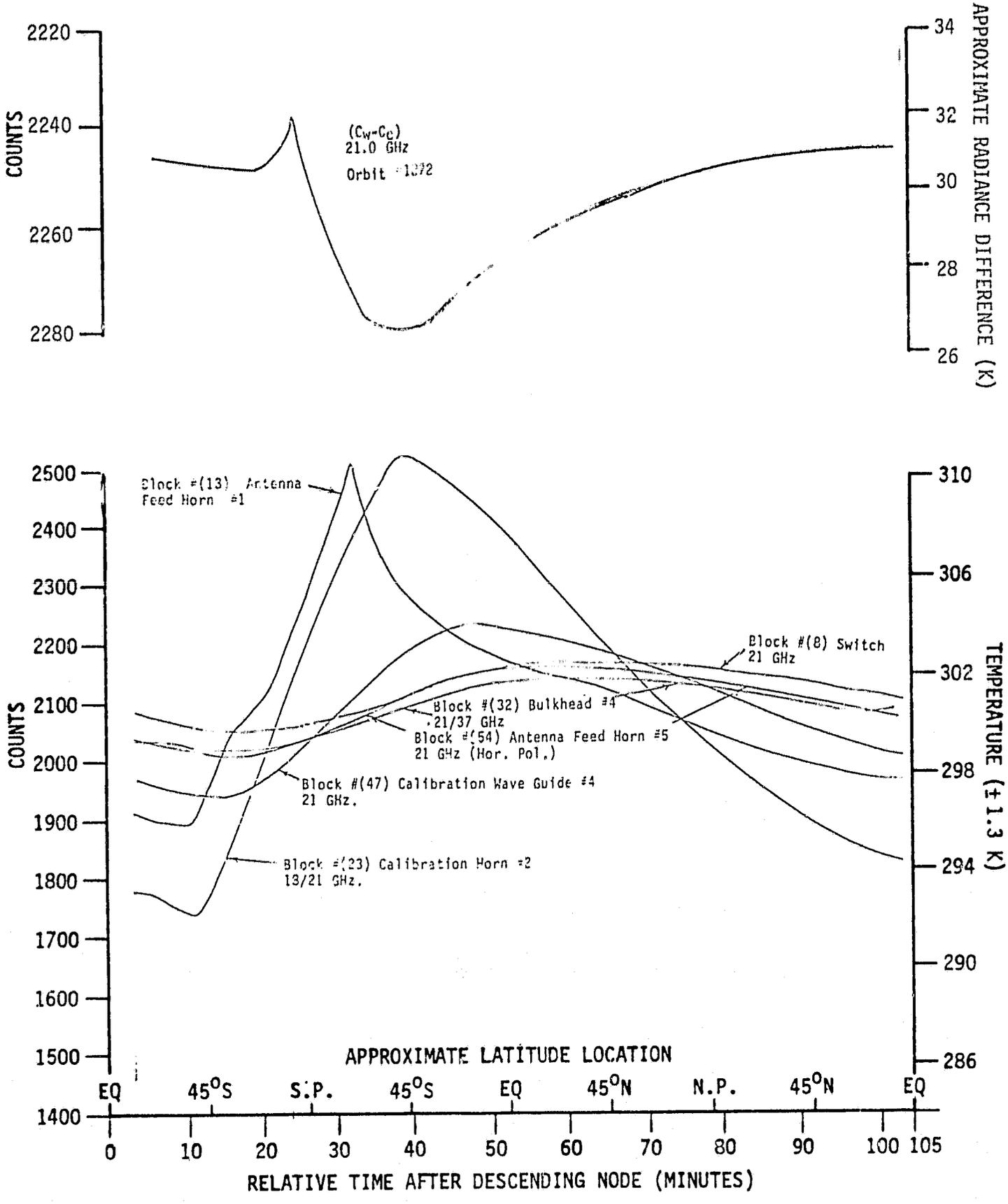

Fig. 36 SMMR 21 GHz horizontal polarization transmission path counts/ temperatures vs. orbit times/latitudes compared with (C_w-C_c) radiances. Orbit #1272, 24 January 1979.

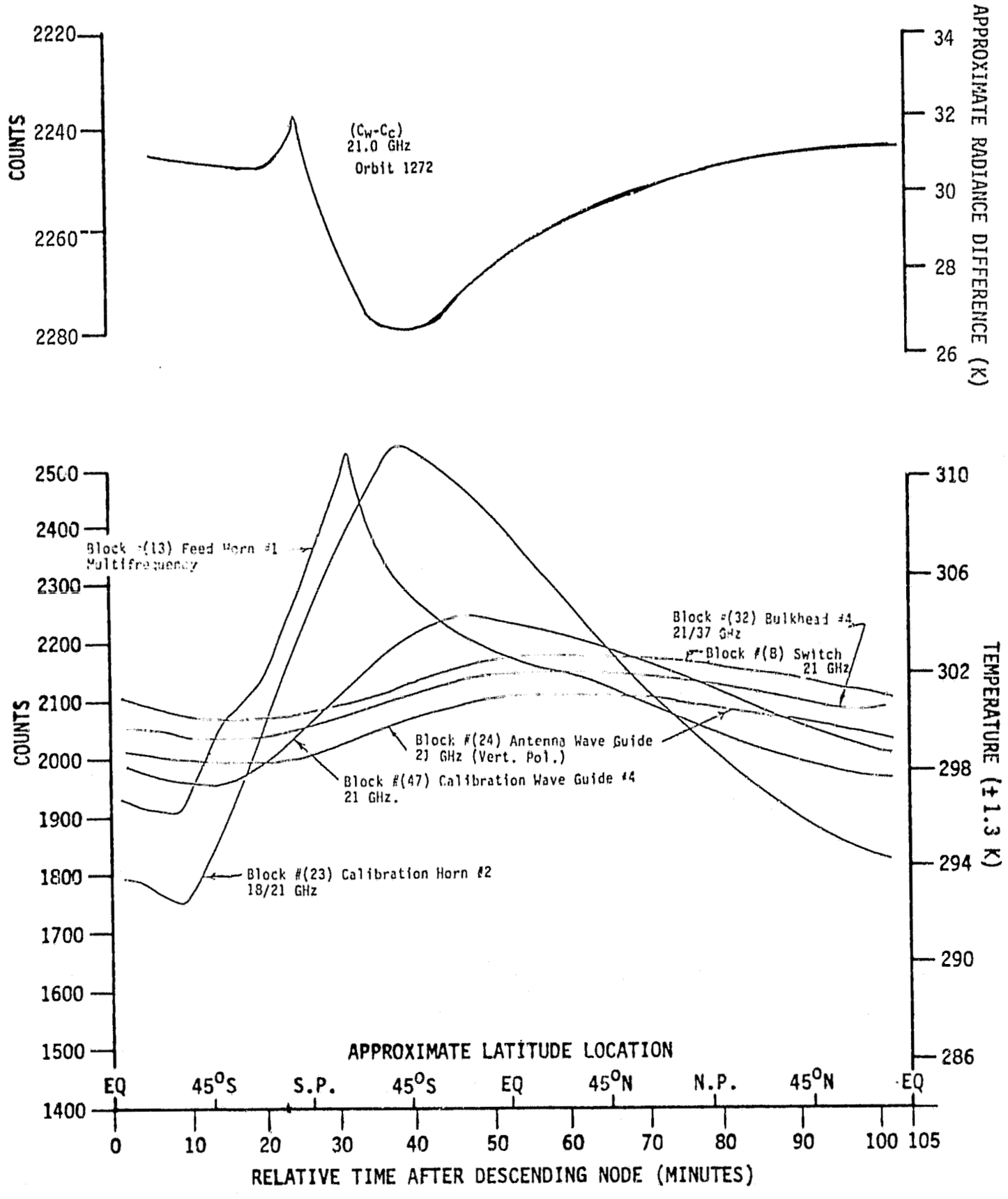

Fig. 37 SMMR 21 GHz vertical polarization transmission path counts/ temperatures vs. orbit times/latitudes compared with (C_W-C_C) radiances. Orbit #1272, 24 January 1979.

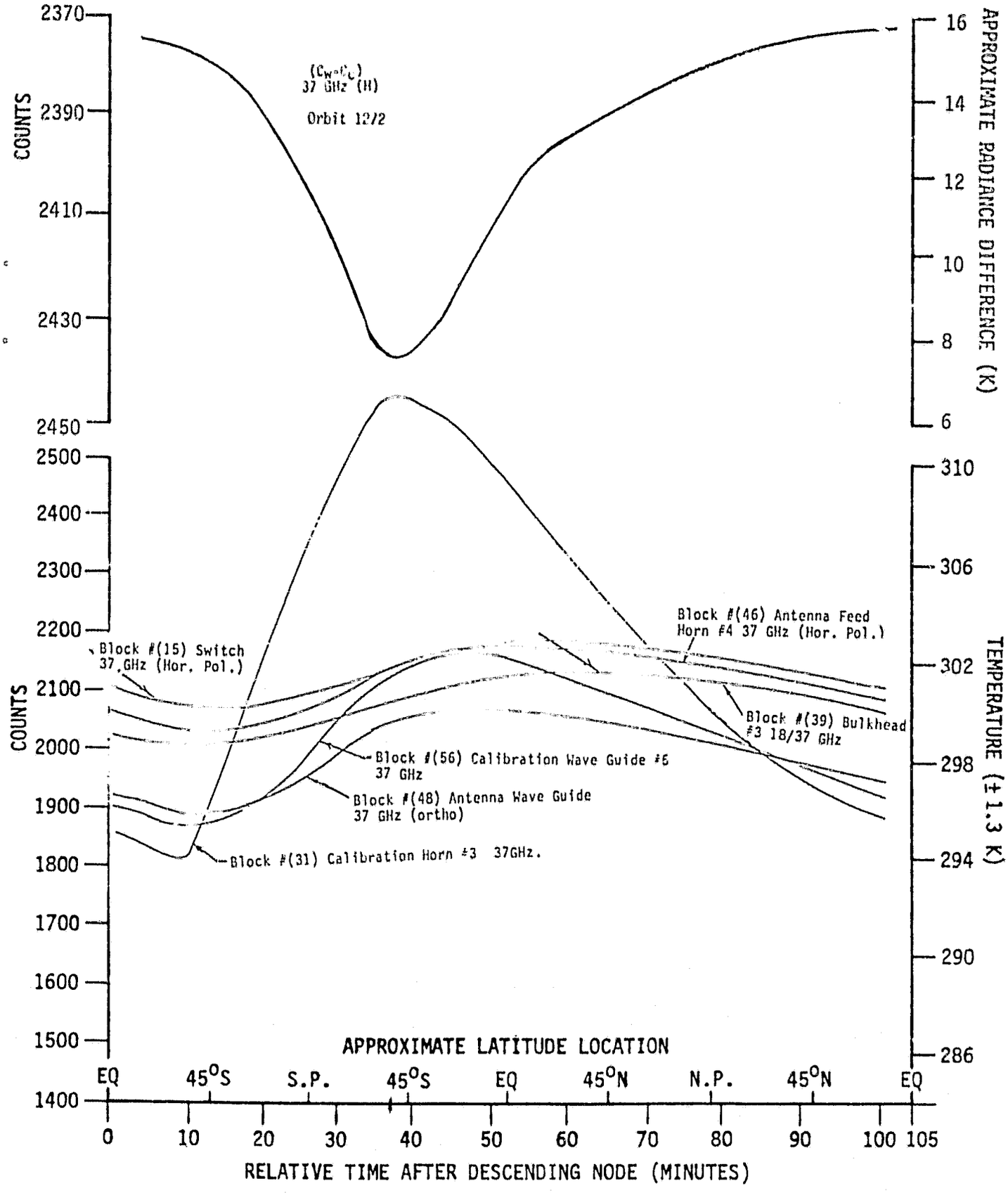

Fig. 38 SMMR 37 GHz horizontal polarization transmission path counts/ temperatures vs. orbit times/latitudes compared with (C_W-C_C) radiances. Orbit #1269, 24 January 1979.

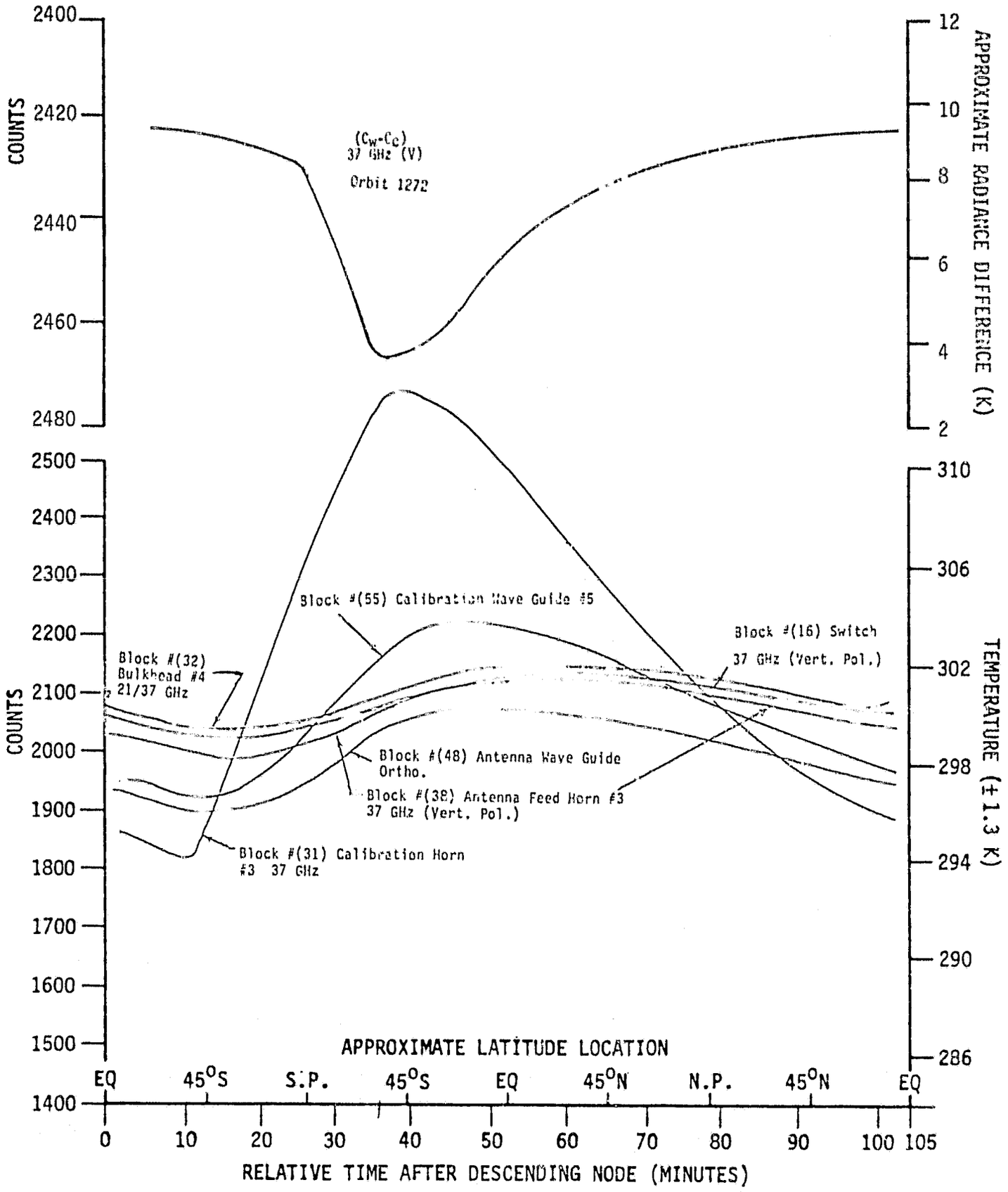

Fig. 39 SMMR 37 GHz vertical polarization transmission path counts/ temperatures vs. orbit times/latitudes compared with (C_W-C_C) radiances. Orbit #1269, 24 January 1979.

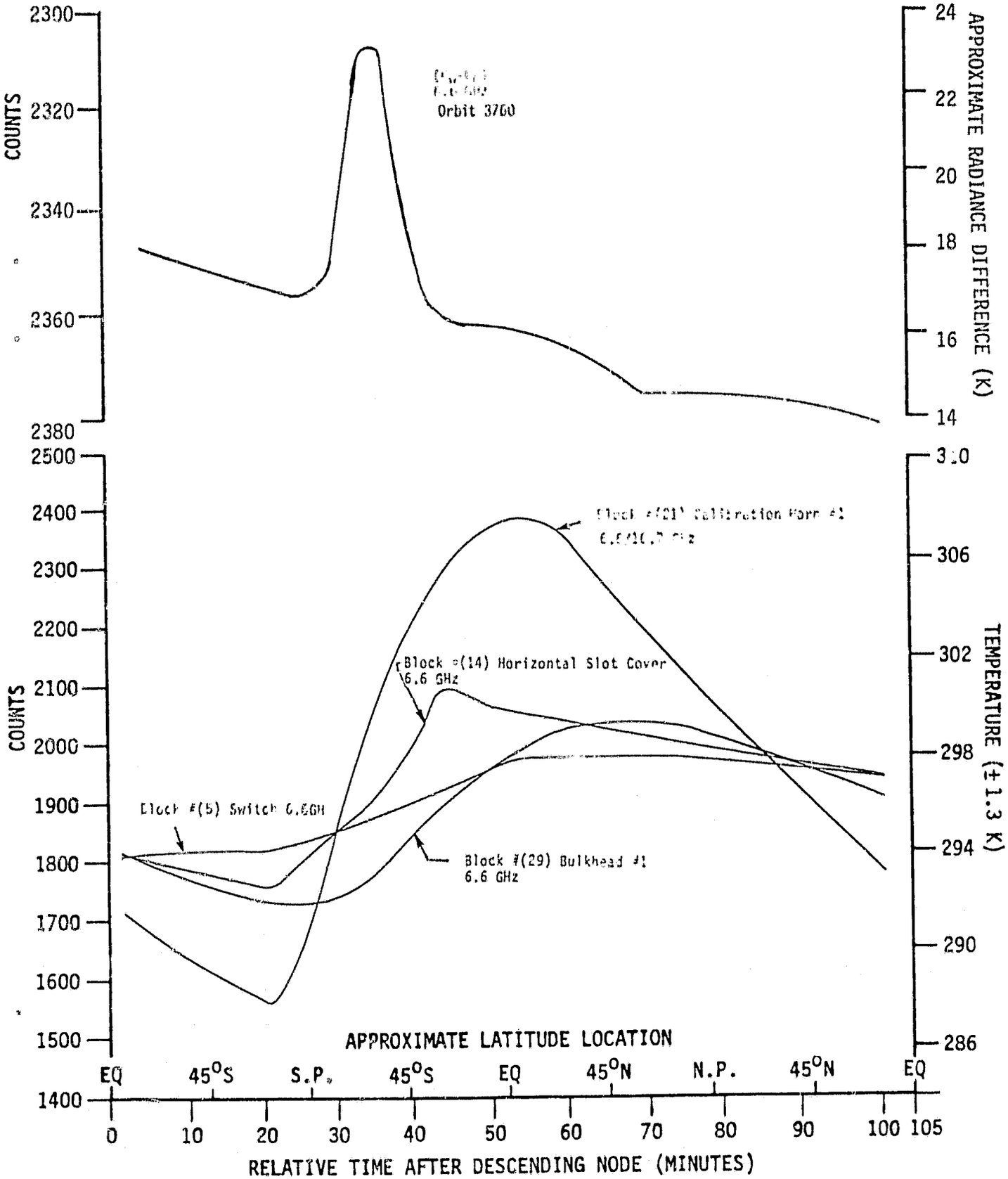

Fig. 40 SMMR 6.6 GHz horizontal polarization transmission path counts/ temperatures vs. orbit times/latitudes compared with (C_W-C_C) radiances. Orbit #3760, 23 July 1979.

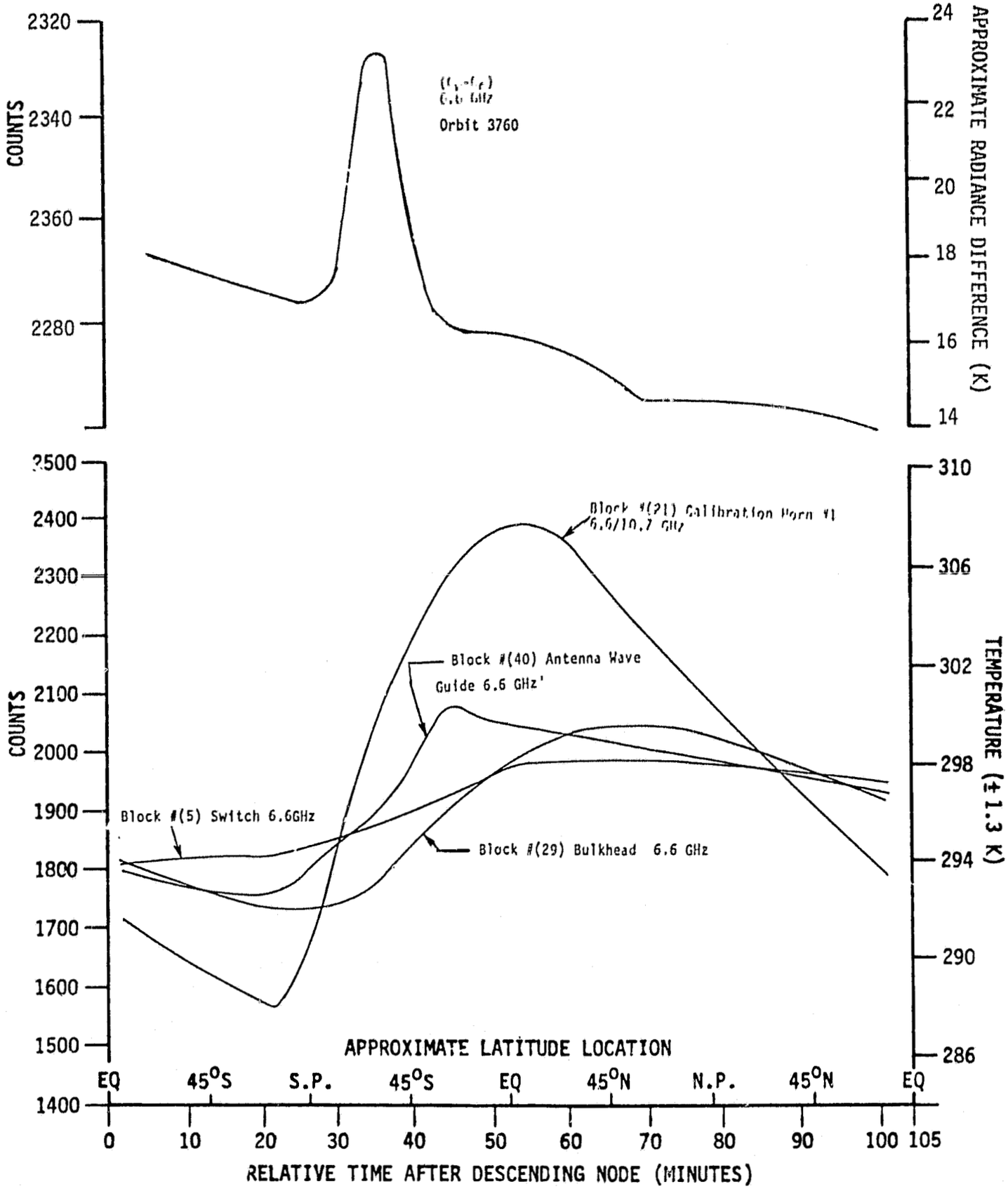

Fig. 41 SMMR 6.6 GHz vertical polarization transmission path counts/ temperatures vs. orbit times/latitudes compared with (C_W-C_C) radiances. Orbit #3760, 23 July 1979.

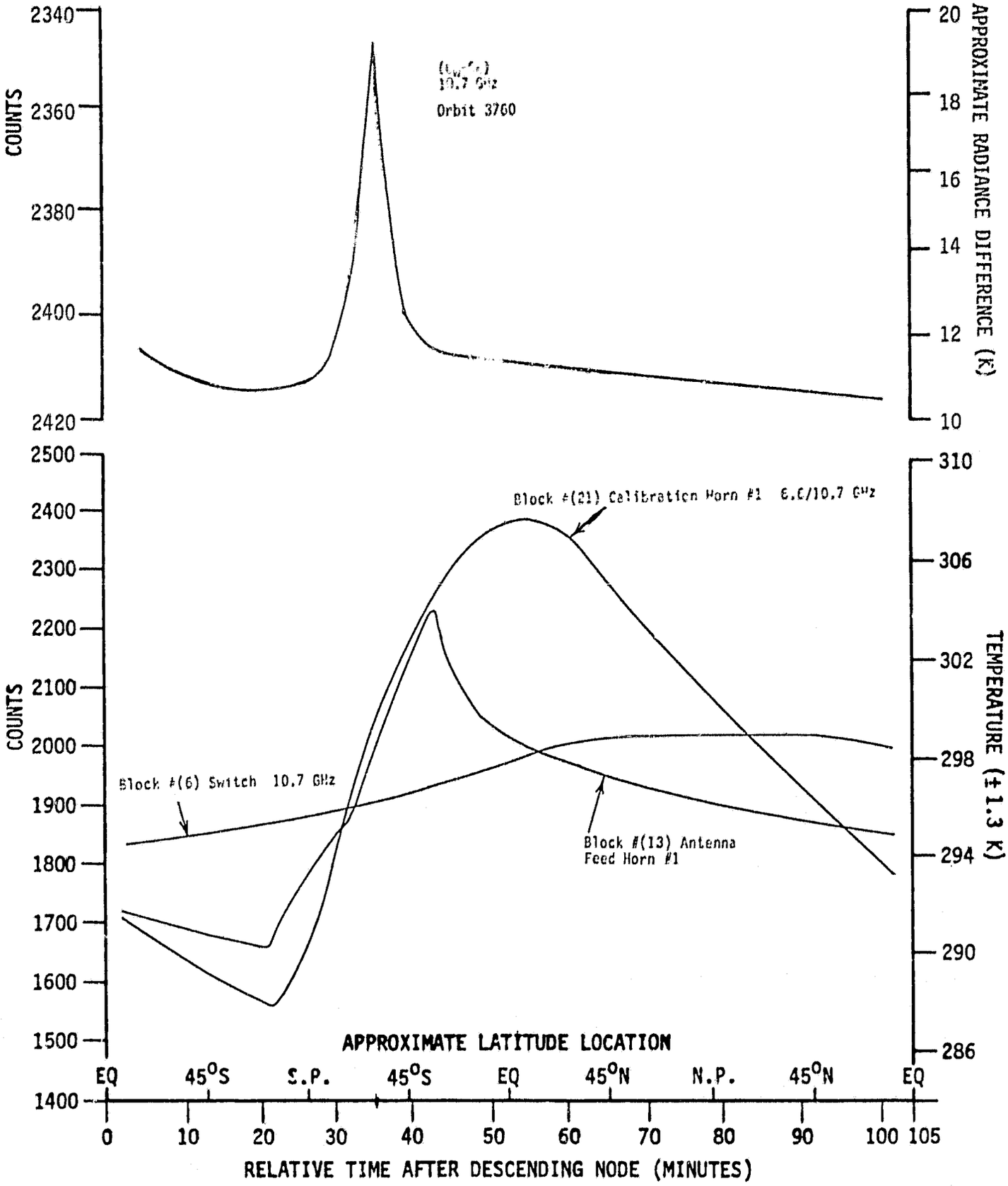

Fig. 42 SMMR 10.7 GHz polarization transmission path counts/temperatures vs. orbit times/latitudes compared with (C_W-C_C) radiances. Orbit #3760, 23 July 1979.

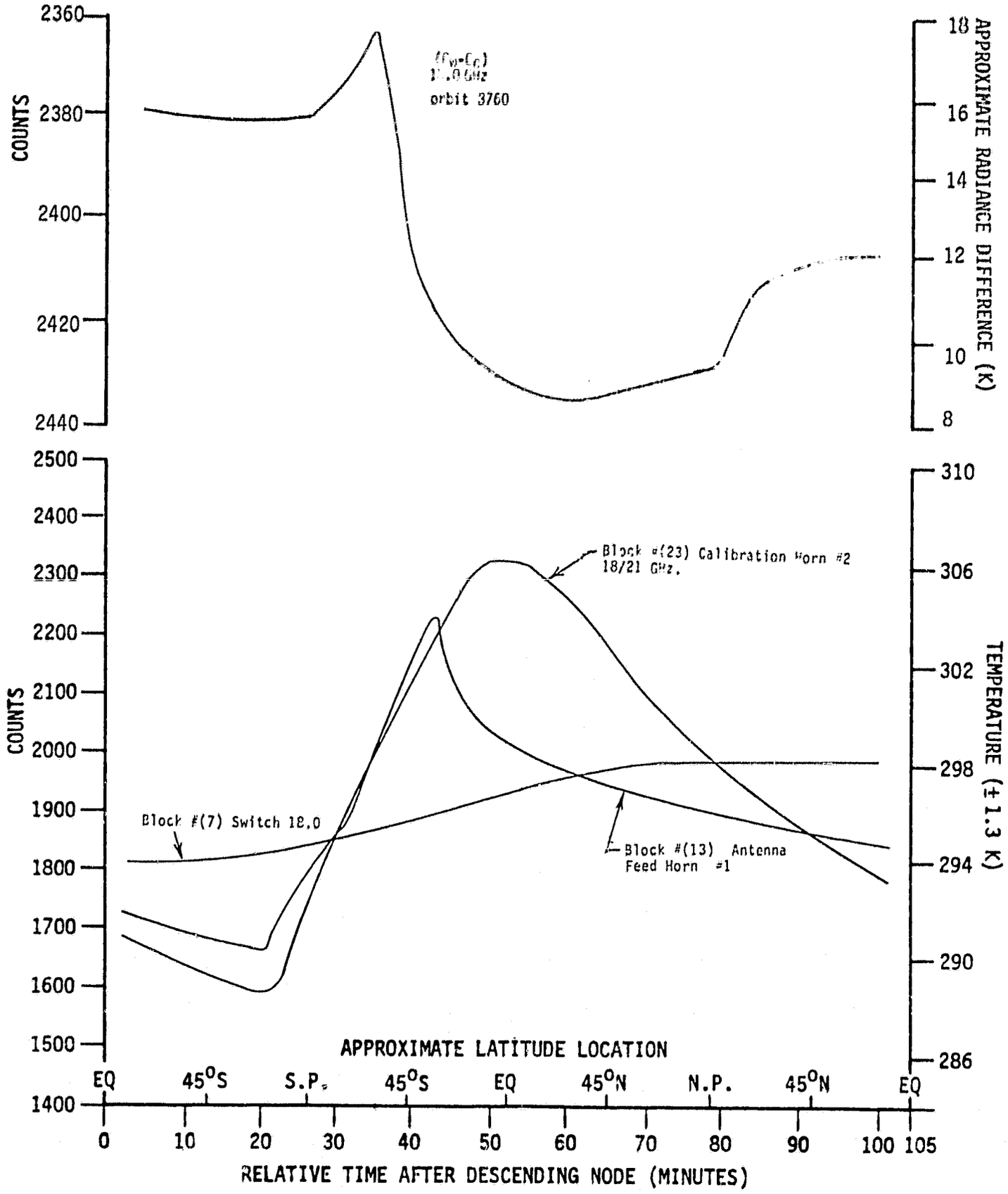

Fig. 43 SMMR 18 GHz horizontal polarization transmission path counts/ temperatures vs. orbit times/latitudes compared with (C_W-C_C) radiances. Orbit #3760, 23 July 1979.

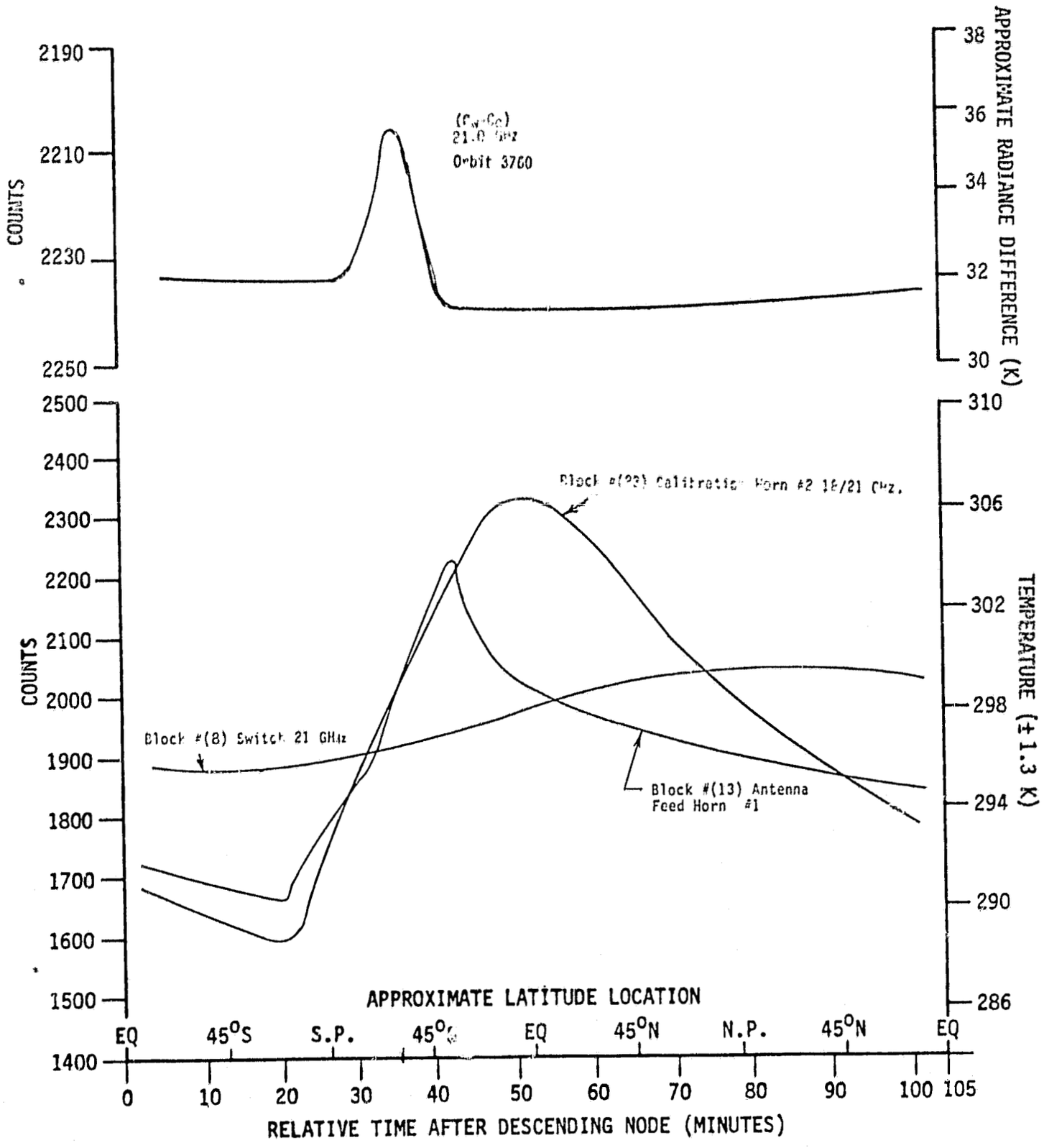

Fig. 44 SMMR 21 GHz horizontal polarization transmission path counts/ temperatures vs. orbit times/latitudes compared with (Cw-Cc) radiances. Orbit #3760, 23 July 1979.

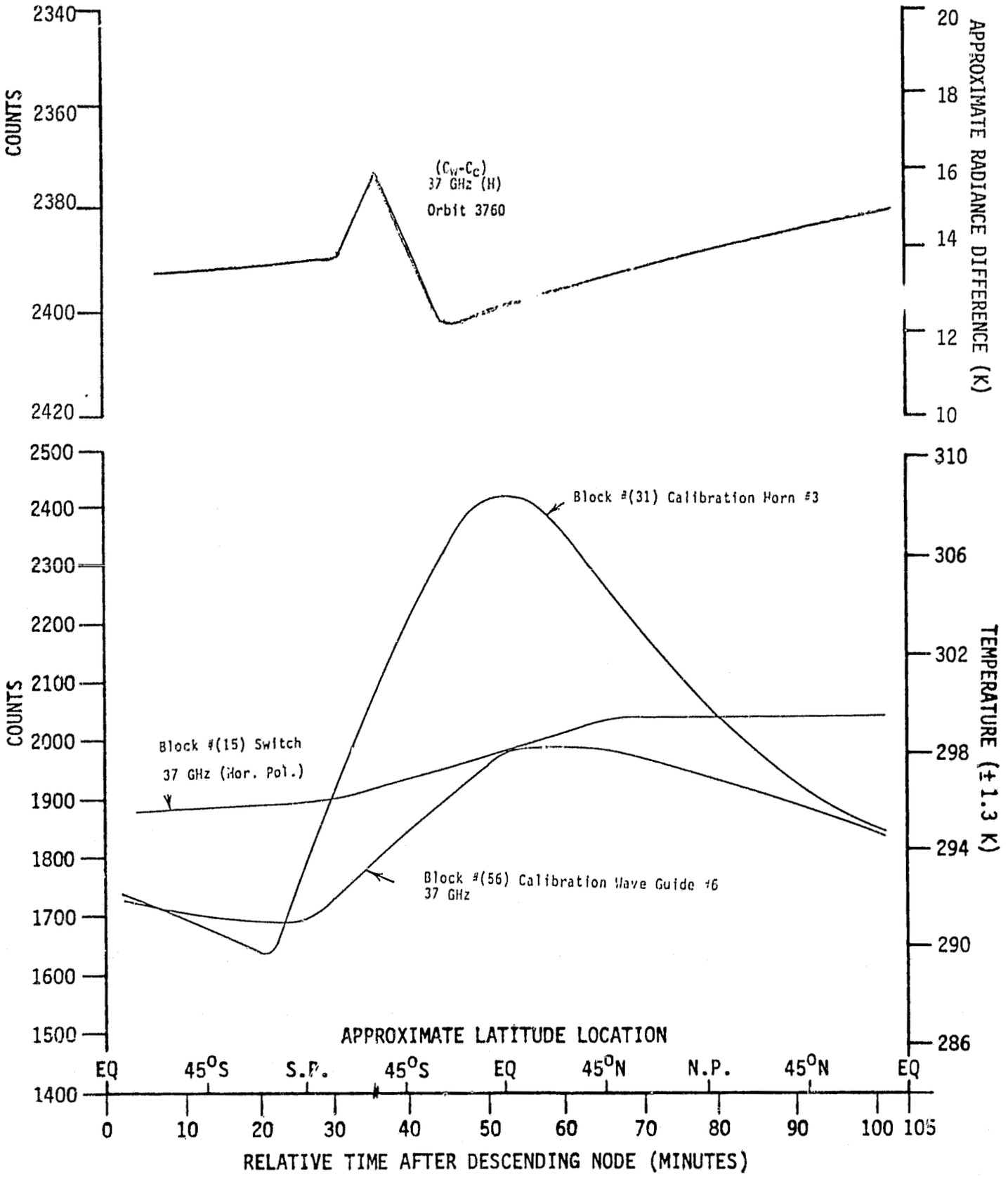

Fig. 45 SMMR 37 GHz horizontal polarization transmission path counts/ temperatures vs. orbit times/latitudes compared with (C_W-C_C) radiances. Orbit #3760, 23 July 1979.

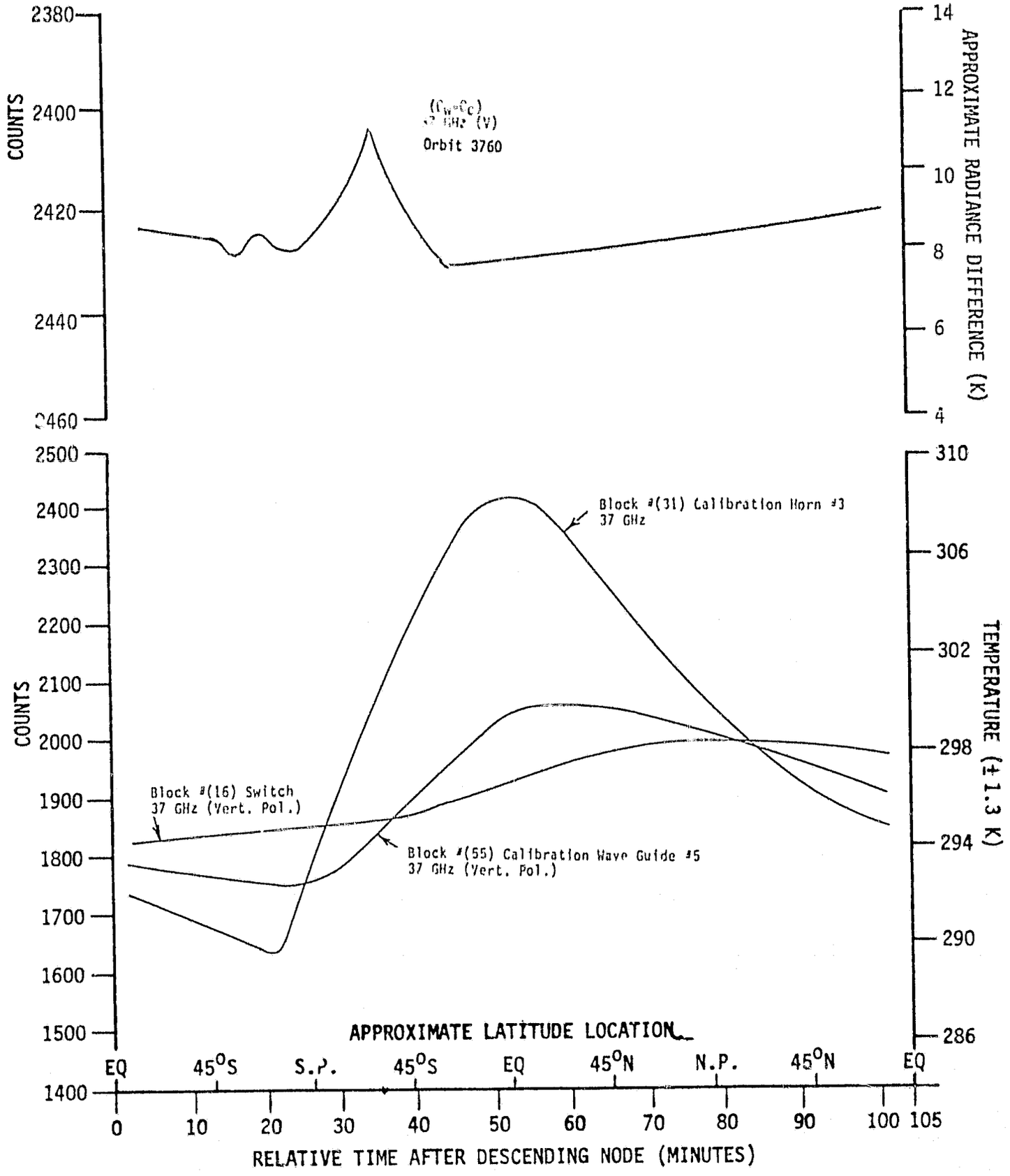

Fig. 46 SMMR 37 GHz vertical polarization transmission path counts/ temperatures vs. orbit times/latitudes compared with (C_W-C_C) radiances. Orbit #3760, 23 July 1979.

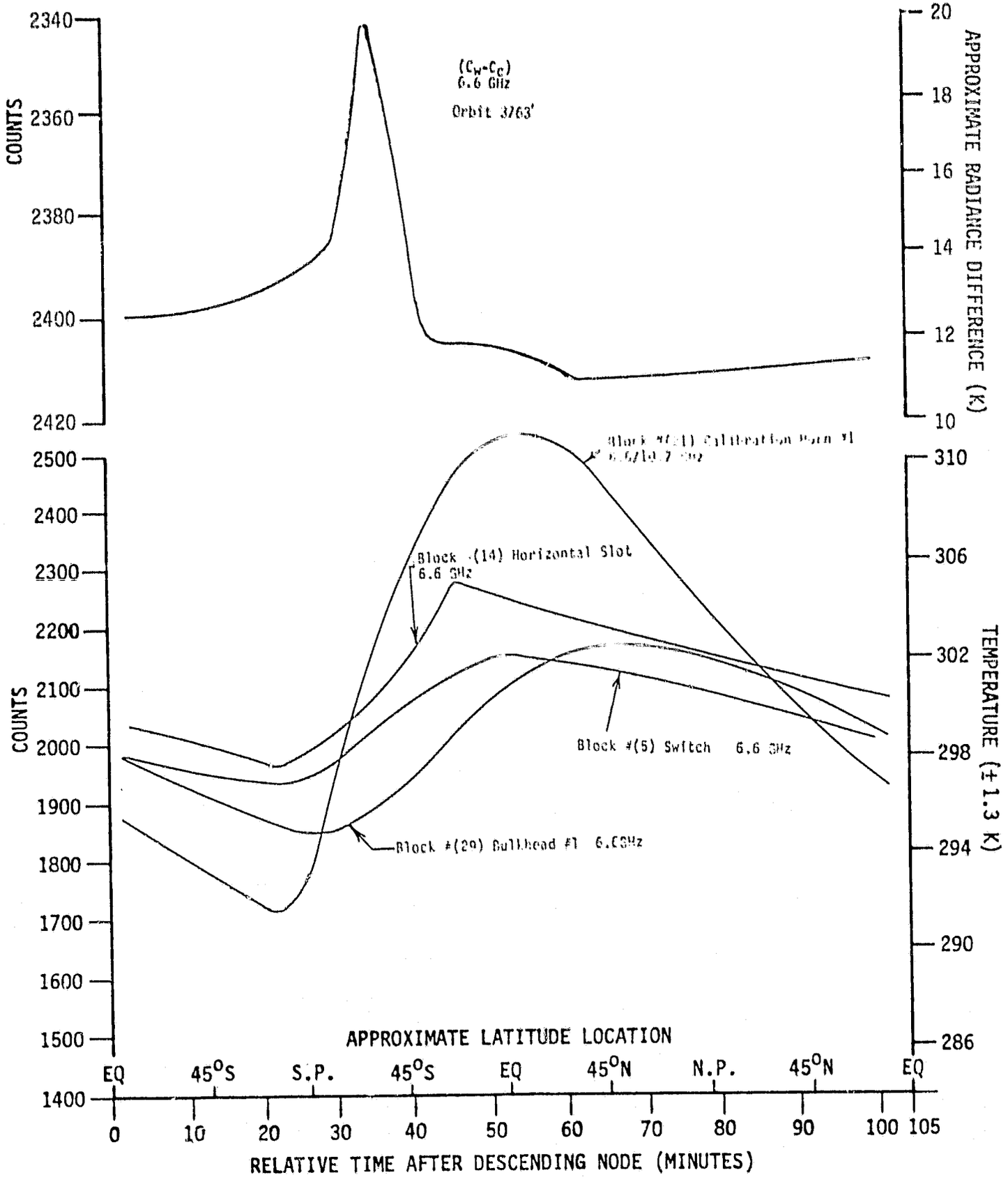

Fig. 47 SMMR 6.6 GHz horizontal polarization transmission path counts/ temperatures vs. orbit times/latitudes compared with (C_W-C_C) radiances. Orbit #3763, 23 July 1979.

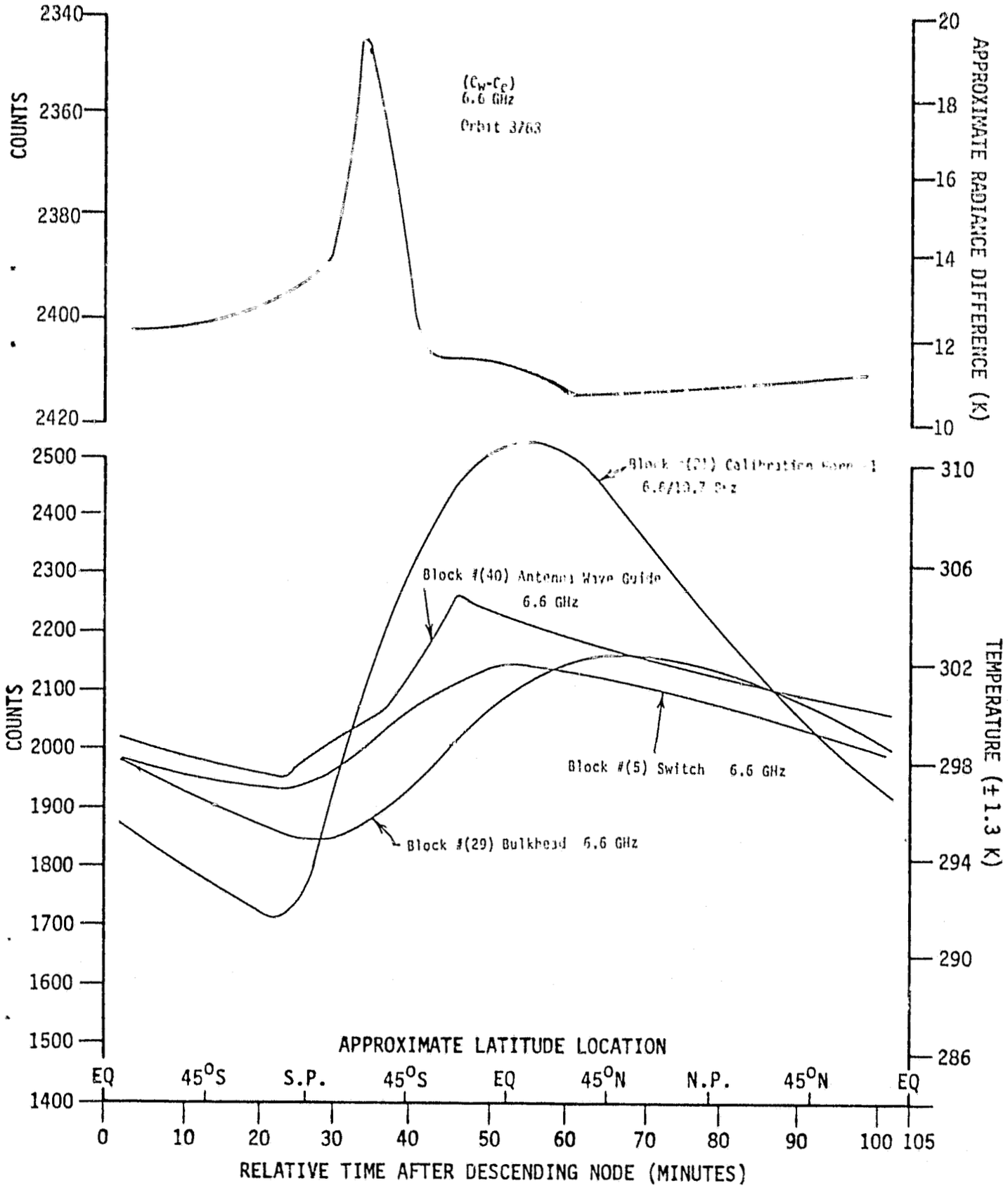

Fig. 48 SMMR 6.6 GHz vertical polarization transmission path counts/ temperatures vs. orbit times/latitudes compared with (C_W-C_C) radiances. Orbit #3763, 23 July 1979.

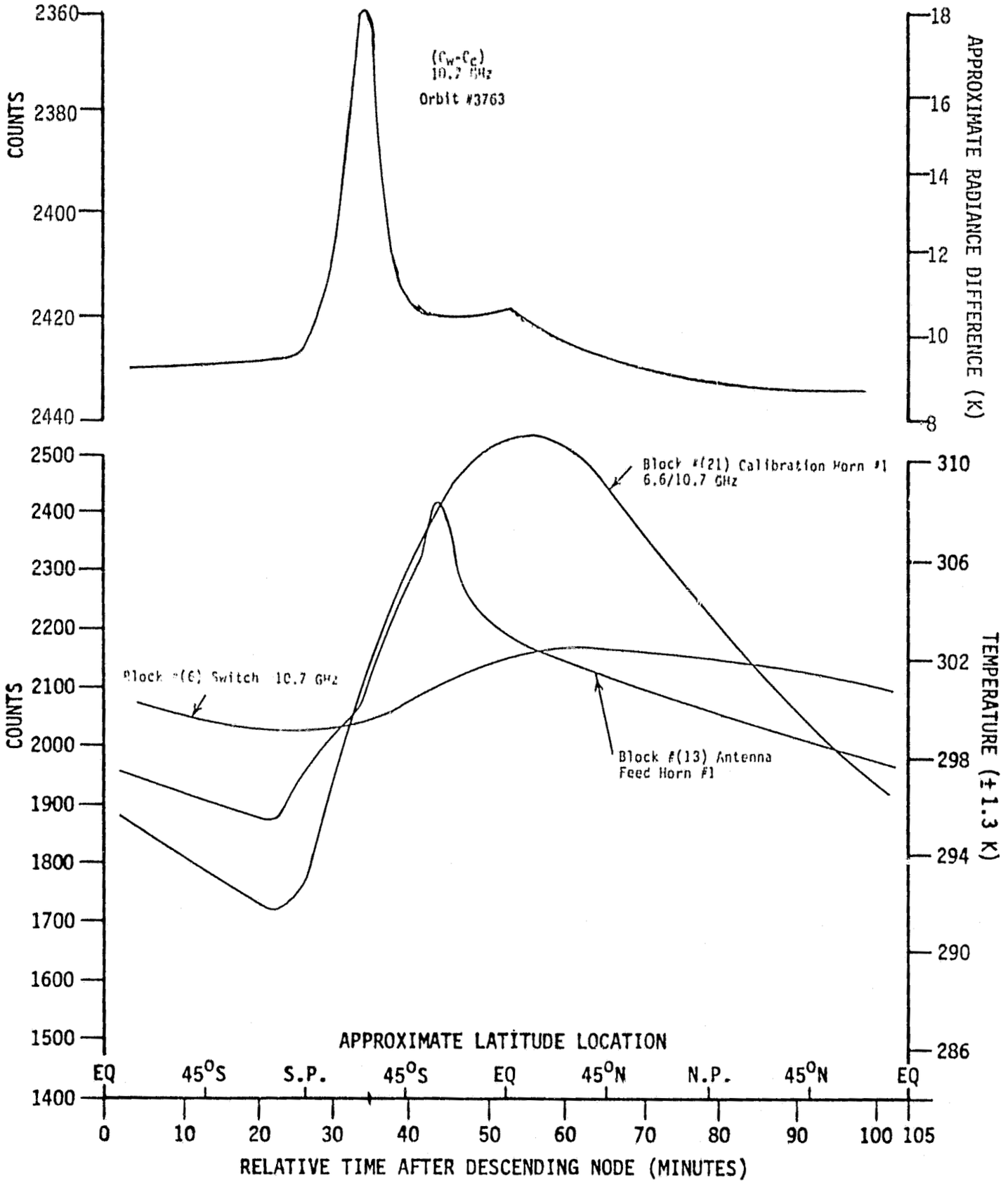

Fig. 49 SMMR 10.7 GHz polarization transmission path counts/temperatures vs. orbit times/latitudes compared with (C_W-C_C) radiances. Orbit #3763, 23 July 1979.

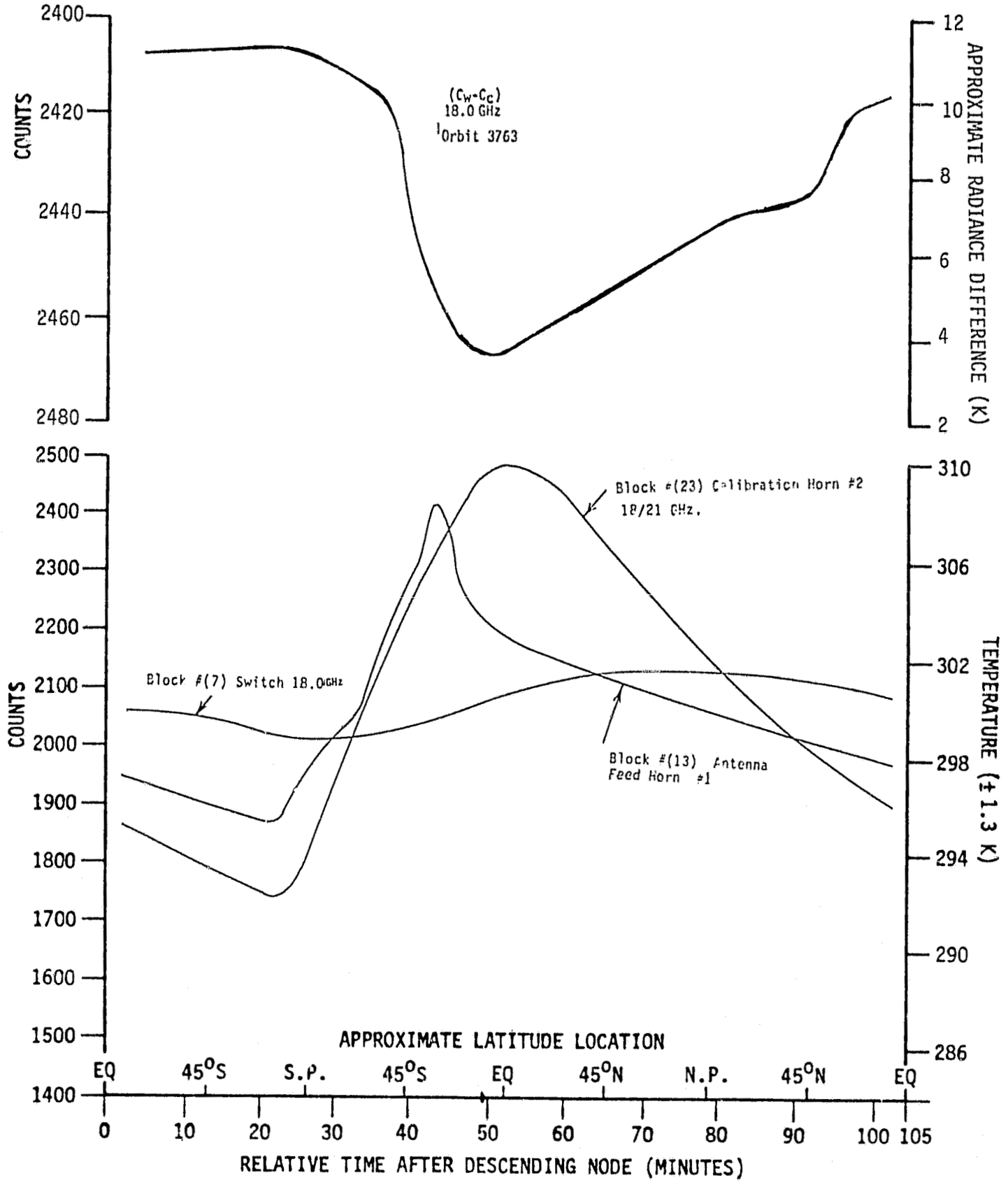

Fig. 50 SMMR 18 GHz horizontal polarization transmission path counts/ temperatures vs. orbit times/latitudes compared with (C_W-C_C) radiances. Orbit #3763, 23 July 1979.

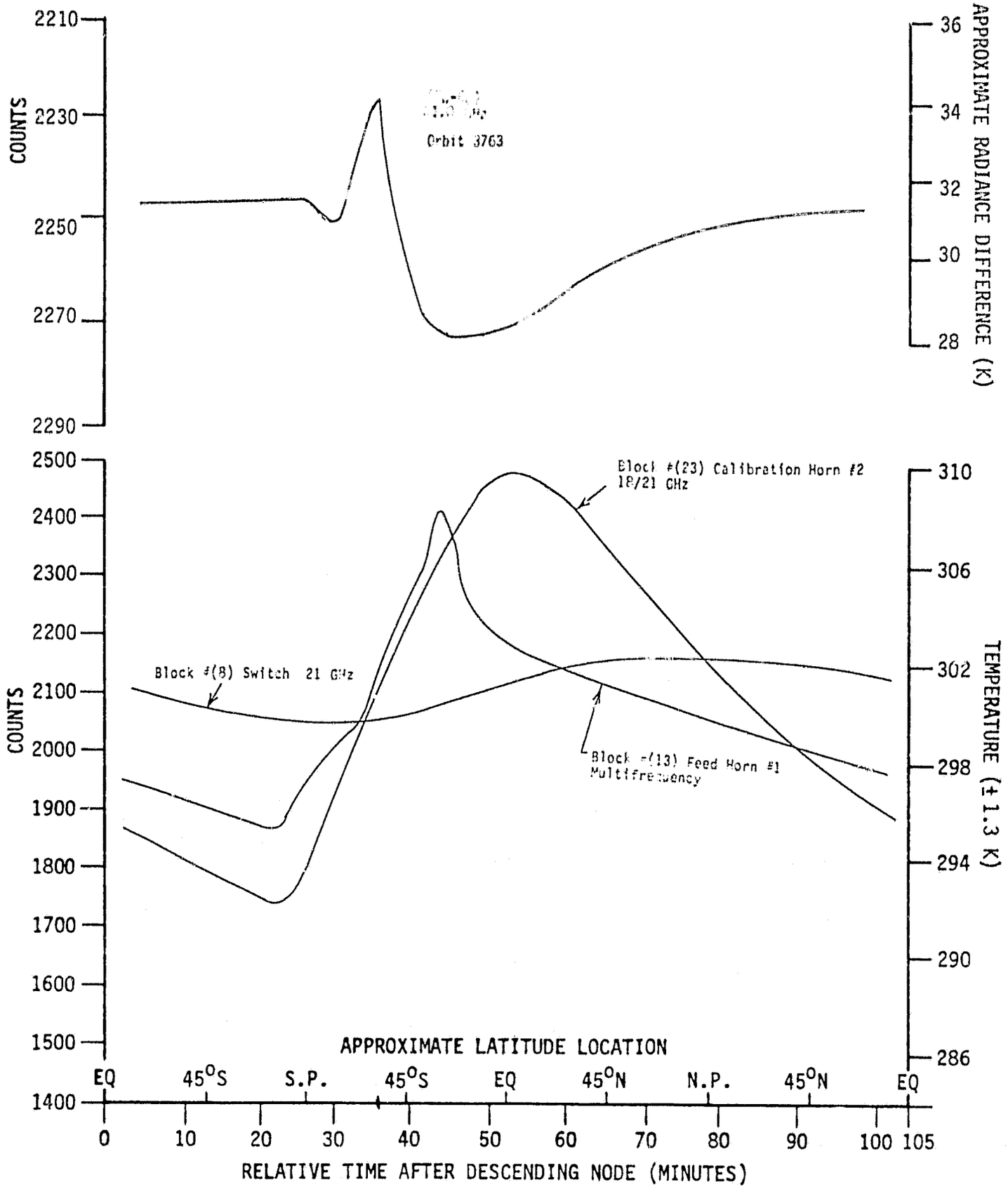

Fig. 51 SMMR 21 GHz horizontal polarization transmission path counts/ temperatures vs. orbit times/latitudes compared with (C_W-C_C) radiances. Orbit #3763, 23 July 1979.

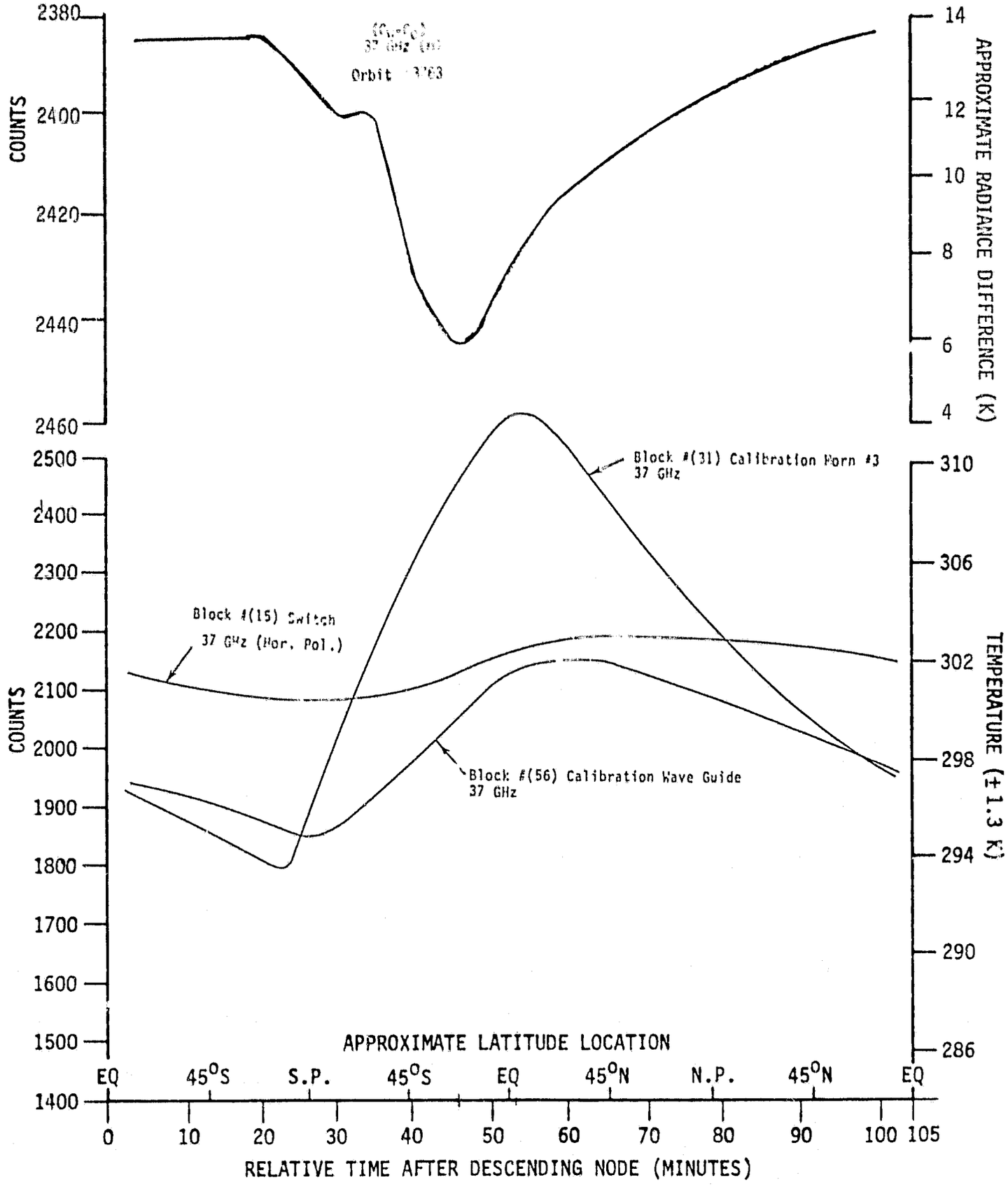

Fig. 52 SMMR 37 GHz horizontal polarization transmission path counts/ temperatures vs. orbit times/latitudes compared with (C_W-C_C) radiances. Orbit #3763, 23 July 1979.

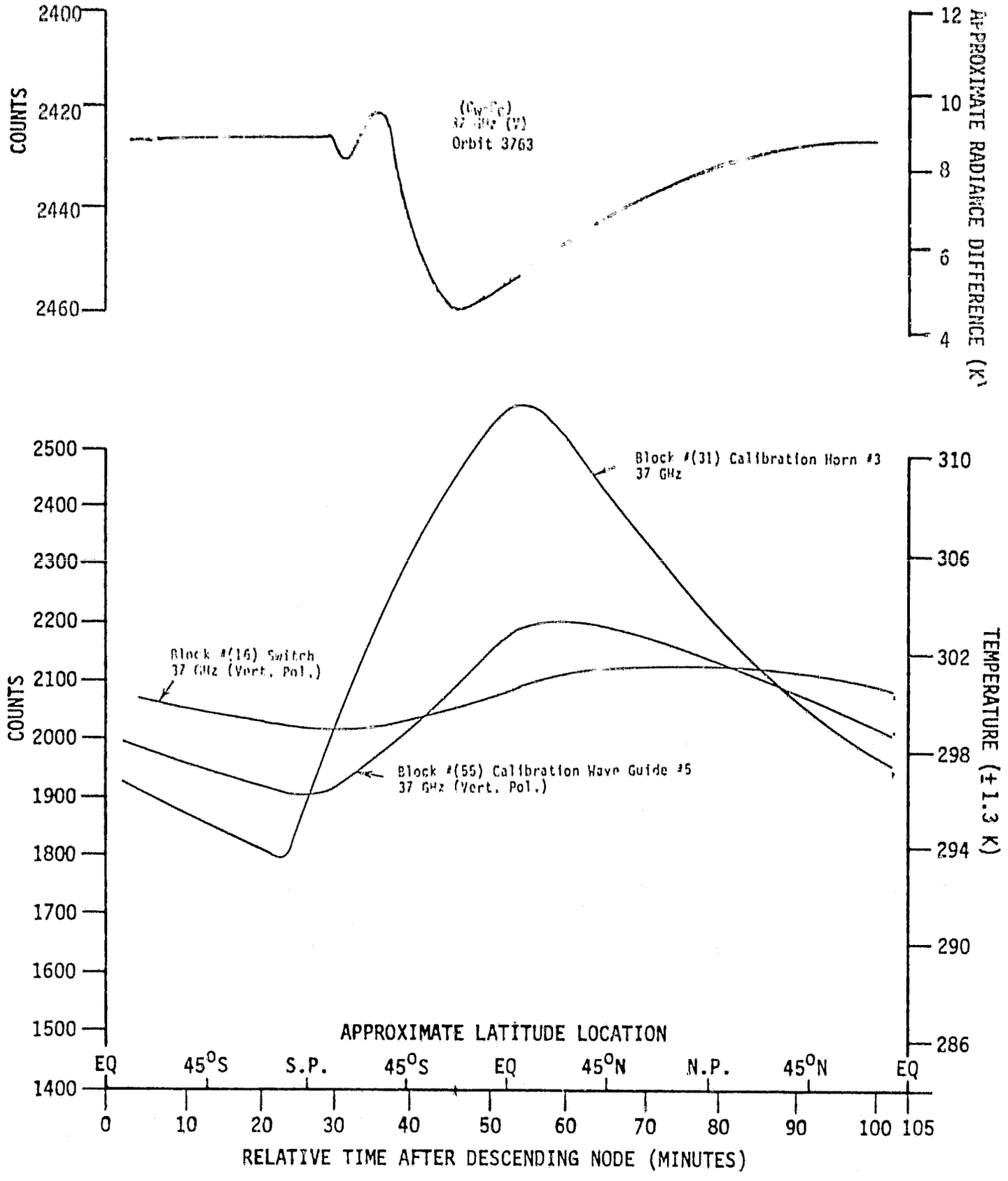

Fig. 53 SMMR 37 GHz vertical polarization transmission path counts/ temperatures vs. orbit times/latitudes compared with (C_W-C_C) radiances. Orbit #3763, 23 July 1979.

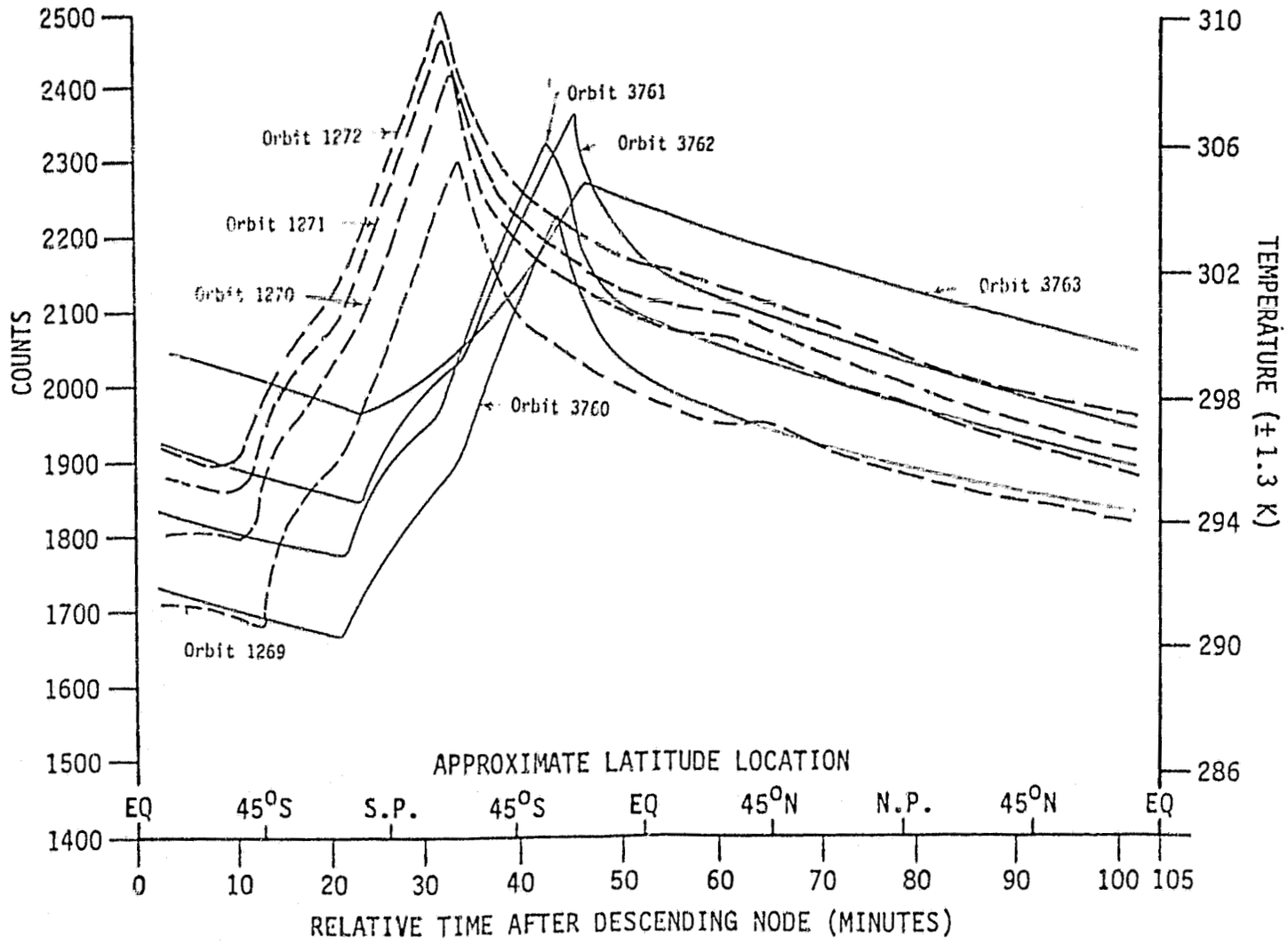

Figure 54. Comparison of the multiple frequency feed-horn temperatures for orbits 1269-1272 (24 Jan. 1979) and those measured on orbits 3760-3763 (23 July 1979). (format word #13).

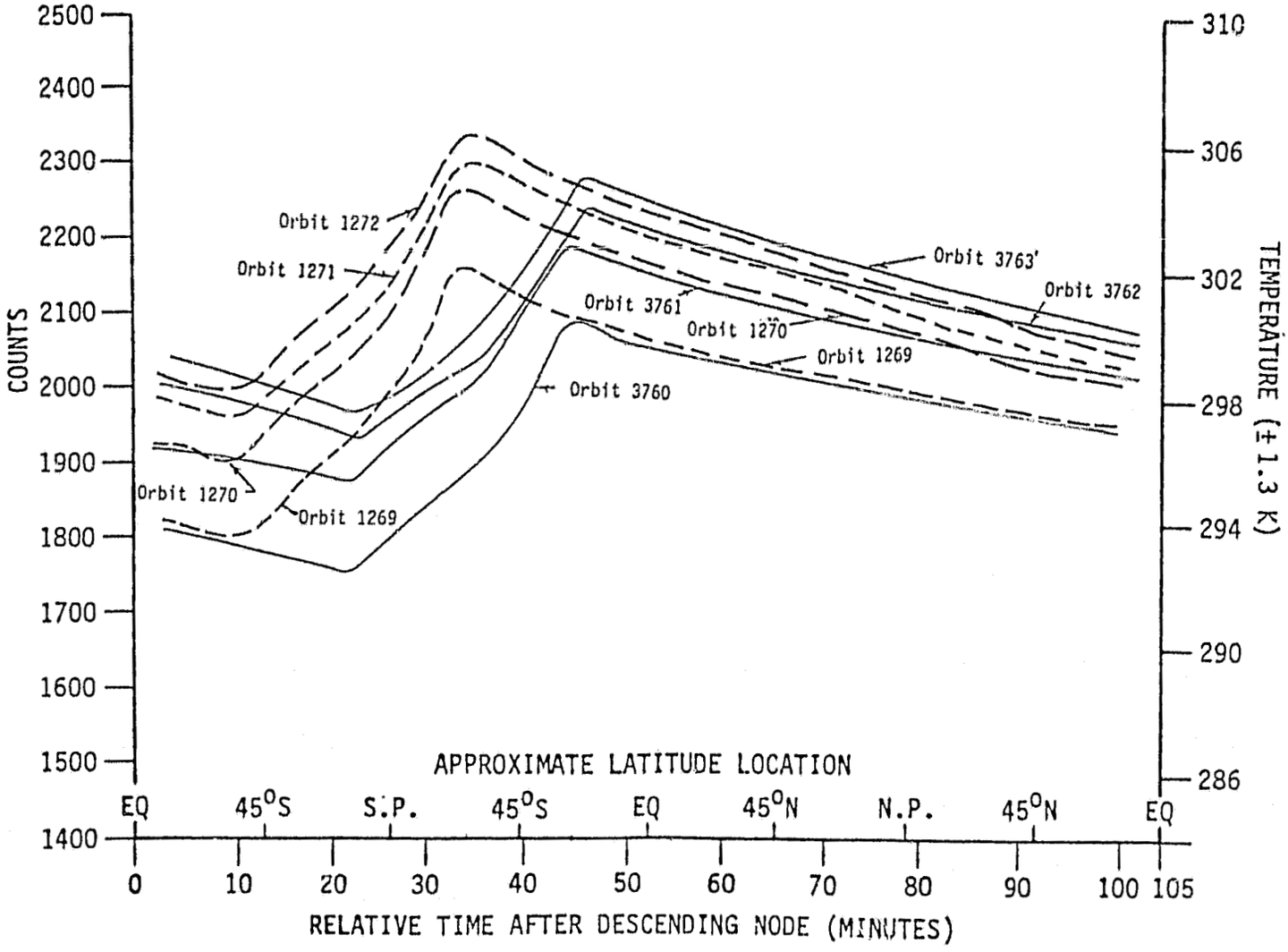

Figure 55. Comparison of 6.6 GHz horizontal polarization antenna feed-horn (format word #14) temperatures for orbits 1269-1272 (24 Jan. 1979) and those measured on orbits 3760-3763 (23 July 1979).

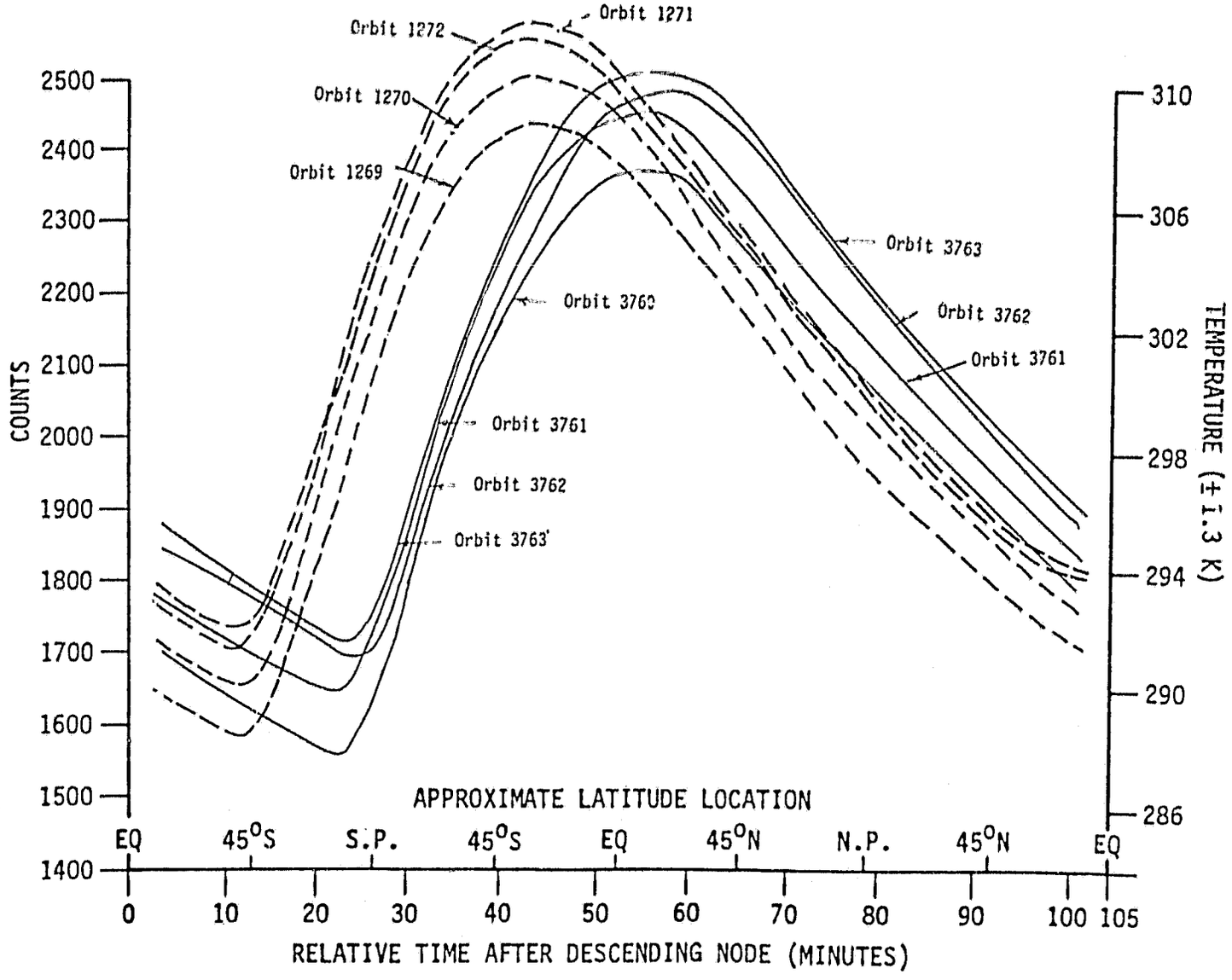

Figure 56. Comparison of the 6.6/10.7 GHz calibration horn temperatures (format word #21) for orbits 1269-1272 (24 Jan. 1979) and those measured on orbits 3760-3763 (23 July 1979).

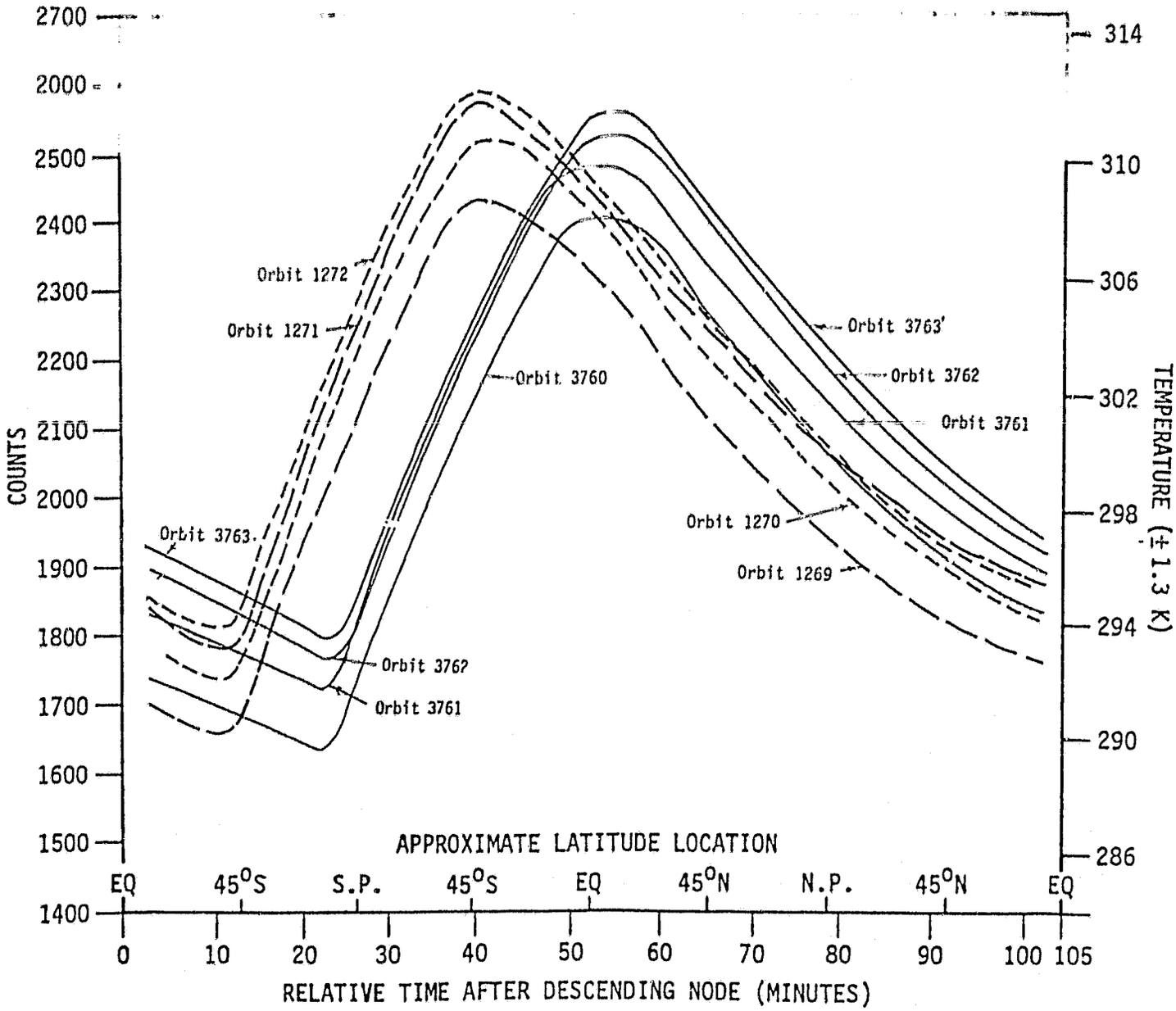

Figure 57. Comparison of the 37.0 GHz calibration horn temperatures (format word #31) for orbits 1269-1272 (24 Jan. 1979) and those measured on orbits 3760-3763 (23 July 1979).

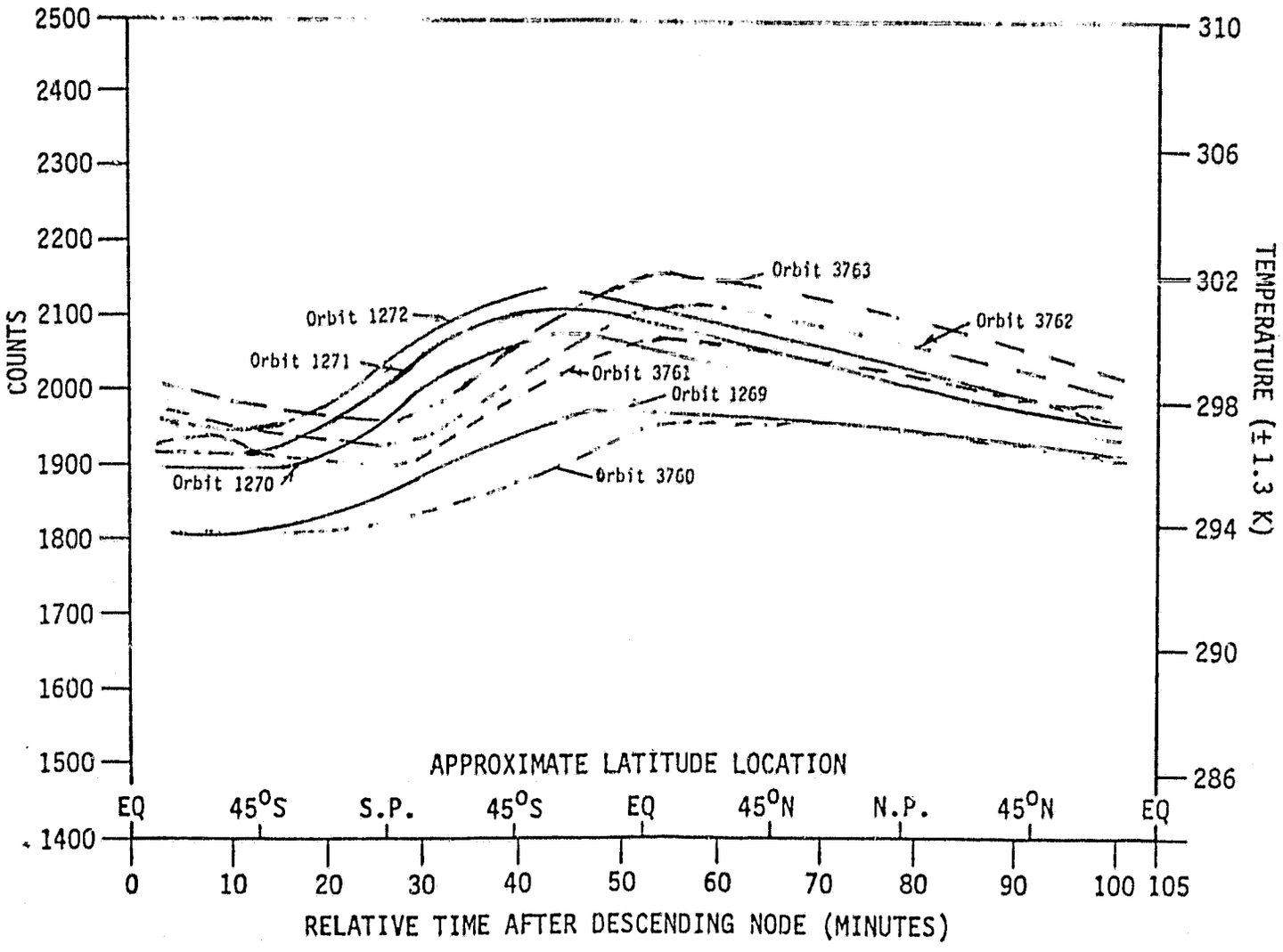

Figure 58. Comparison of the 6.6 GHz Dicke switch temperatures (word #5) for for orbits 1269-1272 (24 Jan. 1979) and those measured on orbits 3760-3763 (23 July 1979).

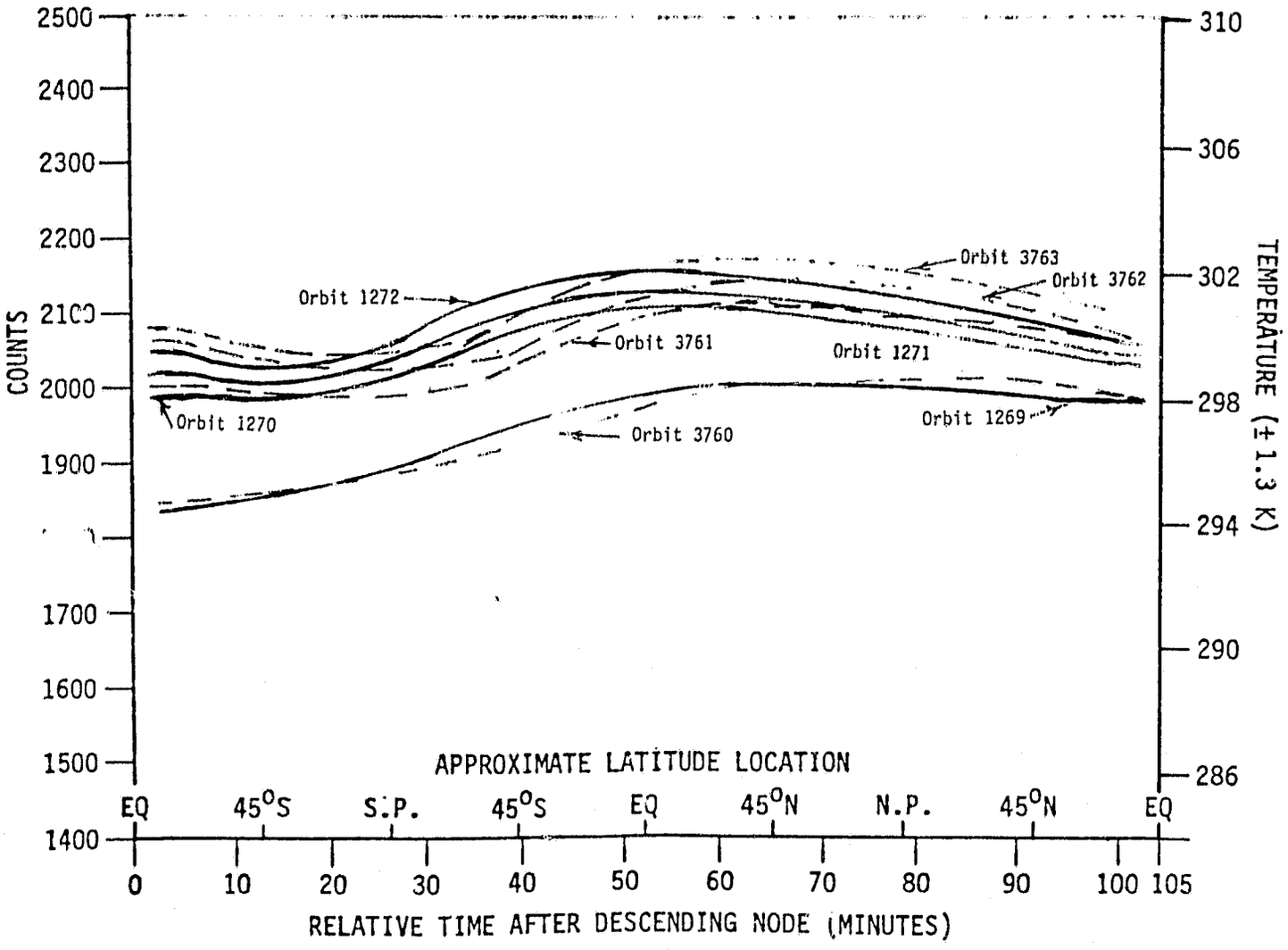

Figure 59. Comparison of the 10.7 GHz Dicke switch temperatures for orbits 1269-1272 (24 Jan. 1979) and those measured on orbits 3760-3763 (23 July 1979).

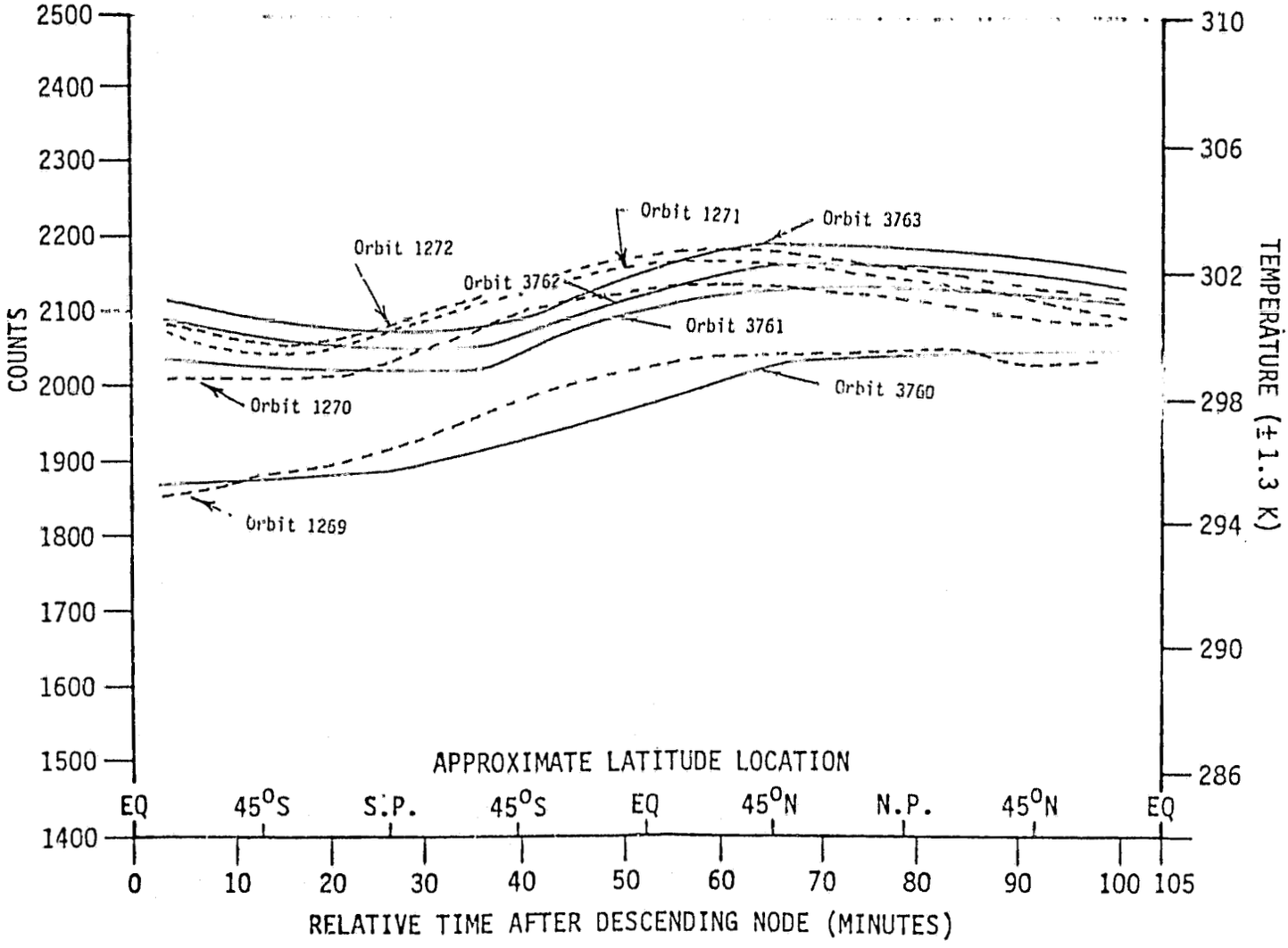

Figure 60. Comparison of the horizontally polarized 37.0 GHz Dicke switch temperatures (word #15) for orbits 1269-1272 (24 Jan. 1979) and those measured on orbits 3760-3763 (23 July 1979).

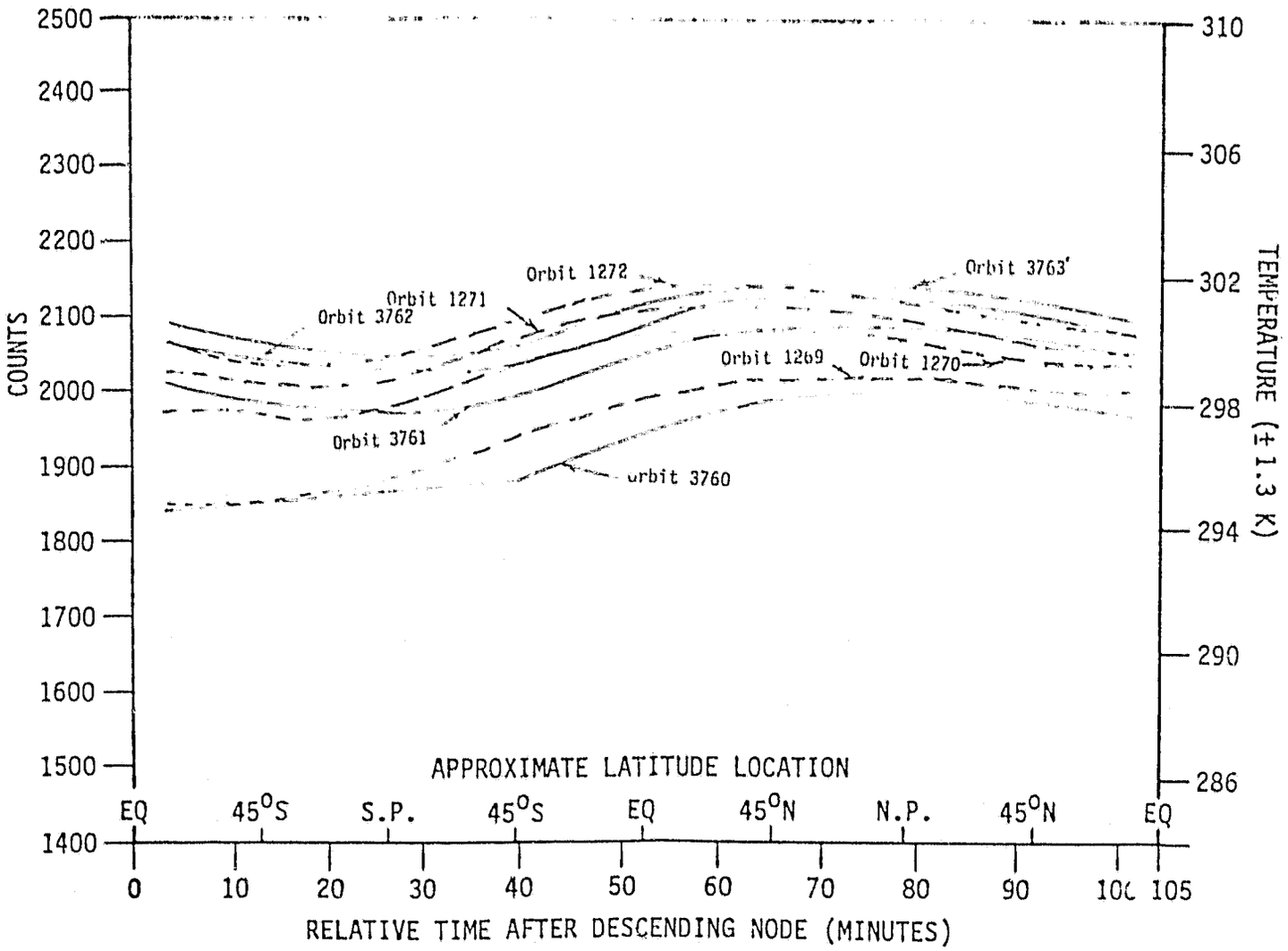

Figure 61. Comparison of the vertically polarized 37.0 GHz Dicke switch temperatures (word #16) for orbits 1269 through 1272 (24 Jan. 1979) and those measured on orbits 3760 through 3763 (23 July 1979).